Bioorganic Studies on *cis*-Jasmone and Pyrethrins Biosynthesized via the OPDA Isomerizing Pathway

(OPDA 異性化経路により生合成される *cis*-ジャスモン及びピレスリンに関する生物有機化学的研究)

北海道大学　大学院農学院

農学専攻　応用生命フロンティアコース

応用生物化学ユニット　英語コース

博士後期課程

井上 史朗

Table of contents

1. Introduction

1.1. Jasmonate: A Plant Hormone

Jasmonates (JAs) play pivotal roles in diverse biological processes, including responses to biotic and abiotic stresses as well as the development of reproductive organs. They act as key regulators of plant defense against environmental challenges such as insect herbivory and pathogen infection. The biosynthesis of JAs is rapidly induced by wounding stress such as insect or herbivore attack. Subsequently, JAs activate the expression of

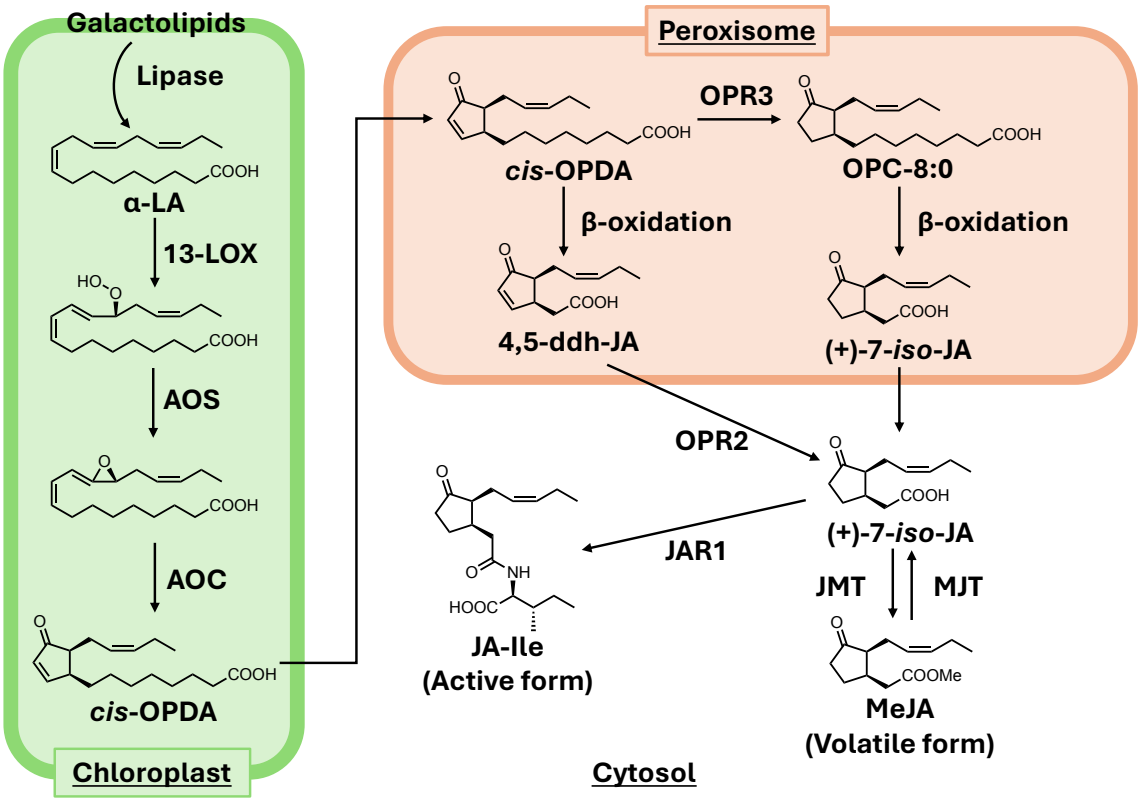

Figure 1.1. Biosynthetic pathway of jasmonates.

Abbreviations: Compounds: α-linolenic acid (α-LA), *cis*-12-oxo-phytodienoic acid (*cis*-OPDA), 3-oxo-2-(2'-[*Z*]-pentenyl)cyclopentane-1-octanoic acid (OPC-8:0), (+)-7-*iso*-jasmonic acid ((+)-7-*iso*-JA), 4,5-didehydro-(+)-7-*iso*- jasmonic acid (4,5-ddh-JA), (-)-7-*iso*-jasmonoyl-L-isoleucine (JA-Ile), methyl (+)-7-*iso*-Jasmonate (MeJA).
Enzymes: allene oxide cyclase (AOC), allene oxide synthase (AOS), JA carboxyl methyltransferase (JMT), MeJA esterase (MJE), OPDA reductase 2 (OPR2), OPDA reductase 3 (OPR3), 13-lipoxygenase (13-LOX).

genes encoding protease inhibitors (PIs), which suppress herbivore feeding, and pathogenesis-related (PR) proteins, which restrict pathogen invasion[1]. Moreover, JAs promote resistance against necrotrophic pathogens by upregulating the biosynthesis of phytoalexins, thereby strengthening the overall immune capacity of plants[2].

The biosynthesis of JAs begins with the release of α-linolenic acid (α-LA) from galactolipids of chloroplast membranes[3], and the released α-LA undergo peroxidation by 13-lipoxygenase (13-LOX)[4], epoxidation by allene oxide synthase (AOS)[5], and cyclization by allene oxide cyclase (AOC)[6] to produce *cis*-12-oxo-phytodienoic acid (*cis*-OPDA). *cis*-OPDA is then transported to peroxisomes and is reduced by OPDA-reductase 3 (OPR3) to form 3-oxo-2-(2'-[*Z*]-pentenyl)-cyclopentane-1-octanoic acid (OPC-8:0)[7]. Then, OPC-8:0 undergoes three β-oxidation steps to produce (+)-7-*iso*-jasmonic acid ((+)-7-*iso*-JA). Furthermore, (+)-7-*iso*-JA was conjugated with L-isoleucine via jasmonate amino synthase (JASMONATE RESISTANT1: JAR1) to give (-)-7-*iso*-jasmonyl-L-isoleucine (JA-Ile)[8]. Among jasmonates, JA-Ile represents the primary bioactive molecule responsible for regulating jasmonate signaling pathways. The volatile form of jasmonates, methyl (+)-7-*iso*-jasmonate (MeJA), can induce defence responses in neighboring plants by air transmission. (+)-7-*iso*-MeJA is produced from (+)-7-*iso*-JA by JA carboxyl methyltransferase (JMT)[9], whereas MeJA is hydrolysed to (+)-7-*iso*-JA by MeJA esterase (MJE)[10]. Recently, a supplemental JA biosynthetic pathway involving 4,5-didehydro-(+)-7-*iso*-JA (4,5-ddh-JA) as an intermediate was discovered[11]. In this pathway, 4,5-ddh-JA is generated from *cis*-OPDA by three β-oxidation steps and then reduced by *cis*-OPDA reductase 2 (OPR2) to form (+)-7-*iso*-JA in cytosol.

In jasmonate signaling, JA-Ile is perceived by the CORONATINE INSENSITIVE 1 (COI1)-JASMONATE-ZIM DOMAIN (JAZ) co-receptor[12] (Figure 1.2). COI1 is an F-box protein that

functions as a component of the SCF-type E3 ubiquitin ligase complex, forming the COI1 complex together with Cul1, Skp1, and Rbx1[13]. In the absence of JA-Ile, JAZ, the repressor protein, binds to transcription factors such as MYC2, thereby suppressing their transcriptional activity. Upon various stress, endogenous levels of JA-Ile increase, promoting the JA-Ile-dependent interaction of JAZ with COI1 and the formation of the COI1-JAZ complex. Once bound to COI1, JAZ proteins are ubiquitinated to be degraded by the 26S proteasome. The dissociation of MYC2 from JAZ allows MYC2 to associate with the basal transcriptional machinery to initiate transcription inducing the expression of downstream JA-responsive genes.

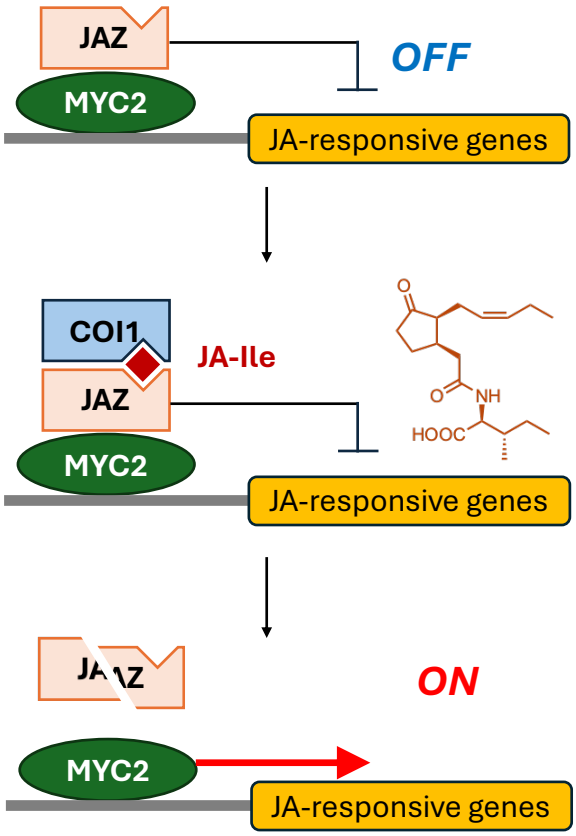

Figure 1.2. Model of JA-Ile perception and signaling

Abbreviations: JASMONATE ZIM-DOMAIN (JAZ), CORONATINE INSENSITIVE 1 (COI1).

1.2. *cis*-Jasmone: A Fragrant Compound

The essential oil of jasminum flowers has long been used in the perfume industry due to its excellent fragrance. *cis*-Jasmone (CJ) and MeJA were identified in the essential oil[14, 15]. CJ is also found in the absolutes of neroli (*Citrus bigaradia*), jonquil (*Narcissus jonquilla L.*), and bergamot (*Citrus bergamia*) plants and in plants of the Pittosporum family[16]. Today, CJ is an important industrial material used to produce many commodities, such as perfumes, cosmetics, and food additives. The biological functions of CJ have been studied extensively in previous studies. First, it was noted that CJ is released from flowers in many cases and attracts olive flies[16]. CJ has also received attention as a wounding signal as well as a beneficial ingredient that attracts pollinator insects. Small amounts of CJ are released from cotton leaves during wounding, and the releasing CJ exterminates aphids by attracting natural enemies of the aphids as well as aphid parasitoids[17]. Futhermore, CJ acts as a signal to trigger plant defence responses, similar to MeJA. Brassica plants treated with CJ were less attractive to and less suitable for *Myzus persicae* aphids[18], and CJ-treated leaflets of tomato significantly reduced *Tuta absoluta* leaf-mining activity[19]. Wheat treated with CJ accumulated phenolic acids, which act as defensive substances[20]. Interestingly, CJ triggers a signaling pathway different from that of jasmonates[21]. Expression of CJ-responsive genes is not affected in *coi1* or *jar1* mutants.

To date, two pathways have been proposed for CJ biosynthesis from *cis*-OPDA (Figure 1.3). The first pathway is the OPDA-reducing pathway involving the biosynthesis of 7-*iso*-JA from *cis*-OPDA by OPRs. In this pathway, 7-*iso*-JA is oxidized to form 3,7-didehydro-JA (3,7-ddh-JA), which undergoes a decarboxylation reaction to produce CJ.

The second pathway is the OPDA-isomerizing pathway, which converts the C11–C10 double bond in *cis*-OPDA to the C13–C9 position, producing *iso*-OPDA (Figure 1.3).

Inspired by the commonality of the chemical structure in CJ with that of JAs, Koch *et al.* fed deuterium-labelled (±)-JA and 3,7-ddh-MeJA to lima beans (*Phaseolus lunatus*), willow (*Salix alba*) and jasmine (*Jasminum rincospernum*), which found that the labelled compounds were converted to deuterium-labelled CJ[22]. From the results of the experiment, it was determined that CJ was biosynthesized via the OPDA-reducing pathway. On the other hand, OPDA-isomerizing pathway that biosynthesizes CJ via *iso*-OPDA was proposed by Dabrowska *et al.*, who showed that deuterium-labelled methyl *iso*-OPDA was converted to deuterium-labelled CJ in seven kinds of plants[16]. Recently, it was reported that CJ, a biosynthetic intermediate of pyrethrin II, is biosynthesized in pyrethrum (*Tanacetum cinerariifolium*) via the OPDA-isomerizing pathway rather than the OPDA-reducing pathway[23]. However, the key enzyme in the OPDA-isomerizing pathway, OPDA isomerase, has not been identified in any plant species.

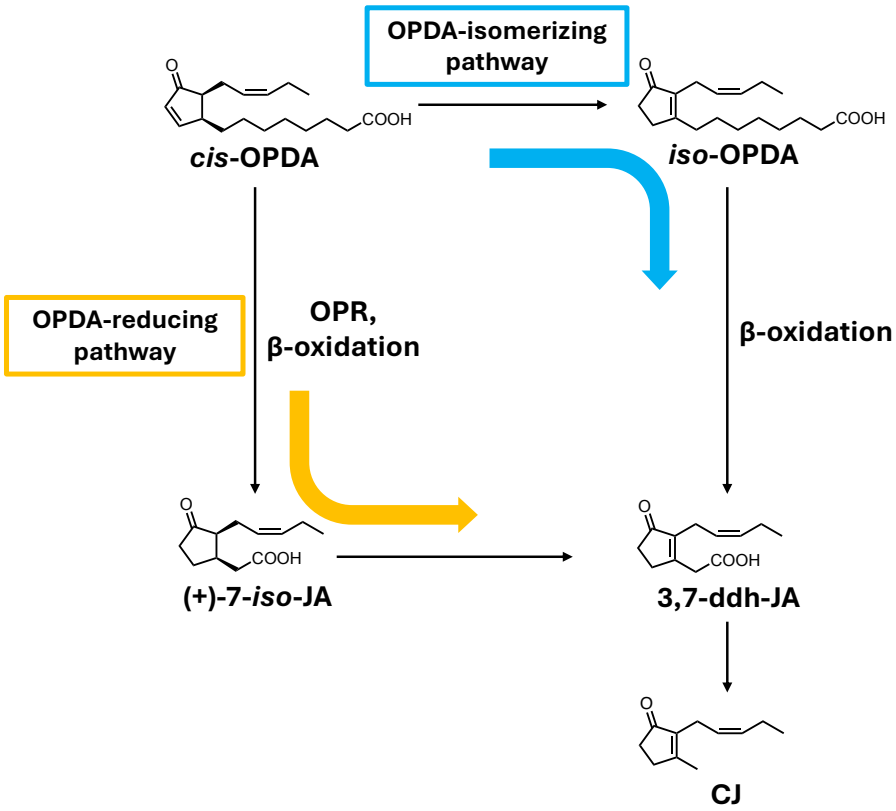

Figure 1.3. Proposed biosynthetic pathway of *cis*-jasmone (CJ)

1.3. Pyrethrins: Natural Pesticide Compounds

Pyrethrins are natural insecticides produced by pyrethrum (*Tanecetum cinerariifolium*). The history of pyrethrins is long, and products made from pyrethrum have been used for pest control since medieval times[24]. Natural insecticides derived from pyrethrum are called as pyrethrins, while synthetic insecticides designed from pyrethrins are called as pyrethroids. Pyrethroids having higher insecticidal activity and stability than those of pyrethrins have been invented, and the market for pyrethrins has been replaced by synthetic pyrethroids. In recent years, the adverse effects of synthetic pesticides on the environment and human health have become an issue, and natural pyrethrins are receiving attention again due to their low impact on the environment. The industrial production of naturally derived pyrethrin still relies on extraction from mature flowers of pyrethrum. It was found that the highest levels of production were observed in flowers, whereas a smaller amount was observed in leaves. It is estimated that the world production of pyrethrum reaches or exceeds 30,000 metric tons[24].

Natural pyrethrins comprise six esters, pyrethrin I/II, jasmolin I /II, and cinerin I/II, produced by the esterification of the acid moiety of chrysanthemic and pyrethric acids with the alcohol moiety of pyrethrolone, cinerolone, and jasmolone[25]. Chrysathemic and pyrethric acids are biosynthesized from two molecules of dimethylallyl diphosphate (DMAPP) via the monoterpenoid pathway[26], and the complete biosynthetic pathway for the acid moiety has been fully elucidated[27, 28]. However, the biosynthesis of the alochol moiety remains less understood. As described above, the alcohol moiety is derived from α-LA via CJ through the OPDA isomerizing pathway. But, OPDA isomerase has not been identified to date in pyrethrum. From CJ, jasmolone, pyrethlone, and cinerolone are subsequently

produced[29, 30]. While the biosynthetic pathways of jasmolone and pyrethlone have been elucidated, that of cinerolone remains unknown.

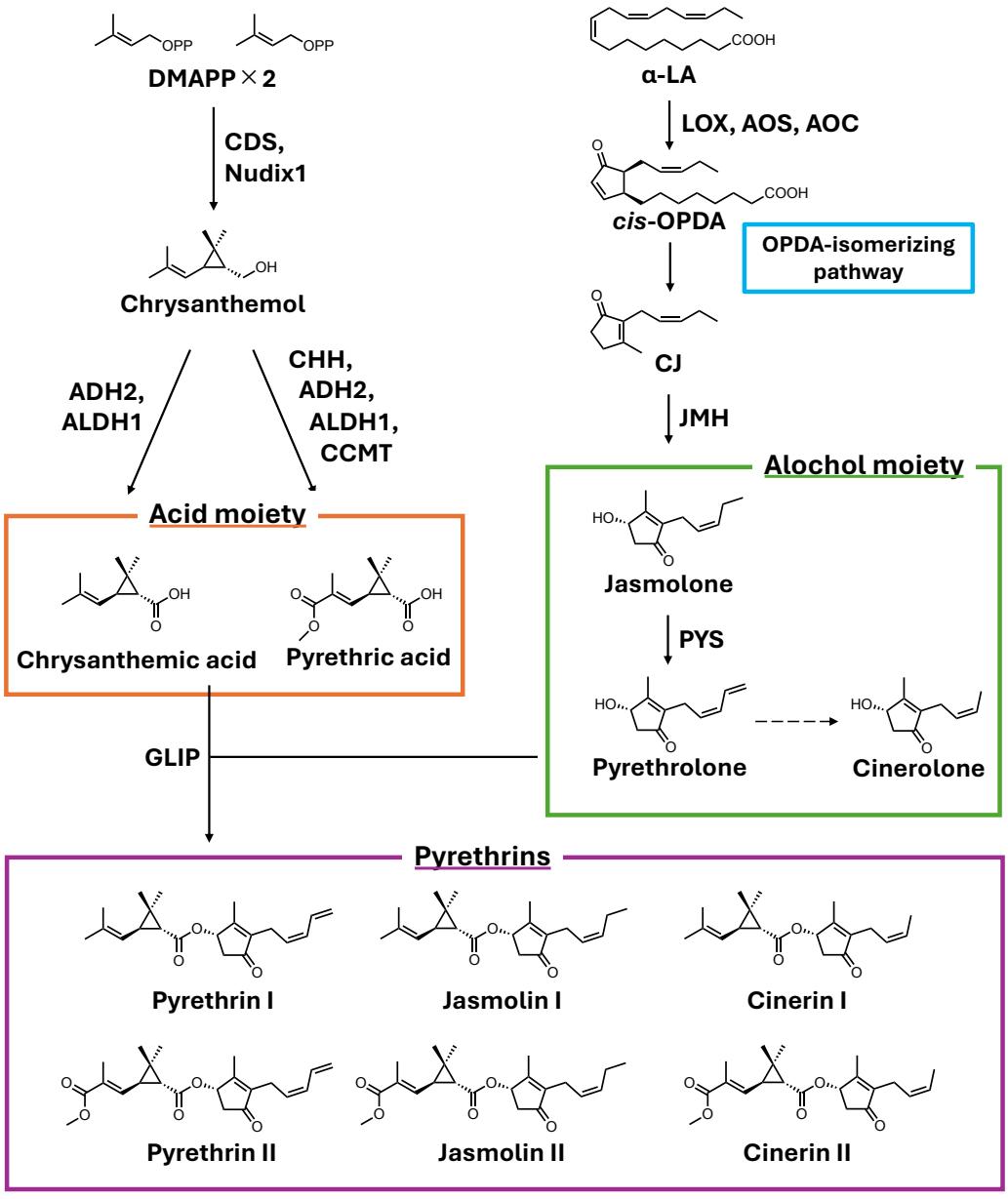

Figure 1.4. Biosynthesis pathway of pyrethrins

Abbreviations: Compound: dimethylallyl pyrophosphate (DMAPP), Enzyme: alcohol dehydrogenase 2 (ADH2), aldehyde dehydrogenase 1 (ALDH1),10-carboxychrysanthemic acid methyltransferase (CCMT), chrysanthemyl diphosphate synthase (CDS), chrysanthemyl monophosphate (CMP), dimethylallyl diphosphate (DMADP), GDSL lipase-like protein (GLIP), jasmone hydroxylase (JMH), pyrethrolone synthase (PYS)

1.4. dn-*iso*-OPDA: Jasmonate Ligands of Ancestral Land Plants

Plants originated from charophytic algae and subsequently underwent major evolutionary transitions, including terrestrialization, the development of vascular tissues, the emergence of seeds, and the generation of flowers. As a result of these innovations, land plants evolved into the major groups present today, including bryophytes, lycophytes, gymnosperms, and angiosperms. The mechanisms of phytohormone signaling have also undergone extensive evolutionary modification during plant evolution.

In vascular plants such as *Arabidopsis thaliana*, the bioactive ligand of the COI1–JAZ co-receptor complex is JA-Ile. By contrast, the liverwort *Marchantia polymorpha*, which represents an early-diverging lineage of land plants, possesses homologs of COI1 and JAZ but lacks a functional homolog of JAR1, the enzyme that catalyzes the conjugation of jasmonic acid (JA) and L-isoleucine to form JA-Ile[31]. Consistently, endogenous JA-Ile has not been detected in this species[32]. Instead, the *M. polymorpha* COI1–JAZ (MpCOI1-MpJAZ) complex specifically recognizes dinor-*iso*-OPDA (dn-*iso*-OPDA), while showing no binding affinity for JA-Ile[33]. During the evolution of land plants, the COI1-JAZ receptor

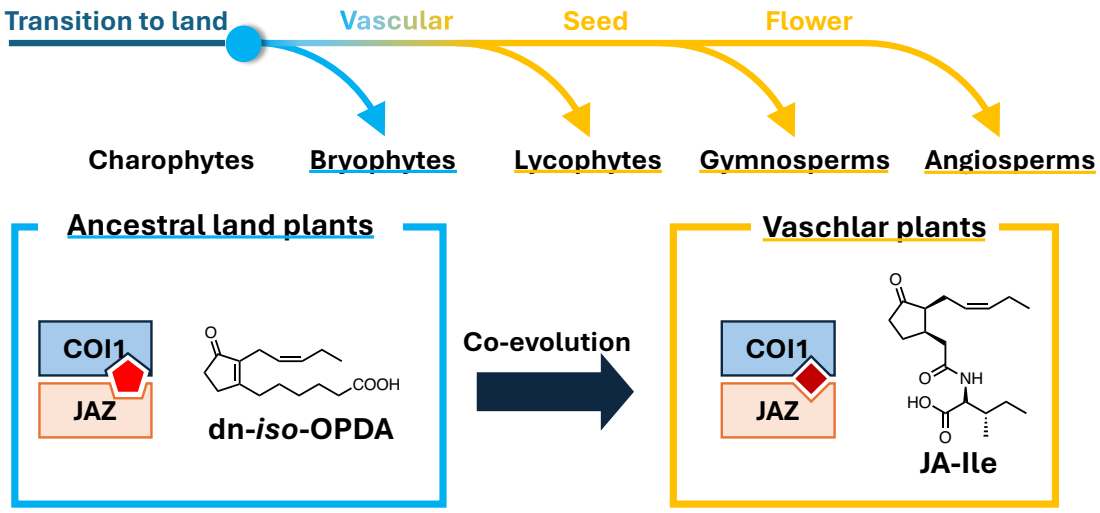

Figure 1.5. Ligand-receptor co-evolution in jasmonate signaling

module and its ligands co-evolved in association with ligand specificity shift from dn-*iso*-OPDA in bryophytes to JA-Ile in vascular plants[34].

It has been suggested that dn-*iso*-OPDA is synthesized via the OPDA isomerizing pathway (Figure 1.6.). Two biosynthetic routes have been proposed for dn-OPDAs, originating from α-LA and hexadecatrienoic acid (HTA). In the HTA-derived pathway, dn-*iso*-OPDA are biosynthesized by LOX, AOS, AOC, and OPDA isomerase. By contrast, in the α-LA-derived pathway, dn-*iso*-OPDA are biosynthesized by these four enzymes coupled with β-oxidation. MpFAD5 (fatty-acid desaturase 5) mainly converts palmitic acid (C16:0) to palmitoleic acid (C16:1) and ultimately contributes to the biosynthesis of HTA (C16:3) through the early stage of the biosynthetic pathway. In *M. polymorpha*, knockout of *fatty-acid-desaturase 5* (*fad5*) abolished the accumulation of HTA, while α-LA levels decreased to 40–50% of wild-type levels but remained detectable[35]. The levels of dn-*iso*-OPDA and dn-*cis*-OPDA were reduced by approximately 95% in the mutants. These data indicated that the HTA-derived pathway is the major route for dn-*iso*-OPDA biosynthesis in *M. polymorpha*, rather than the α-LA-derived pathway.

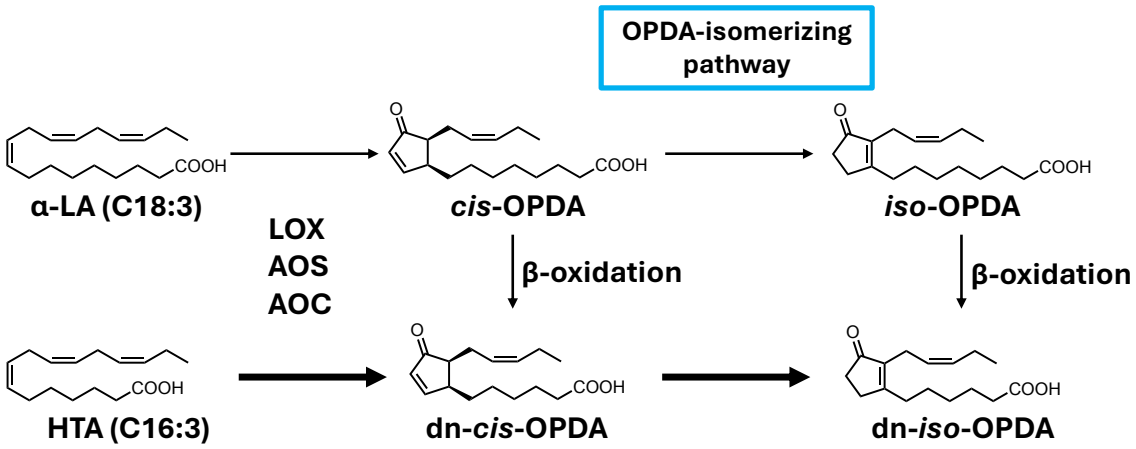

Figure 1.6. Biosynthetic pathway of dn-*iso*-OPDA

1.5. Purpose of this study

The OPDA-isomerizing pathway was proposed only recently, and its biochemical and physiological details remain largely unresolved. Despite increasing interest in this pathway, experimental tools and direct evidence supporting its biological role have been limited. Therefore, the purpose of this study was to advance the understanding of the OPDA-isomerizing pathway through three research projects described in Chapters 2, 3, and 4.

In Chapter 2, a synthetic method for *iso*-OPDA was established, which was applicable to the synthesis of *iso*-OPDA derivatives.

In Chapter 3, the biosynthetic pathway of CJ in plants was investigated using isotope-labeled compounds to evaluate the involvement of the OPDA-isomerizing pathway.

In Chapter 4, stress and phytohormone treatments that induce pyrethrin accumulation in pyrethrum were explored.

2. Establishment of a method for synthesis of *iso*-OPDA

2.1 Introduction

As described above, *iso*-OPDA is a key intermediate in the recently elucidated OPDA isomerizing pathway. However, the chemical synthesis of *iso*-OPDA has only been reported once, in a study by Lauchli *et al*[36]. In the study by Lauchi *et al.*, *iso*-OPDA was synthesized from cyclopentane-1,3-dione, and the method was further adapted for the synthesis of [$^2H_1$-9, $^2H_1$-10]-*iso*-OPDA.

This study aimed to develop a synthetic route to *iso*-OPDA from (±)-MeJA and to apply this method to the synthesis of [$^2H_1$-10, $^2H_2$-11, $^2H_3$-12]-*iso*-OPDA, which contains six deuterium atoms in the pentenyl side chain. The synthetic strategy in this study is composed by three key functional-group transformations. First, the -CH_2-COOMe side chain was extended via a Horner–Wadsworth–Emmons (HWE) reaction. Second, Ru-catalyzed oxidative cleavage of an alkene was combined with a Wittig reaction to enable the incorporation of deuterium into the pentenyl unit. Third, a double bond was introduced into the cyclopentanone ring, and subsequent migration of the double bond.

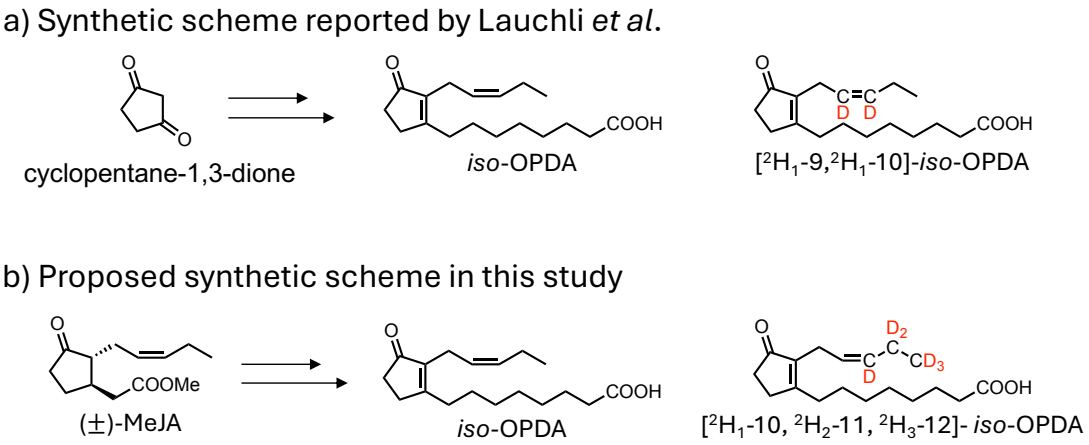

Figure 2.1. Proposed synthetic scheme for *iso*-OPDA synthesis

2.2 Material and Method

・Methyl 2-[3-oxo-2-(2-oxoethyl)cyclopentyl]acetate (**2**)

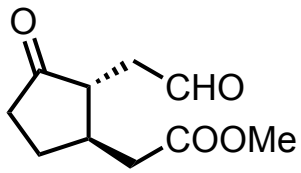

2

To a stirred solution of (±)-MeJA (**1**) (5.0 g, 22 mmol) in 1,2-dichloroethane (53 mL) and water (42 mL) were added a solution of 3.5 M $RuCl_4$ aq. (10 mL) and $NaIO_4$ (14 g, 10 mmol), and the mixture was stirred at room temperature for 1 h. The reaction was quenched by sat. $Na_2S_2O_3$, and the reaction mixture was separated with H_2O and $CHCl_3$. The organic layer was washed with brine and dried over Na_2SO_4. The volatile components of the organic layer were removed under reduced pressure to give an oil, which was subjected to a silica gel column chromatography (EtOAc:*n*-hexane=4:6) to provide **2** (4.0 g, 20 mmol, 91%).

^{1}H-NMR ($CDCl_3$, 270 MHz) δ_H: 9.73 (1H, s), 3.74 (3H, s), 2.94-2.19 (10H, m)

・Methyl 2-{6-[(1,3-dixolan-2-yl)metgyl]-1,4-dioxaspiro[4,4]nonan-7-yl}acetate (**3**)

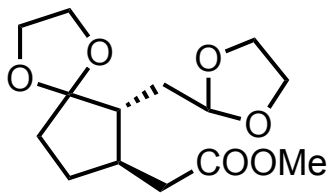

3

To a stirred solution of **2** (8.0 g, 40 mmol) in toluene (200 mL) were added ethylene glycol (15 mL) and PPTS (20 mg, 0.080 mmol), and the mixture was stirred for 16 h at 120 °C under reflux. The water generated as a result of dehydration condensation reaction was removed using Dean-Stark trap. After cooling to room temperature, the reaction mixture was washed with brine and dried with Na_2SO_4. The volatile components of the organic layer were removed under reduced pressure to give an oil, which was subjected to a silica gel column chromatography (EtOAc:*n*-hexane = 1:1) to provide **3** (10 g, 35 mmol, 87%).

^{1}H-NMR ($CDCl_3$, 270 MHz) δ_H: 4.92 (1H, m), 3.97-3.77 (8H, m), 3.64 (3H, s), 2.66 (1H, m), 2.30-1.30 (9H, m).

・2-{6-[(1,3-Dioxolan-3-yl)methyl]-1,4-dioxaspiro[4.4]nonan-7-yl}acetaldehyde (**4**)

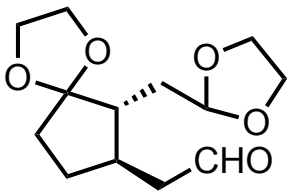

4

To a stirred mixture of **3** (3.3 g, 12 mmol) in CH_2Cl_2 (120 mL) at -78 °C under atmosphere of N_2 was added a solution of 1 M DIBAL-H (14 mL, 14 mmol), and the mixture was stirred for 30 min. MeOH (10 mL) and Saturated Rochelle salt solution (200 mL) were added to the reaction solution, and the reaction solution was stirred until temperature became room temperature. The reaction mixture was extracted with $CHCl_3$, and the volatile components of the organic layer were removed under reduced pressure to give an oil, which was subjected to a silica gel column chromatography (EtOAc) to provide **4** (2.4 g, 9.4 mmol, 82%).

^{1}H-NMR ($CDCl_3$, 270 MHz) δ_H: 9.73 (1H, s), 4.90 (1H, m), 3.96-3.76 (8H, m), 2.78-2.70 (1H, m), 2.41-2.17 (2H, m), 2.01-1.20 (7H, m).

・(*E*)-4-Bromobut-2-en-1-ol (**6**)

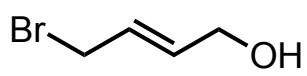

6

To a stirred mixture of methyl 4-bromocrotonate (**5**) (3.0 g, 17 mmol) in CH_2Cl_2 (120 mL) at -78 °C under atmosphere of N_2 was added a solution of 1 M DIBAL-H (43 mL, 43 mmol) and mixture was stirred for 2 h. The reaction mixture was added 50% aqueous acetic acid (5.0 mL, 44 mmol), and the mixture was warmed to room temperature with stirring. After celite filtration, the filtrate was dried over Na_2SO_4. The volatile components of the organic layer were removed under

reduced pressure to give an oil, which was subjected to a silica gel column chromatography (EtOAc *n*-hexane = 3:7) to provide **6** (1.9 g, 13 mmol, 74%).

^{1}H-NMR ($CDCl_3$, 400 MHz) δ_H: 5.93 (2H, m), 4.18 (2H, m), 3,96 (2H, m), 1.53(1H, s)

・(*E*)-4-Bromobut-2-enal (**7**)

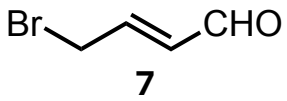

7

To a stirred solution of **6** (3.0 g, 20 mmol) in CH_2Cl_2 (180 mL) was added MnO_2 (50 g, 0.58 mol), and the mixture was stirred for 2 h at room temperature. After celite filtration, the filtrate was evaporated to provide **7** (2,5 g, 17 mmol, 84%).

^{1}H-NMR ($CDCl_3$, 270 MHz) δ_H: 9.59 (1H, m), 6.84 (1H, m), 6.25 (1H, m), 4,09 (2H, m)

・Ethyl (4*E*)-6-bromohexa-2,4-dienoate (**8**)

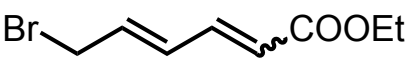

8

To a stirred solution of **7** (2.5 g, 17 mmol) in $CHCl_3$ (50 mL) was added ethyl (triphenylphosphoranylidene)acetate (7.1 g, 21 mmol), and the mixture was stirred for 16 h at room temperature. The volatile components of the organic layer were removed under reduced pressure to give an oil, which was subjected to a silica gel column chromatography (EtOAc:*n*-hexane=2:8) to provide **8** (2.0 g, 9.1 mmol, 54%).

^{1}H-NMR ($CDCl_3$, 270 MHz) δ_H: 9.73 (1H, s), 3.74 (3H, s), 2.94-2.19 (10H, m)

・Ethyl (4*E*)-6-(diethoxyphosphoryl)hexa-2,4-dienoate (**9**)

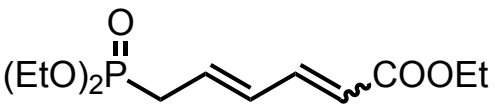

9

Compound **8** (2.5 g, 11 mmol) was dissolved in triethyl phosphite (2.5 ml, 16 mmol), and the mixture was refluxed for 6 h at 120 °C. The

reactionmixture was subjected to a silica gel column chromatography (EtOAc) provided **9** (2.2 g, 8.0 mmol, 86%).

^{1}H-NMR ($CDCl_3$, 270 MHz) δ_H: 7.60-5.40 (4H, m), 4.10 (6H, m), 2.70 (2H, m), 1.25 (9H, m)

・Ethyl (2*E*/*Z*,4*E*,6*E*)-8-((6*R*,7*R*)-6-((1,3-dioxolan-2-yl)methyl)-1,4-dioxaspiro[4.4]nonan-7-yl)octa-2,4,6-trienoate (**10**)

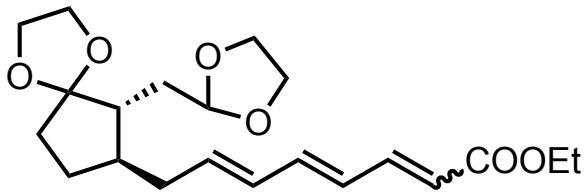

10

To a stirred mixture of **9** (0.88 g, 1.9 mmol) in THF (60 mL) at -78 °C under atmosphere of N_2 was added a solution of 1 M LiHMDS (1.9 mL, 1.9 mmol), and the mixture was stirred for 30 min. To the reaction solution, a solution of **4** (0.48 g, 2.0 mmol) in THF (60 mL) was added, and the reaction solution was stirred for 16 h. The temperature was gradually increased from −78 °C to room temperature. The reaction was quenched by adding a solution of sat. NH_4Cl (30 mL). The reaction mixture was extracted with EtOAc and the volatile components of the organic layer were removed under reduced pressure to give a oil, which was subjected to a silica gel column chromatography (EtOAc:*n*-hexane = 4:6) provided **10** (0.50 mg, 1.3 mmol, 70%).

^{1}H-NMR ($CDCl_3$, 270 MHz) δ_H: 7.31-5.78 (6H, m), 4.92 (1H, m), 4.16 (2H, q, *J*=7.30 Hz), 3.85 (8H, m) 2.15-1.53 (10H, m), 1.25 (3H, t, *J*=7.30 Hz)

・Ethyl 8-((6*R*,7*S*)-6-((1,3-dioxolan-2-yl)methyl)-1,4-dioxaspiro[4.4]nonan-7-yl)octanoate (**11**)

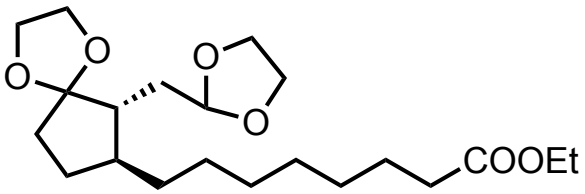

11

To a stirred solution of **10** (0.50 g, 1.3 mmol) in MeOH (3.0 mL) was added Pd/C. Under an atmosphere of H_2, the reaction mixture was stirred for 6 h at room temperature. After filtration through celite, the filtrate was concentrated under reduced pressure to provide compound **11** (0.51 g, 1.3 mmol, *quant.*).

^{1}H-NMR ($CDCl_3$, 270 MHz) δ_H: 4.94 (1H, m), 4.12 (2H, q, *J*=7.3 Hz), 3.88 (8H, m), 2.60 (2H, m), 1.93-1.20 (23H, m)

・Ethyl 8-((1*S*,2*R*)-3-oxo-2-(2-oxoethyl)cyclopentyl)octanoate (**12**)

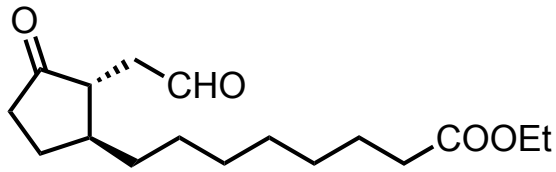

12

To a stirred solution of **11** (0.10 g, 0.26 mmol) in THF (7.5 mL) was added 1 M HCl (7.5 ml), and the reaction mixture was stirred for 18 h at 25 °C. The reaction was quenched by adding a solution of sat. $NaHCO_3$ (50 mL). The reaction mixture was extracted with EtOAc. The organic layer was washed with brine and dried over Na_2SO_4. The volatile components of the organic layer were removed under reduced pressure to give an oil, which was subjected to a silica gel column chromatography (EtOAc:*n*-hexane = 3:7) to provide **12** (66 mg, 0.23 mmol, 85%).

^{1}H-NMR ($CDCl_3$, 270 MHz) δ_H: 9.75 (1H, s), 4.11 (2H, q, *J*=7.3 Hz), 2.69 (2H, m), 2.40-1.19 (23H, m)

・Ethyl OPC-8:0 (**13**)

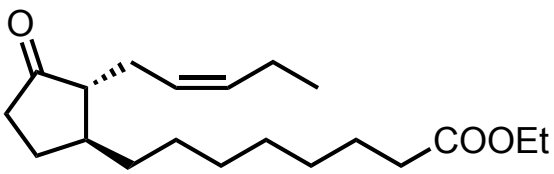

13

To a stirred mixture of propyltriphenylphosphonium iodide ($I^-Ph_3P^+CH_2CH_2CH_3$) (250 mg, 0.82 mmol) in CH_2Cl_2 (25 mL) at -78 °C under atmosphere of N_2 was added a solution of 0.6 M NaHMDS (1.3 ml, 0.82 mmol), and the mixture was stirred for 30 min. To the reaction mixture was added a solution of **12** (124 mg, 0.42 mmol) in CH_2Cl_2 (5 mL) and the reaction solution was stirred for 16 h. The temperature was gradually increased from −78 °C to room temperature. The reaction was quenched by adding a solution of sat. NH_4Cl, and the reaction mixture was extracted with $CHCl_3$. The organic layer was washed with brine and dried over Na_2SO_4. The volatile components of the organic layer were removed under reduced pressure to give an oil, which was subjected to a silica gel column chromatography (EtOAc:*n*-hexane = 1:9) provided **13** (82 mg, 0.25 mmol, 60%).

^{1}H-NMR ($CDCl_3$, 270 MHz) δ_H: 5.40 (1H, m), 5.23 (1H, m), 4.10 (2H, q, *J*=7.3 Hz), 2.32-1.52 (14H, m), 1.40-1.20 (13H, m), 0.94 (3H, t, *J*=7.6 Hz)

・Ethyl *trans*-OPDA (**14**)

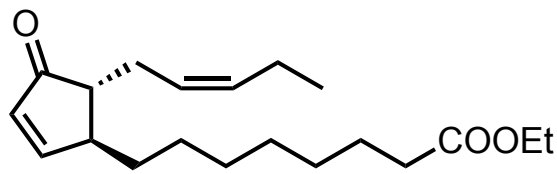

14

To a stirred solution of **13** (63 mg, 0.20 mmol) in *N*,*N*-dimethylformamide (5 mL) under an atmosphere of N_2 at 80°C was added diethyl allyl phosphate (75 μL, 0.40 mmol), Na_2CO_3 (53 mg, 0.48 mmol), and palladium acetate (6.0 mg, 0.030 mmol), and the reaction mixture was stirred for 24 h at the same temperature. After dilution with EtOAc, the

organic layer was washed with a solution of sat. $NaHCO_3$ and brine, and dried over Na_2SO_4. The volatile components of the organic layer were removed under reduced pressure to give an oil, which was subjected to a silica gel column chromatography (EtOAc:*n*-hexane = 2:8) to provide **14** (47 mg, 0.15 mmol, 75%). ^{1}H-NMR ($CDCl_3$, 270 MHz) δ_H: 7.57 (1H, dd, *J*=5.4, 2.3 Hz), 6.09 (1H, dd, *J*=5.4, 1.8 Hz), 4.10 (2H, *J*=4.3 Hz), 2.55 (1H, m), 2.42 (1H, m), 2.26 (3H, m), 2.01 (3H, m), 1.60-1.20 (15H, m), 0.93 (3H, t, *J*= 7.6 Hz)

・Methyl *iso*-OPDA (**15**)

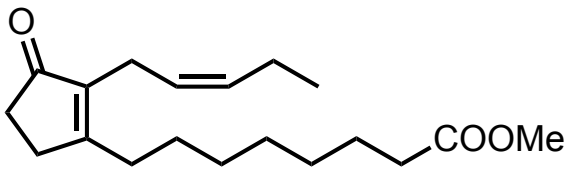

15

Under an atmosphere of N_2, to a stirred solution of **14** (58 mg, 0.19 mmol) in MeOH (5 mL) was added a solution of CH_3ONa (30 mg, 0.57 mmol) in MeOH (5 mL), and the reaction mixture was stirred for 72 h at 80 °C. The reaction was quenched by a solution of sat. NH_4Cl. After dilution with EtOAc, the organic layer was washed with brine, and dried with Na_2SO_4. The volatile components of the organic layer were removed under reduced pressure to give an oil, which was subjected to a silica gel column chromatography (EtOAc:*n*-hexane = 2:8) to provide **15** (40 mg, 0.13 mmol, 70%).

^{1}H-NMR ($CDCl_3$, 270 MHz) δ_H: 7.57 (1H, dd, *J*=5.4, 2.3 Hz), 6.09 (1H, dd, *J*=5.4, 1.8 Hz), 4.10 (2H, *J*=4.3 Hz), 2.55 (1H, m), 2.42 (1H, m), 2.26 (3H, m), 2.01 (3H, m), 1.60-1.20 (15H, m), 0.93 (3H, t, *J*= 7.6 Hz)

・*iso*-OPDA (**16**)

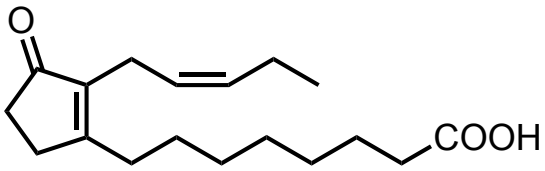

***iso*-OPDA (16)**

To a stirred solution of **15** (24 mg, 0.08 mmol) in 100 mM phosphate buffer pH 8.0 (8 mL) and MeOH (1.5 mL) was added esterase from porcine liver (5 mg, Sigma), and the reaction mixture was stirred for 5 d at room temperature. After dilution with EtOAc (100 ml), the organic layer was washed with 1 M HCl and brine, and dried over Na_2SO_4. The volatile components of the organic layer were removed under reduced pressure to provide *iso*-OPDA (18 mg, 80%).

^{1}H-NMR ($CDCl_3$, 500 MHz; Appendix Chart 1) δ_H: 5.34 (1H, m), 5.19 (1H, m), 2.91 (2H, d, *J*=7.3 Hz), 2.47 (2H, m), 2.40 (2H, m), 2.37-2.28 (4H, m), 2.13 (2H, m), 1.62 (2H, m), 1.50 (2H, m), 1.39-1.27 (6H, m), 0.97 (3H, t, *J*=7.5 Hz).

^{13}C-NMR ($CDCl_3$, 125 MHz; Appendix Chart 2) δ_C: 209.6, 179.1, 174.4, 139.2, 132.2, 125.3, 34.2, 33.9, 31.3, 29.5, 29.2, 29.0, 28.9, 27.3, 24.6, 21.2, 20.6, 14.1.

HMBC (Appendix Chart 3).

HSQC (Appendix Chart 4).

^{1}H-^{1}H COSY (Appendix Chart 5).

HR-FD-MS (Appendix Chart 6): $[M+H]^+$ calcd. for $^{12}C_{18}{}^1H_{29}{}^{16}O_3$: *m*/*z* 293.21167, found: *m*/*z* 293.21072.

2.3. Result

An overview of the *iso*-OPDA synthetic route proposed in this work are shown in Schemes 2.1, 2 and 3. As shown in Scheme 2.1, aldehyde **4** was synthesized from (±)-MeJA (**1**) to provide the required substrate for the HWE reaction. Ru-catalyzed oxidative cleavage of (±)-MeJA (**1**) afforded aldehyde **2**. The ketone and aldehyde moieties of **2** were protected as acetals using ethylene glycol, affording compound **3**. Reduction of ester **3** with DIBAL subsequently afforded aldehyde **4**, which was used as the substrate for the subsequent HWE reaction.

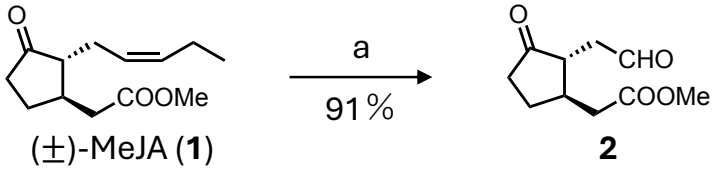

(±)-MeJA (**1**) **2**

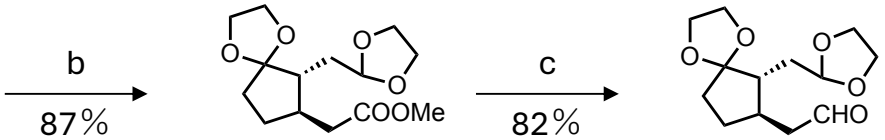

3 **4**

Scheme 2.1. Synthesis of Aldehyde 4

(a) $RuCl_3$ aq, $NaIO_4$, 1,2-dichloroethane/H_2O, rt, 1 h

(b) Ethylene glycol, PPTS, toluene, reflux, 16 h

(c) DIBAL-H, CH_2Cl_2, -78 °C, 30 min

In Scheme 2.2, the HWE salt was prepared. In general, HWE reaction between an alkyl phosphonate and aldehyde or ketone provides *E*-selective carbon–carbon double bonds when stabilized phosphonates are used. In this study, an HWE phosphonate containing an additional alkene moiety was employed to improve the efficiency of side-chain elongation. The newly generated double bond in the product forms conjugates with the pre-existing alkene, thereby increasing the thermodynamic stability of the product. This thermodynamic

advantage is considered to promote the six-carbon side-chain elongation reaction. Ester **5** was reduced with DIBAL to afford alcohol **6**. The resulting alcohol was then oxidized with manganese dioxide to give aldehyde **7**. Condensation of aldehyde **7** with the acetate ylide (Ph_3P=CHCOOEt) yielded ester **8** as an *E*/*Z* mixture. Finally, treatment of **8** with triethyl phosphite under reflux conditions afforded the HWE salt **9**.

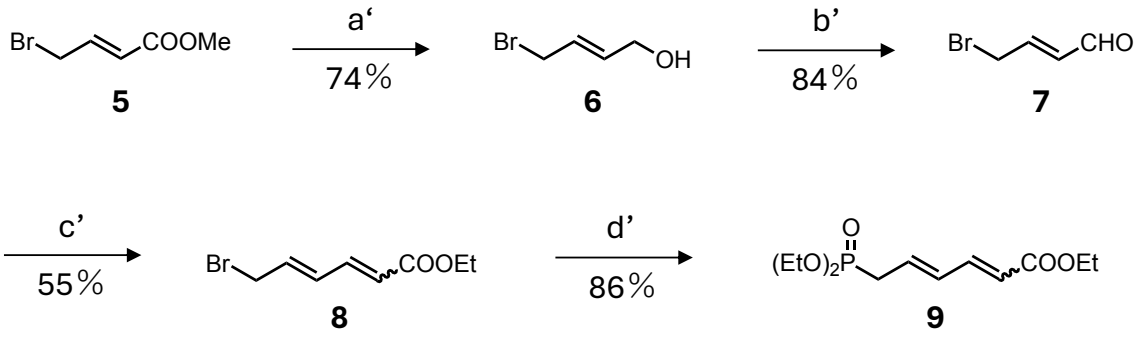

Scheme 2.2. Synthesis of HWE salt 9

(a’) DIBAL-H, CH_2Cl_2, -78 °C, 4 h

(b’) MnO_2, CH_2Cl_2, rt., 4 h

(c’) Ph_3P=CHCOOMe, toluene, 90 °C, 3 h

(d’) Triethyl phosphite, reflux, 3 h

In Scheme 2.3, *iso*-OPDA was synthesized by following series of reactions, side-chain elongation via the HWE reaction, formation of the pentenyl side chain by the Witting reaction, introduction of a double bond into the cyclopentanone ring, and subsequent migration of the double bond to afford *iso*-OPDA (**16**). Aldehyde **4** was firstly subjected to a HWE reaction with HWE salt **9** using LiHMDS to afford compound **10**. Hydrogenation of **10** using Pd/C provided compound **11**, which was then deprotected under acidic conditions to give aldehyde **12**. Aldehyde **12** was subjected to Wittig reaction with the phosphonium ylide derived from triphenyl(propyl)phosphonium iodide ($I^-Ph_3P^+CH_2CH_2CH_3$) to yield ethyl OPC 8 (**13**). Oxidation of OPC 8 (**13**) catalyzed by palladium (II) acetate afforded ethyl *trans*-

OPDA (**14**). Under basic conditions, keto–enol tautomerization of ethyl *trans*-OPDA (**14**) promoted, and conjugative stabilization drived migration of the C10-C11 double bond to the C9-C13 position, yielding methyl *iso*-OPDA (**15**). Methyl *iso*-OPDA (**15**) was hydrolyzed by esterase from porcine liver to yield *iso*-OPDA (**16**).

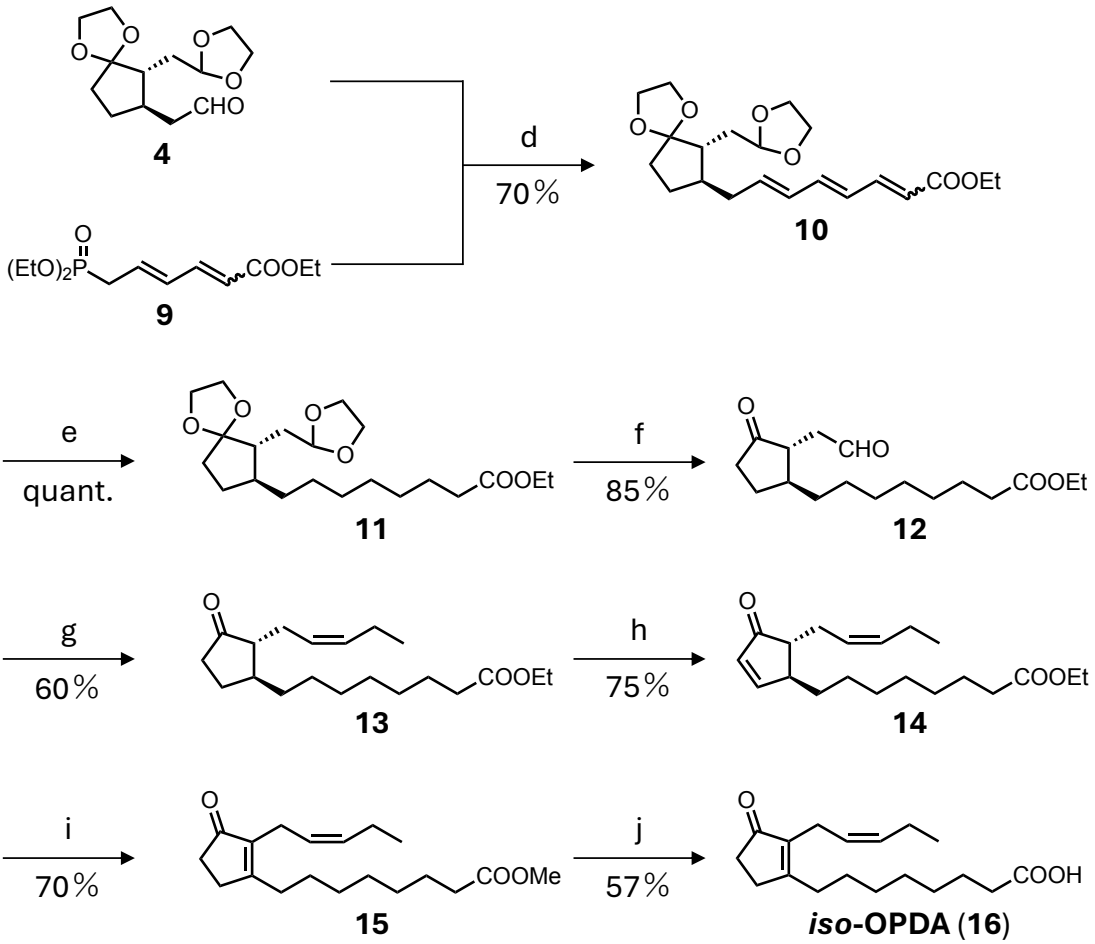

Scheme 2.3. Synthesis of *iso*-OPDA

(d) LiHMDS, THF, -78 °C→0 °C, 16 h

(e) H_2, Pd/C, MeOH, rt, 6 h

(f) HCl aq., THF, 35 °C, 16 h

(g) $I^-Ph_3P^+CH_2CH_2CH_3$, NaHMDS, CH_2Cl_2, -78 °C→0 °C, 16 h

(h) Palladium (Ⅱ) acetate, diethylallyl phosphate, Na_2CO_3, DMF, 80 °C, 24 h

(i) CH_3ONa, MeOH, 60 °C, 24 h

(j) Esterase from porcine liver, MeOH, phosphate buffer (pH 8.0), rt, 3 days

2.4. Conclusion

In this study, *iso*-OPDA was synthesized from (±)-MeJA in 10 steps with an overall yield of 6.9%. By replacing the triphenyl(propyl)phosphonium iodide ($I^-Ph_3P^+CH_2CH_2CH_3$) used in the reaction into its deuterated analogue, triphenyl(propyl-d7)phosphonium iodide ($I^-Ph_3P^+CD_2CD_2CD_3$), *iso*-OPDA-d6 would be synthesized instead of *iso*-OPDA. Furthermore, hydrolysis of ethyl OPC-8:0 (**13**) and ethyl *trans*-OPDA (**14**) affords OPC-8:0 and *trans*-OPDA, respectively. This strategy enables the systematic synthesis of OPC-8:0-d6, *trans*-OPDA-d6, and *iso*-OPDA-d6 from a single synthetic route.

Furthermore, replacing the C6 HWE salt with the corresponding C4 HWE salt would also enable the synthesis of dn-*iso*-OPDA and dn-*iso*-OPDA-d6.

3. Investigation of *cis*-jasmone biosynthetic pathway in plants

3.1. Introduction

As mentioned before, the biosynthesis of CJ has been proposed to proceed via two distinct pathways, the OPDA-reducing pathway and the isomerizing pathway, and remains to be controversial. This study explored plants accumulating large amount of CJ and investigated its biosynthetic pathways. In order to achieve the objective, the biosynthetic relationships among (+)-7-*iso*-JA, 4,5-ddh-JA, and 3,7-ddh-JA, which represent downstream branching points of the pathways, were examined.

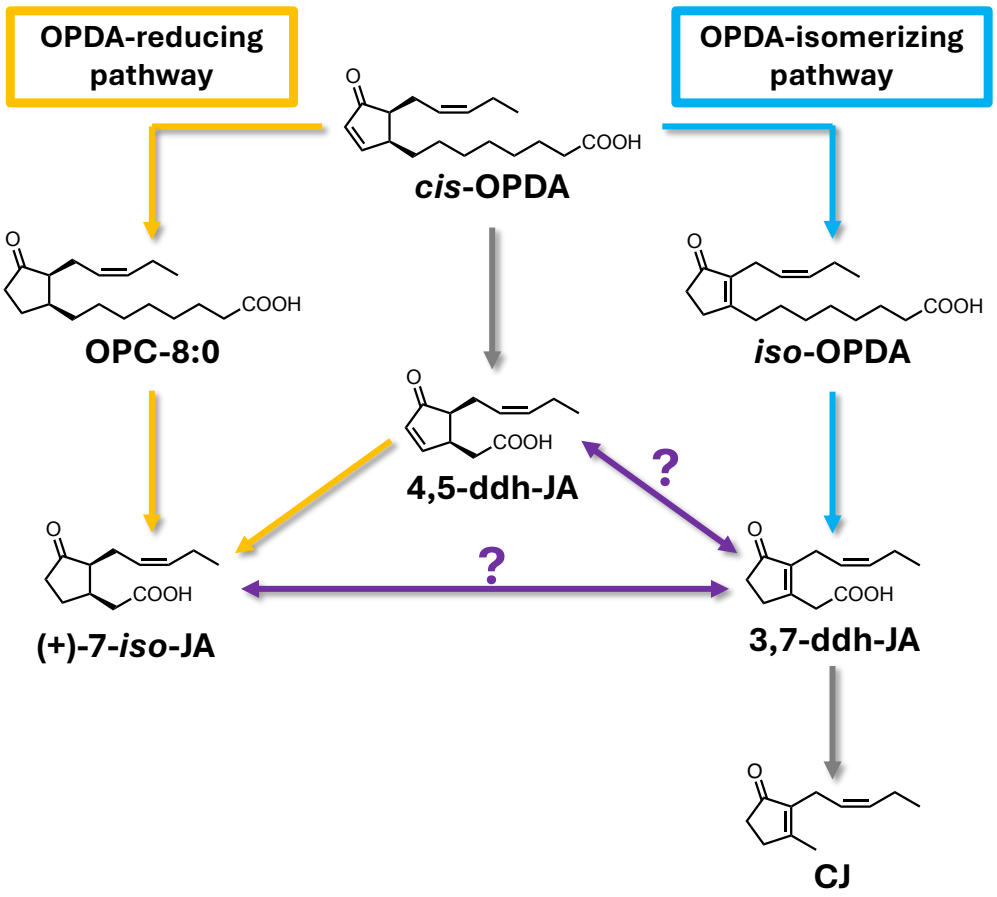

Figure 3.1. Proposed biosynthtic pathway of CJ

3.2. Material and Method

General experimental procedures: NMR spectra were recorded using a JNM-ECZ400 FT-NMR spectrometer (JEOL; 400 MHz for ^{1}H-NMR and 100 MHz for ^{13}C-NMR) and JNM-EX270 FT-NMR spectrometer (JEOL; 270 MHz for ^{1}H-NMR). FD-MS spectra were recorded using a JMS-T100GCV (JEOL). GC-MS analyses were performed on Varian CP-3800 gas chromatograph coupled to a Varian 1200 L quadrupole MS/MS (Varian).

GC–MS conditions: The injection temperature was set at 250 °C. Separation was achieved using a fused-silica capillary column (TC-5; 30 m × 0.25 mm i.d., 0.25 μm film thickness; GL Sciences). The oven temperature was initially held at 40 °C for 1 min, then ramped at 22 °C/min to 290 °C, which was maintained for 20 min. Helium was used as the carrier gas at a linear velocity of 1.2 mL/min. All spectra were acquired in the *m*/*z* range of 10–520, and collision-induced dissociation was performed at a collision energy of 170 eV.

Plant material and growth condition: Seeds were planted into a Jiffy-7 (ϕ 42 mm) pot, which had absorbed 20 mL of water, and seedlings were grown in the growth chamber. The temperature and moisture of the chamber were set at 23 °C and 60%, respectively, and the conditions of day length were light for 14 h and dark for 10 h.

Screening for the plants that produce CJ: Approximately 1 g of the plant was frozen, crushed, and extracted with ethyl acetate. The extract was filtered and concentrated at approximately 20 °C using a rotary evaporator to yield an oil. The resulting oil was redissolved with EtOAc (200 μL). The volatile components of the solution were reduced under reduced pressure, and the resultant oil was dissolved in EtOAc (200 μL). A portion of

the solution was subjected to GC-MS analysis. In the quantitative analysis of CJ in Lamiaceae plants, CJ-d7 (10 μg) was added to the EtOAc solution. For evaluation of the endogenous amount, area ratios of the ions of *m/z* 164 and 171 were used to determine the amounts.

Feeding experiments of airborne deuterium-labeled compounds: Plants grown for 6 weeks under long-day conditions and filter paper soaked with the compound to 1 mg/L (relative to the volume of the container) were placed in a transparent, semi-closed container and left under long-day conditions for one week, referring to the reports by Tamogami *et al*., Oki *et al*., and Rishni *et al.*[37-39]. After 1 week, the plants were frozen, crushed, and extracted with EtOAc. The extract was filtered and concentrated to yield an oil. The resulting oil was redissolved with EtOAc and successfully treated with CH_2N_2 to convert the carboxylic acid moiety to methyl ester. A portion of the solution was subjected to GC-MS analysis.

Synthesis of (±)-MeJA-d6 (19), (±)-4,5-ddh-MeJA-d6 (20) and 3,7-ddh-MeJA-d6 (21):

・Triphenyl([$^2H_2$-1, $^2H_2$-2, $^2H_3$-3]-propyl) phosphonium iodide (**18**)

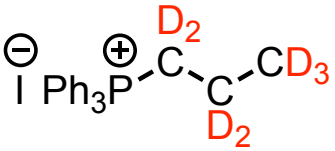

18

To a stirred solution of [$^2H_2$-1, $^2H_2$-2, $^2H_3$-3]-1-iodepropane (**17**) (5.0 g, 28 mmol) in 100 mL of CH_3CN was added triphenyl phosphine (11 g, 42 mmol) and, the mixture was refluxed for 16 h. The volatile components were removed under reduced pressure, and the resulting material was dissolved in a small amount of $CHCl_3$. The precipitate formed by adding *n*-hexane to this solution was collected by suction filtration to afford **18** (19.0 g, 79%).

・[$^{2}H_3$-12, $^{2}H_2$-11, $^{2}H_1$-10]-(±)-MeJA (MeJA-d6, **19**)

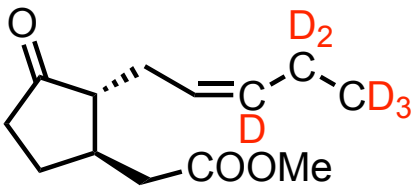

MeJA-d6 (**19**)

To a stirred mixture of **18** (1.5 g, 3.5 mmol) in CH_2Cl_2 (100 mL) at -78 °C under atmosphere of N_2 was added a solution of 0.6 M NaHMDS (5.9 ml, 3.5 mmol). To the reaction mixture was added a solution of **2** (0.65 g, 13.3 mmol) in CH_2Cl_2 (10 ml), and the reaction solution was stirred for 16 h. The temperature was gradually increased from -78 °C to room temperature. The reaction was quenched by adding sat. NH_4Cl, and the reaction mixture was extracted with $CHCl_3$. The organic layer was washed with brine and dried over Na_2SO_4. The volatile components of the organic layer were removed under reduced pressure to give an oil, which was subjected to a silica gel column chromatography (EtOAc:*n*-hexane = 2:8) to provide (±)-MeJA-d6 (0.47 g, 2.0 mmol, 60%).

^{1}H-NMR ($CDCl_3$, 400 MHz; Appendix Chart 7) δ_H: 5.24 (1H, m), 3.68 (3H, s), 2.70 (1H, m), 2.40-1.40 (9H, m).

^{13}C-NMR ($CDCl_3$, 100 MHz; Appendix Chart 8) δ_C: 209.1, 172.6, 124.8, 54.0, 51.7, 38.8, 38.0, 37.8, 27.3, 25.5.

HR-FD-MS (Appendix Chart 9): *m*/*z* $[M]^+$ calcd. for $^{12}C_{13}{}^{1}H_{14}{}^{2}H_6{}^{16}O_3$: 230.17890. Found: 230.17812.

・[$^{2}H_3$-12, $^{2}H_2$-11, $^{2}H_1$-10]-(±)-4,5-didehydroMeJA (4,5-ddh-MeJA-d6, **20**)

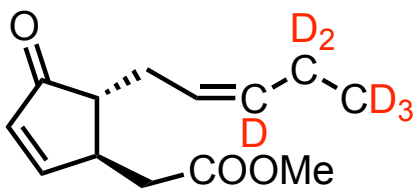

4,5-ddh-MeJA-d6 (**20**)

To a stirred solution of **19** (0.47 g, 2.0 mmol) in *N*,*N*-dimethylformamide (40 mL) under an atmosphere of N_2 at 80°C was added diethyl allyl phosphate (0.71 mL, 4.0 mmol), Na_2CO_3 (0.51 g, 4.8

mmol) and palladium(II) acetate (55 mg, 0.24 mmol), and the reaction mixture was stirred for 48 h at 80 °C. After dilution with EtOAc, the organic layer was washed with sat. $NaHCO_3$ and brine and dried with Na_2SO_4. The volatile components of the organic layer were removed under reduced pressure to give an oil, which was subjected to a silica gel column chromatography (EtOAc:*n*-hexane = 3:7) to provide 4,5-ddh-MeJA-d6 (0.18 g, 0.77 mmol, 38%).

^{1}H-NMR ($CDCl_3$, 400 MHz; Appendix Chart 10) δ_H: 7.61 (1H, dd, J=5.6, 2.4 Hz), 6.16 (1H, dd, *J*=5.6, 2.0 Hz), 5.24 (1H, m), 3.68 (3H, s), 2.99 (1H, m), 2.62-2.40 (3H, m), 2,29 (1H, m), 2.07(1H, m).

^{13}C-NMR ($CDCl_3$, 100 MHz; Appendix Chart 11) δ_C: 210.3, 171.9, 165.4, 133.9, 124.4, 51.9, 51.1, 43.3, 38.2, 27.7.

HR-FD-MS (Appendix Chart 12): $[M]^+$ calcd. for $^{12}C_{13}{}^1H_{12}{}^2H_6{}^{16}O_3$: *m*/*z*. 228.16325, found: *m*/*z* 228.16274.

・[$^2H_3$-12, $^2H_2$-11, $^2H_1$-10]-3,7-didehydroMeJA (3,7-ddh-MeJA-d6, **21**)

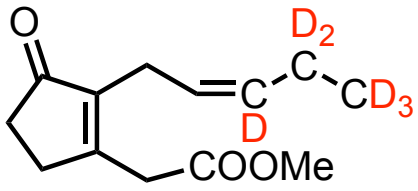

3,7-ddh-MeJA-d6 (**21**)

To a stirred solution of **20** (93 mg, 0.41 mmol) in MeOH (15 mL) under an atmosphere of N_2 was added a solution of CH_3ONa (54 mg, 1.0 mmol) in dry MeOH (15 mL), and the reaction mixture was stirred for 6 h at 80 °C. The reaction was quenched by a solution of sat. NH_4Cl. After dilution with EtOAc, the organic layer was washed with brine and dried with Na_2SO_4. The volatile components of the organic layer were removed under reduced pressure to give an oil, which was subjected to a silica gel column chromatography (EtOAc:*n*-hexane = 3:7) to provide 3,7-ddh-MeJA-d6 (55 mg, 0.24 mmol, 59%).

^{1}H-NMR ($CDCl_3$, 400 MHz; Appendix Chart 13) δ_H: 5.18 (1H, m), 3.70 (3H, s), 3.45 (2H, s), 2.95 (2H, m), 2.60 (2H, m), 2.40 (2H, m).

^{13}C-NMR ($CDCl_3$, 100 MHz; Appendix Chart 14) δ_C: 208.7, 169.6, 164.1, 141.9, 124.3, 52.4, 36.7, 34.3, 30.0, 21.3.

HR-FD-MS (Appendix Chart 15): $[M]^+$ calcd. for $^{12}C_{13}{}^{1}H_{12}{}^{2}H_6{}^{16}O_3$: *m*/*z* 228.16325, found: *m*/*z* 228.16355.

3.3. Result

3.3.1 Synthesis of the deuterium labeled compounds

In this study, a few kinds of deuterium-labeled compounds were synthesized to evaluate the biosynthetic relationships between the OPDA-reducing and -isomerizing pathways. [$^2H_3$-12, $^2H_2$-11, $^2H_1$-10]-(±)-MeJA (MeJA-d6, **19**), [$^2H_3$-12, $^2H_2$-11, $^2H_1$-10]-(±)-4,5-didehydroMeJA (4,5-ddh-MeJA-d6, **20**), [$^2H_3$-12, $^2H_2$-11, $^2H_1$-10]-3,7-ddh-MeJA (3,7-didehydroMeJA-d6, **21**) were synthesized basically according to the synthetic method giving *iso*-OPDA described in chapter 2. Initially, the pentenyl side chain of MeJA (**1**) was oxidatively cleaved using ruthenium oxidation to yield the corresponding aldehyde (**2**), which was reacted with phosphonium ylide derived from phosphonium salt (**18**) generated using NaHMDS in THF to yield MeJA-d6 (**19**). The α,β-dehydrogenation of MeJA-d6 (**19**) was accomplished using palladium (II) acetate and sodium carbonate, affording 4,5-ddh-MeJA-d6 (**20**). Under basic conditions, keto-enol tautomerization of 4,5-ddh-MeJA-d6 (**20**) promoted, and conjugative stabilization drived migration of the C4-C5 double bond to the C3-C7 position, yielding 3,7-ddh-MeJA-d6 (**21**).

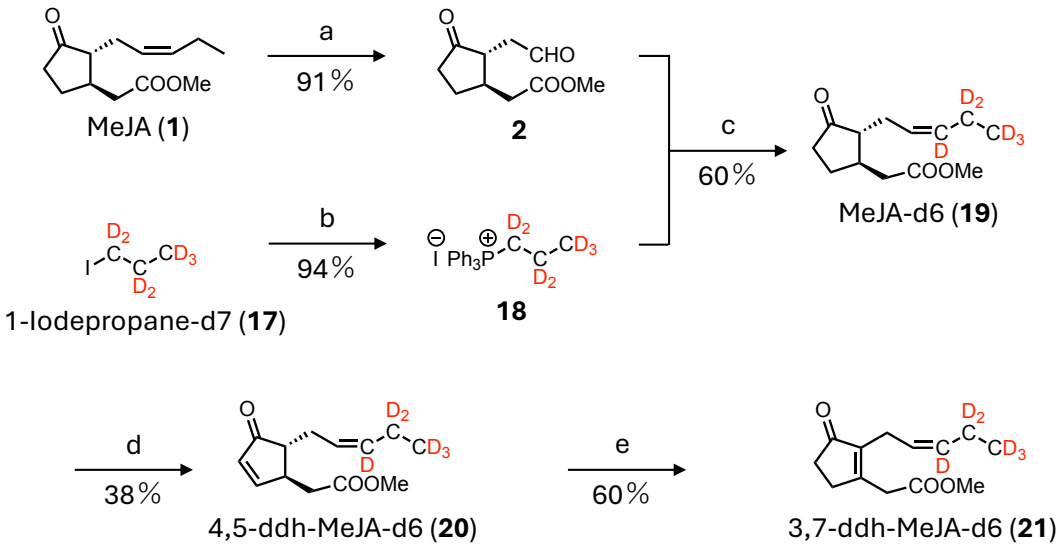

Scheme 3.1. Synthesized deuterium-labeled compounds.

(**a**) $RuCl_3$ aq, $NaIO_4$, 1,2-dichloroethane/H_2O, rt, 1 h, 91%.

(**b**) Ph_3P, CH_3CN, reflux, 16 h, 94%.

(**c**) NaHMDS, CH_2Cl_2,-78 °C→rt, 16 h, 60%.

(**d**) Palladium (II) acetate, diethylallyl phosphate, Na_2CO_3, DMF, 80 °C, 24 h, 38%.

(**e**) CH_3ONa, MeOH, 60 °C, 12 h, 60%.

3.3.2 Screening of plants with high endogenous levels of CJ

CJ is biosynthesized in flowers in many cases, and its production has been reported in a variety of plants, including Honeysuckle (*Lonicera japonica*)[40] and Jasmine (*Jasminum sambac*)[41]. To clarify the relationship between the OPDA-reducing and OPDA-isomerizing pathways for leading CJ, plants having ability to accumulate large amount of CJ were firstly screened by GC-MS analysis after only a single extraction step using EtOAc (Table 3.1). Eleven kinds of plants were examined, and the results are given in Table 3.1.a CJ was detected in the flower part of *L. japonica* and in the leaves and flowers of *Mentha longifolia* (Table 3.1.a). When flowers were used as experimental material, it was thought that it would take a long time to grow for harvesting the flowers. Thus, it was thought that leaves would be more suitable for experiments than flowers, since leaves are not seasonal and the materials can be obtained without waiting for the long time required for growth. Thus, we further analyzed the leaf parts of several Lamiaceae plants (Table 3.1.b), and in this experiment, CJ-d6 was added as an internal standard to strictly evaluate endogenous amount of CJ in the leaves. CJ was detected in *M. longifolia*, *M. suaveolens*, and *M. spicata*, and endogenous amounts of CJ were determined as 32.6, 46.5, and 0.76 μg/g fresh weight, respectively, which revealed that *M. suaveolens* was the highest producer of CJ (Table 1b).

Table 3.1. Screening of plants with the abilitiy to produce CJ.

a)

Plant species	Organ	Production of CJ
Jasminum sambac	flower	n.d.
Nicotiana attenuata	flower	n.d.
Rudbeckia laciniata	flower	n.d.
Linaria vulgaris	flower	n.d.
Allium tuberosum	flower	n.d.
Rosa canina	flower	n.d.
Impatiens textori	flower	n.d.
Tanaxacum officinale	flower	n.d.
Allium caeruleum	flower	n.d.
Lonicera japonica	flower	○
Mentha longifolia	flower, leaf	○

(n.d.; not detected)

b)

Plant Species	CJ (*μ*g/g FW)
Mentha longifolia	32.63 ± 4.15
Mentha suaveolens	46.50 ± 10.12
Mentha spicata	0.76 ± 0.08
Thymus vulgaris	n.d.
Origanum vulgare	n.d.
Salvia officinalis	n.d.
Salvia rosmarinus	0.89 ± 0.04
Ocimum basilicum	n.d.
Lavandula angustifolia	n.d.
Perilla frutescens	n.d.

(n.d.; not detected)

(**a**) Plant species analyzed in this study..

(**b**) Lamiaceae species analyzed in this study.

3.2.3 Feeding experiments with deuterium labeled compounds

Since it was demonstrated that MeJA was able to be applied by air propagation, the synthesized compounds, MeJA-d6 (**19**), 4,5-ddh-MeJA-d6 (**20**) and 3,7-ddh-MeJA-d6 (**21**) were applied to *M. suaveolens* via airborne propagation as described in the reported method[37-39]. After the treatments of the deuterium labeled compounds by air propagation, the aerial parts of the plants were subjected to GC-MS analysis. The results of the feeding experiments using 3,7-ddh-MeJA-d6 (**21**) are shown in Figure 3.2. In case of feeding 3,7-ddh-MeJA-d6 (**21**) via airborne propagation to the plants, a peak indicating almost the same retention time (14.8 min, Figure 3.2.b) as that of authentic CJ (Figure 3.2.d) was detected in the GC chromatogram, although there was no peak with an identical retention time (Figure 3.2.c) to that of authentic MeJA (18.2 min, Figure 3.2.d). The MS/MS cleavage patterns for the peaks with retention times of 14.8 min in Figures 3.2.b and 3.2.d are analyzed in Figure 3.3. In Figure 3.3.a, the MS/MS cleavage pattern for authentic CJ is shown, in which *m/z* 164 was determined as the molecular ion, *m/z* 149 as the ion derived from the methyl group leaving ion from the parent ion and *m/z* 135 as the ethyl group missing ion from the parent ion. In Figure 3.3.b, the MS/MS cleavage pattern is given for the peak assumed to be [$^{2}H_{3}$-11, $^{2}H_{2}$-10, $^{2}H_{1}$-9]-CJ (CJ-d6), whose peak appeared at 14.8 min. The ion with *m*/*z* 170 was determined to be the molecular ion of CJ-d6, *m*/*z* 155 was determined to be the ion derived from the methyl group leaving ion between the C-1 and C-2 carbons, *m*/*z* 152 was determined to be the ion derived from the -CD_3 moiety leaving ion between C-10 and C-11, and *m*/*z* 136 determined to be the ion derived from the -CD_2CD_3 moiety leaving ion between C-9 and C-10 carbons. The MS/MS pattern strongly supported that the compound examined for analysis in Figure 3.3.b was CJ-d6. Based on the obtained results, it was revealed that air-propagated 3,7-ddh-MeJA-d6 (**21**) was metabolized into CJ-

d6 in the treated plants but not into MeJA-d6.

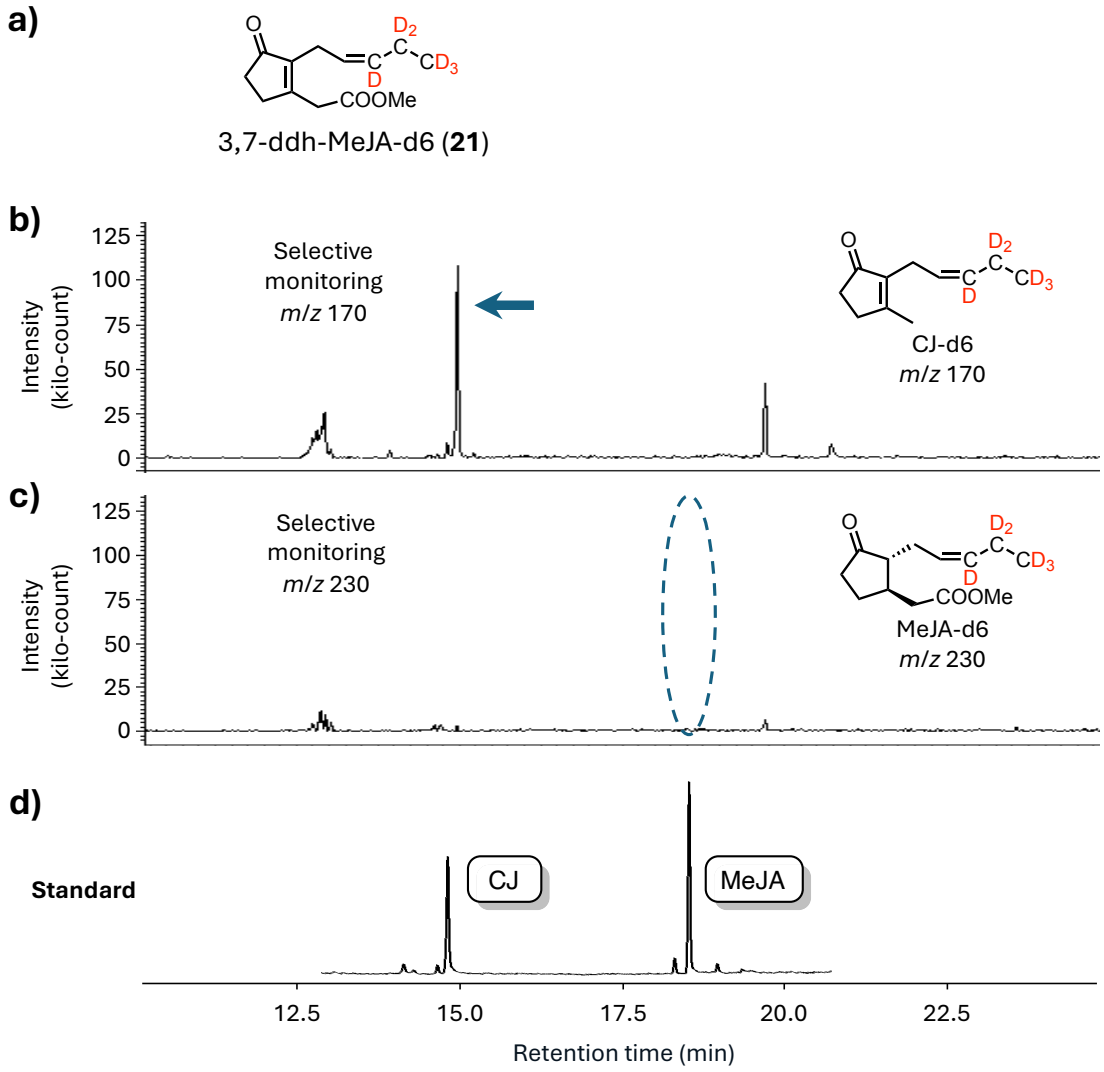

Figure 3.2. **Feeding experiment using deuterium-labeled 3,7-ddh-MeJA.**

(**a**) Chemical structure of 3,7-ddh-MeJA-d6 (**21**).

(**b**) Representative GC–MS chromatogram for detecting CJ-d6 using selected ion monitoring at *m/z* 170.

(**c**) Representative GC–MS chromatogram for measuring MeJA-d6 using selected ion monitoring at *m/z* 230.

(**d**) Representative GC–MS chromatogram for measuring authentic CJ and MeJA using total ion counting mode.

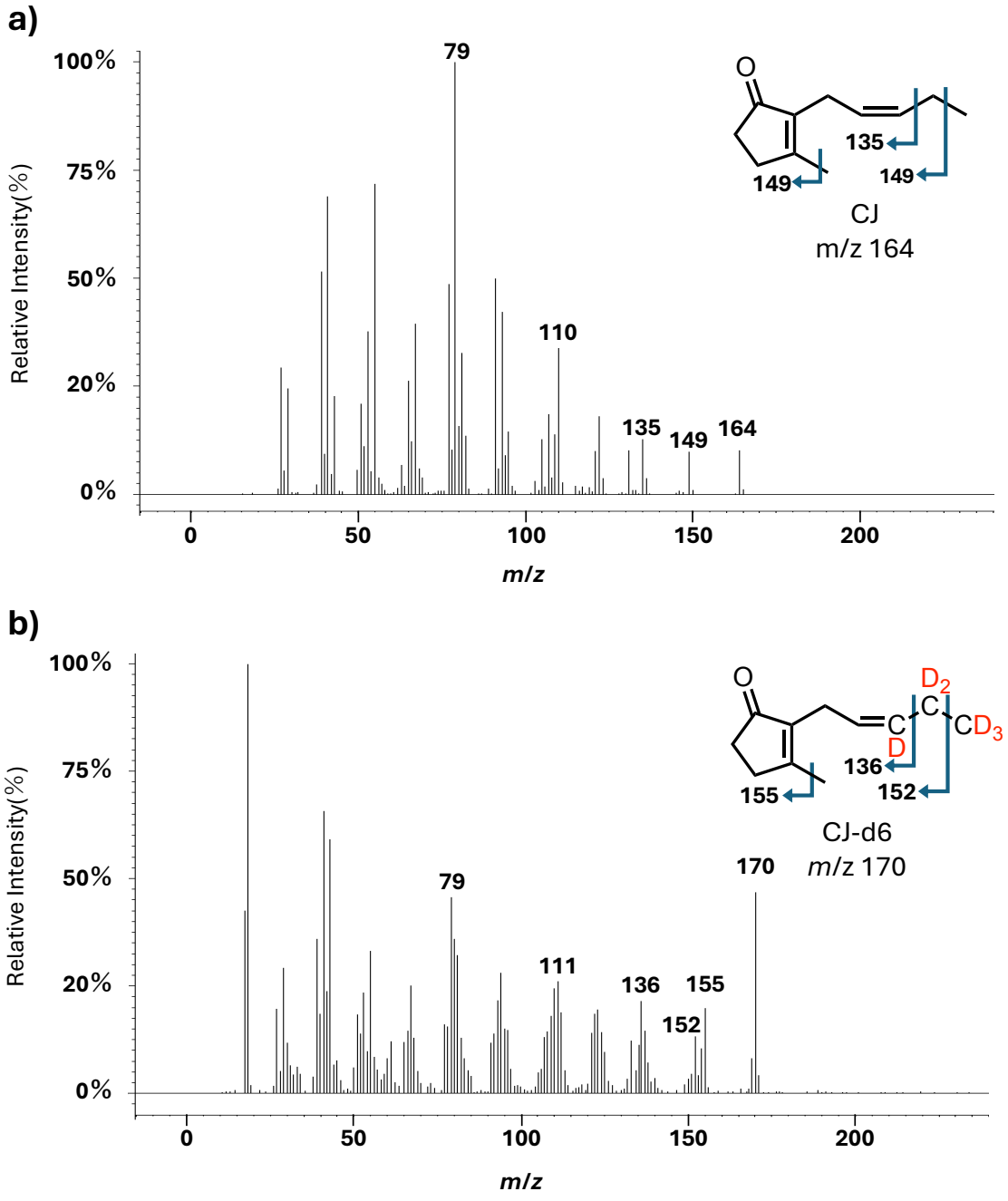

Figure 3.3. Comparison of mass spectra between authentic CJ and deuterium-labeled CJ detected in 3,7-ddh-MeJA-d6 (21) treatment.

(a) Mass spectrum of authentic CJ.

(b) Mass spectrum of labeled CJ detected in plants treated with 3,7-ddh-MeJA-d6 (**21**).

In the case of feeding 4,5-ddh-MeJA-d6 (**20**) via air propagation to the plants (Figure 3.4), a peak having almost the same retention time (18.2 min, Figure 3.4.c) as that of authentic MeJA (Figure 3.4.d) was detected in the GC chromatogram, although here was no peak with an almost identical retention time (Figure 3.4.b) to that of authentic CJ (14.8 min, Figure 3.4.b). The MS/MS cleavage patterns for the peaks in figure 3.5.a and 3.5.b with a retention time of 18.2 min are analyzed in Figure 3.4. In Figure 3.5.a, the MS/MS cleavage pattern for authentic MeJA is shown, in which *m*/*z* 224 was determined as the molecular ion, *m*/*z* 193 as the ion derived from the methyl group leaving ion from the parent ion and *m*/*z* 151 as the -CH_2-$COOCH_3$ moiety missing the ion from the parent ion. The ion with *m*/*z* 230 was determined to be the molecular ion of MeJA-d6, *m*/*z* 199 was determined to be the ion derived from the methyl group leaving ion from the C-1 carbon, *m*/*z* 157 was determined to be the ion derived from the -CH_2-$COOCH_3$ moiety leaving ion. The features of Figures 3.5.a and 3.5.b coincided well except for some peaks having deuterium atom(s), such as *m/z* 230, 199, 157, and 84. Matsui *et al.* reported the GC–MS pattern of MeJA-d6, and it coincided well with that in Figure 3.5.b[42].

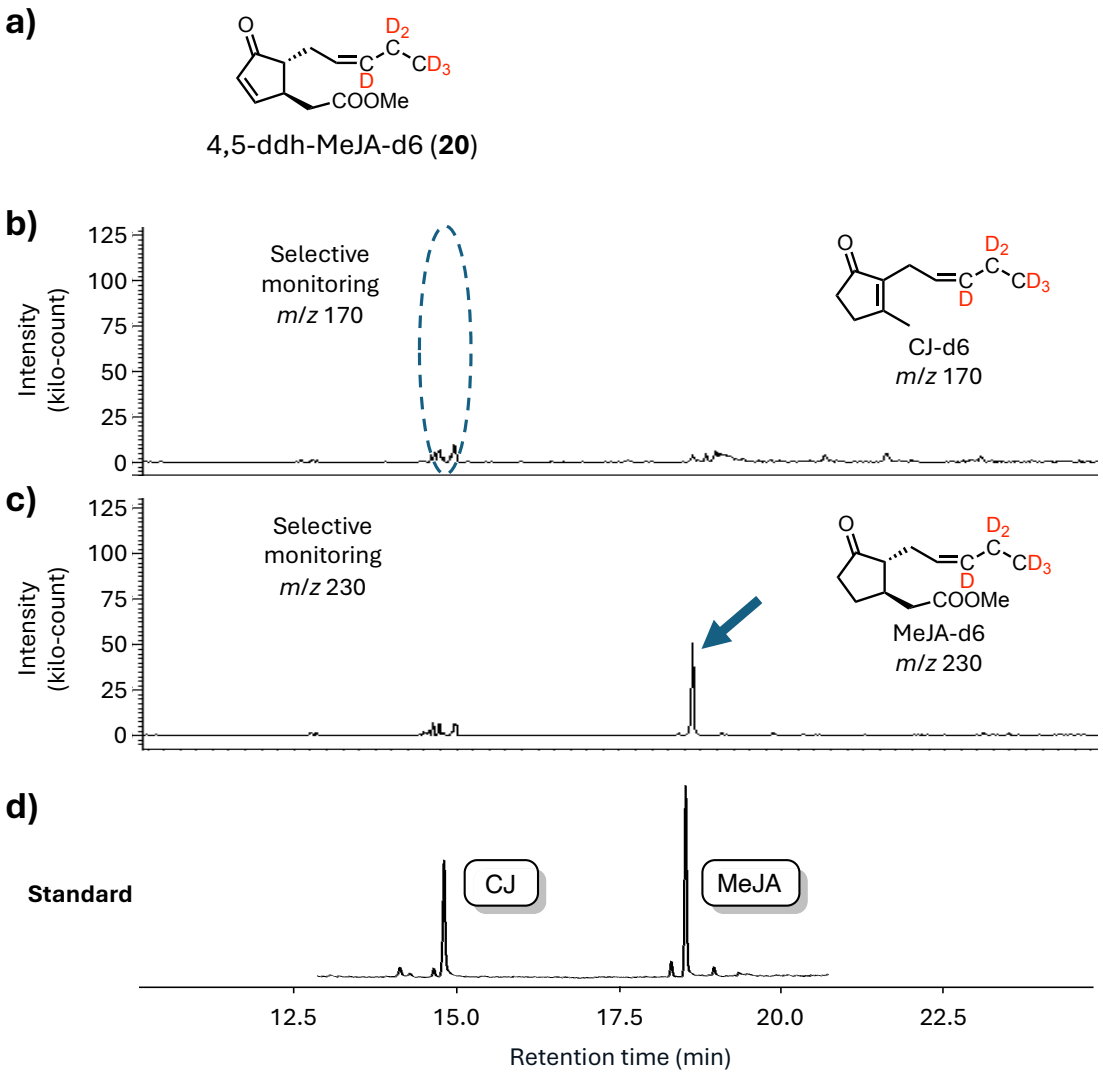

Figure 3.4. **Feeding experiment using deuterium-labeled 4,5-ddh-MeJA.**

(**a**) Chemical structure of 4,5-ddh-MeJA-d6 (**20**).

(**b**) Representative GC-MS chromatogram for detecting CJ-d6 using selected ion monitoring at *m/z* 170.

(**c**) Representative GC-MS chromatogram for measuring MeJA-d6 using selected ion monitoring at *m/z* 230.

(**d**) Representative GC-MS chromatogram for measuring authentic CJ and MeJA using total ion counting mode.

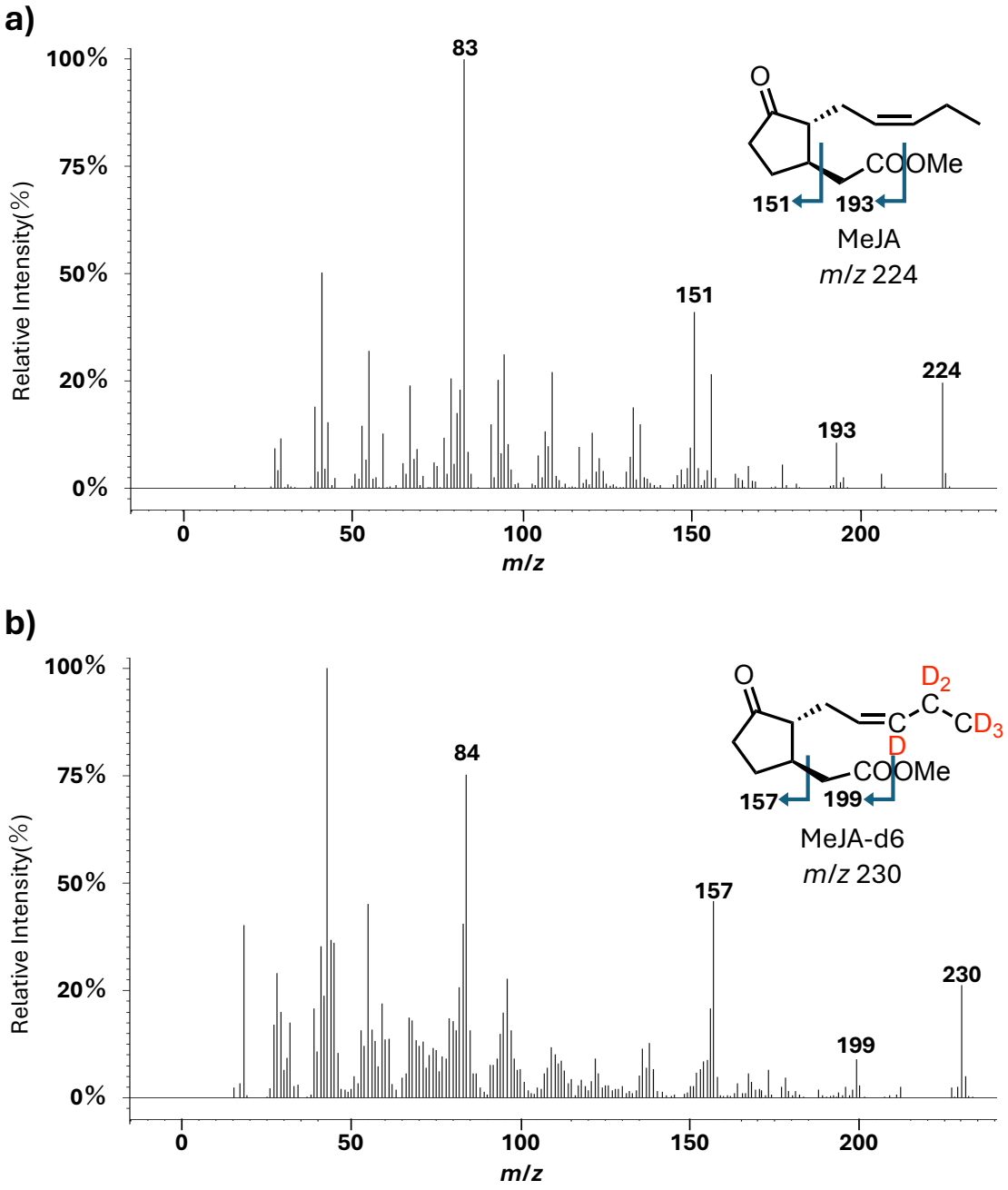

Figure 3.5. Comparison of mass spectra between authentic MeJA and deuterium-labeled MeJA detected in 4,5-ddh-MeJA-d6 (20) treatment.

(**a**) Mass spectrum of authentic MeJA.

(**b**) Mass spectrum of deutrium-labeled MeJA detected in plants treated with 4,5-ddh-MeJA-d6 (**20**).

The results of feeding MeJA-d6 (**19**) via airborne propagation to the plants are presented in Figure 3.6. Comparison of the retention times with those of the authentic compounds (Figure 3.6.d) showed no peak corresponding to CJ-d6, indicating that air-propagated MeJA-d6 was not metabolized into CJ. In Figure 3.6.b, there is a small peak with a retention time overlapping with that of CJ-d6. However, the peak in the MS pattern could not be confirmed to resemble that of CJ-d6 (data not shown).

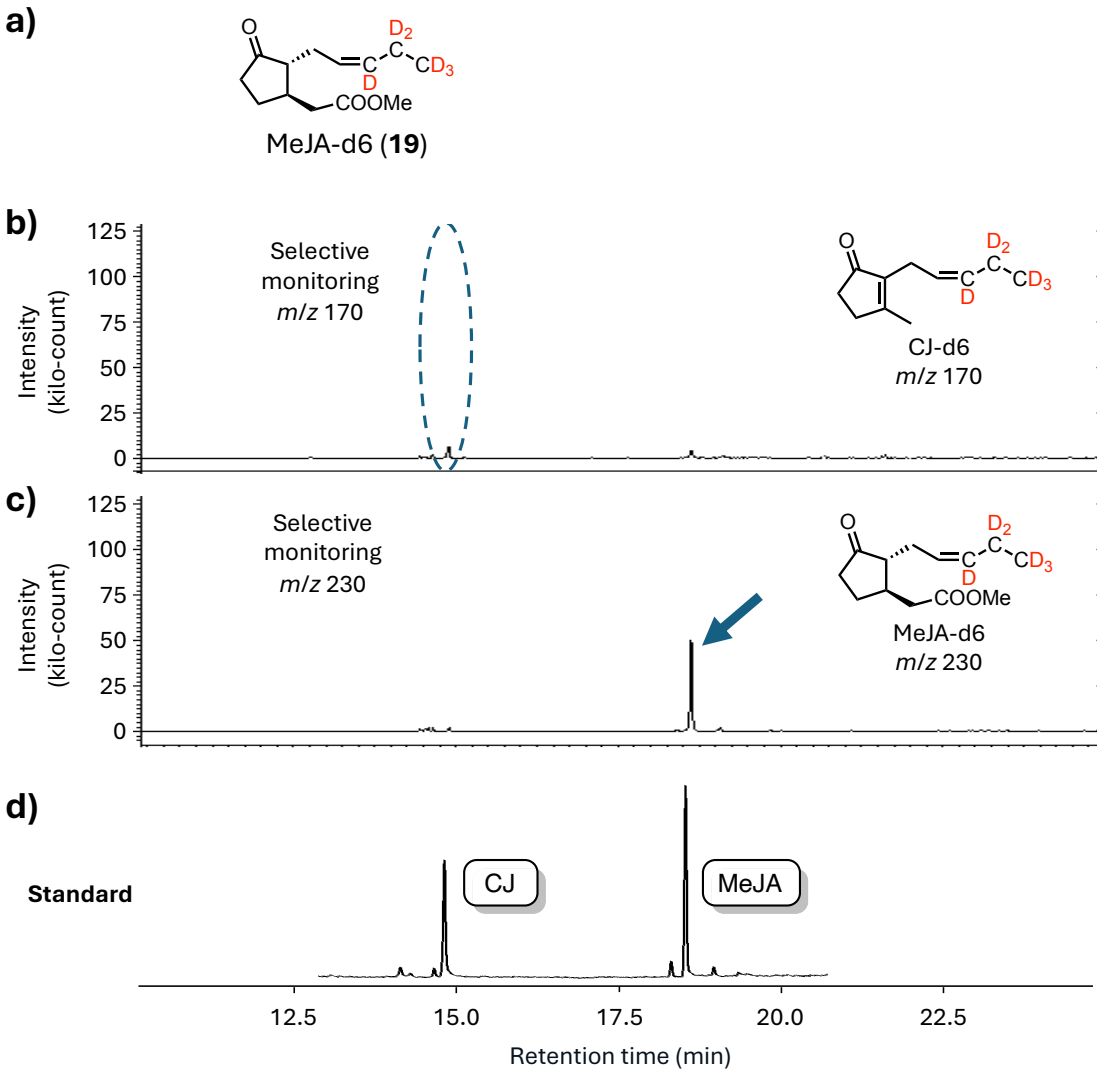

Figure 3.6. **Feeding experiment using deuterium-labeled MeJA.**

(**a**) Chemical structure of MeJA-d6 (**19**).

(**b**) Representative GC–MS chromatogram for detecting CJ-d6 using selected ion monitoring at *m/z* 170.

(**c**) Representative GC–MS chromatogram for measuring MeJA-d6 using selected ion monitoring at *m/z* 230.

(**d**) Representative GC–MS chromatogram for measuring authentic CJ and MeJA using total ion counting mode.

3.4. Conclusion

In this section, three deuterium-labeled compounds, MeJA-d6 (**19**), 4,5-ddh-MeJA-d6 (**20**), and 3,7-ddh-MeJA-d6 (**21**), were synthesized to investigate the CJ biosynthetic pathway (Scheme 3.1). GC-MS analysis revealed that some Lamiaceae plants accumulated CJ in their leaves (Table 3.1). Finally, the biosynthetic relationship between CJ and JA was investigated using *M. suavelons*. Treatment with 3,7-ddh-MeJA-d6 (**21**) resulted in the detection of CJ-d6, whereas JA-d6 was not detected (Figure 3.2). In contrast, treatment with 4,5-ddh-MeJA-d6 (**20**) led to the detection of JA-d6 but not CJ-d6 (Figure 3.4). Moreover, CJ-d6 was not detected following MeJA-d6 (**19**) treatment (Figure 3.6). These results indicate that 3,7-ddh-JA is metabolized into CJ but not into JA, whereas 4,5-ddh-JA and JA are not metabolized into CJ. Collectively, these findings suggested that the OPDA-reducing pathway leading to JA and the OPDA-isomerizing pathway leading to CJ were independent metabolic routes.

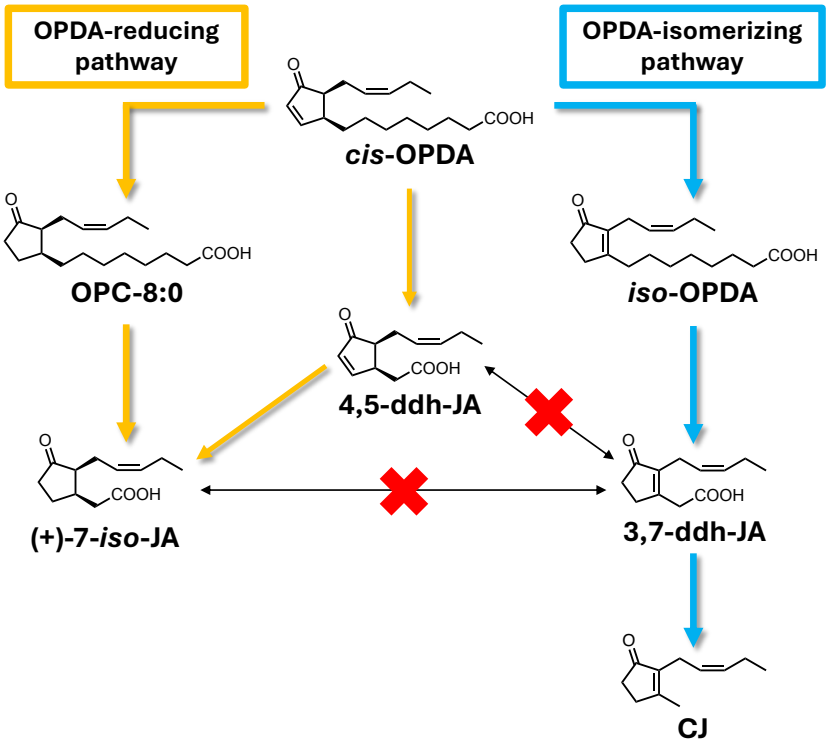

Figure 3.7. Proposed biosynthetic pathway of CJ and JA in this study

4. Exploration of stress treatments that induce pyrethrin accumulation in Pyrethrum

4.1. Introduction

As mentioned before, in recent years, the adverse effects of synthetic pesticides on the environment and human health have become an issue, and natural pyrethrins are receiving attention again due to their low impact on the environment[24]. The industrial production of naturally derived pyrethrin still relies on extraction from mature flowers of pyrethrum. Global pyrethrum production is estimated to reach or exceed 30,000 tons[24]. It was found that the highest levels of accumulation were observed in flowers, whereas pyrethrins were also detected in leaves[25]. In this study, with the goal of improving industrial pyrethrins production, stress treatments that increase the endogenous levels of pyrethrins were explored. Given the current situation where pyrethrum plants being cultivated on a large scale in the field, it is assumed that a foliar application and irrigation treatment of argents stimulating pyrethrins biosynthesis were possible candidate to make better quality of insecticides derived from pyrethrum dry powder. In practical agricultural production, plant hormones and hormone-like compounds are commonly used to improve product quality. Gibberellin is used in seedless grape cultivation[43], and jasmomate, a jasmonic acid derivative, is used as a coloring enhancer for apple fruit[44]. Given the numerous applications of plant hormones in actual agriculture, plant hormones are the first candidates considered

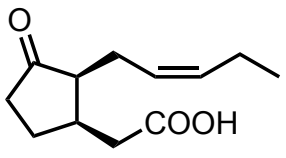

(+)-7-*iso*-Jasmonic acid
(JA)

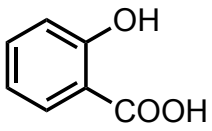

Salicylic acid
(SA)

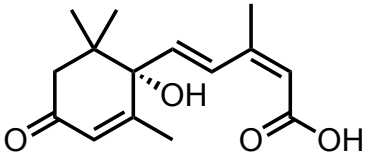

(+)-Abscisic acid
(ABA)

Figure 4.1. Plant hormones examined in this study

as biosynthetic promoters. Among the plant hormones, jasmonic acid (JA), salicylic acid (SA), and abscisic acid (ABA) were examined in this study (Figure 4.1).

As described above, JA is a phytohormone that plays a key role in plant defense against various biotic stresses. It is particularly involved in responses to insect herbivory and necrotrophic pathogen infection, such as *Botrytis cinerea*[45]. Regardless of whether the cells are alive or dead after infection, the pathogens invade the plant cells to get nutrients. The activation of JA-dependent signaling pathways enhances the production of defensive compounds, such as proteinase inhibitors, secondary metabolites, and volatile organic compounds, which prevent insect feeding damage and limit the proliferation of pathogens. In contrast, SA is primarily associated with defense responses against biotrophic pathogens, which require living host cells for their proliferation, such as tobacco mosaic virus[46]. SA-mediated responses often trigger the production of pathogenesis-related (PR) proteins and the activation of systemic acquired resistance (SAR), which enhances the plant's ability to resist the infections[47]. The signaling pathways of JA and SA are known to exhibit crosstalk, frequently acting antagonistically. Through this antagonistic crosstalk, JA-dependent defenses are typically upregulated when SA-mediated defenses are suppressed, and SA-dependent defenses are activated when JA-dependent defenses are downregulated. This regulatory balance enables plants to prioritize the defense pathway most effective for the particular type of attacker. Abscisic acid (ABA), on the other hand, plays a central role in plant responses to abiotic stresses, such as drought, salinity, and cold[48]. ABA regulates physiological processes including stomatal closure, osmoprotectant accumulation, and expression of stress-responsive genes, thereby enhancing the ability of plant to survive under harsh environmental conditions for growing.

Accurate quantification of pyrethrins is essential in this study, but conventional methods

remain problematic. In previous reports, the endogenous amount of pyrethrins was evaluated using an HPLC system[25, 49]. When using an HPLC system to evaluate endogenous amounts of target compounds, the peak assumed to be the target compound is often overlapped by those of other compounds, resulting in inaccurate quantification data. In this study, the use of UPLC-MS/MS in multiple reaction monitoring (MRM) mode enabled to distinguish compounds based on their parent and product ions. This approach effectively erase interference from co-eluting compounds to perform accurate quantification of target compounds. Since it was reported that pyrethrin II was major pyrethrin[23], pyrethrin II was selected as a target for endogenous quantification. [$^{2}H_{1}$-9', $^{2}H_{1}$-8']-Jasmolin I, structure analogs of pyrethrin II, are used as an internal standard. The advantages of using a structurally similar deuterium-labelled compound as an internal standard was listed as following two points. First, since its chemical properties are almost identical to those of the target compound, it can accurately adjust of partial decomposition of the compounds during sample extraction, purification, and other preparatory procedures. Second, in MS/MS analysis, pyrethrin II and [$^{2}H_{1}$-9', $^{2}H_{1}$-8']-jasmolin I were analyzed under identical instrumental conditions (cone voltage: 15 V; collision energy: 12 eV). Both compounds exhibited the same fragmentation behaviour, in which cleavage occurred at the bond between C1 and the adjacent oxygen atom (Figure. 4.2).Thus, [$^{2}H_{1}$-9', $^{2}H_{1}$-8']-jasmolin I produced a transition of *m*/*z* 333.76 → 165.54, whereas pyrethrin II produced a transition of *m*/*z* 373.50 → 161.01. The highly similar MS behavior of the two compounds led to more precise quantification. Solutions having several concentration ratios of [$^{2}H_{1}$-9', $^{2}H_{1}$-8']-jasmolin I and pyrethrin II were made, and a calibration curve was obtained. As a result, the peak area ratio and concentration ratio of [$^{2}H_{1}$-9', $^{2}H_{1}$-8']-jasmolin I and pyrethrin II exhibit a linear relationship, and it was confirmed that [$^{2}H_{1}$-9', $^{2}H_{1}$-8']-jasmolin I was able to be used

as an internal standard. Endogenous amount of pyrethrin II was evaluated based on the calibration curve using [$^2H_1$-9', $^2H_1$-8']-jasmolin I (Figure.4.3).

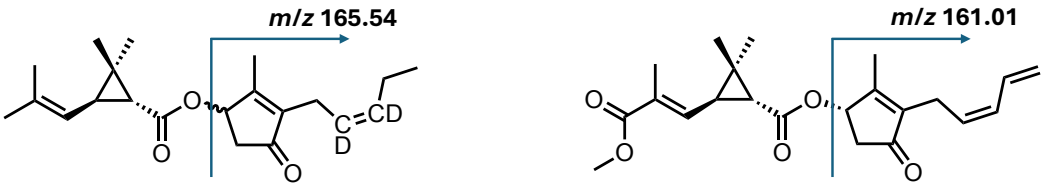

[$^2H_1$-9', $^2H_1$-8']-Jasmolin I
(*m/z* 333.76 → 165.54)

Pyrethrin II
(*m/z* 373.50 →161.01)

Figure 4.2. Structure of [$^2H_1$-9', $^2H_1$-8']-jasmolin I and Pyrethrin II

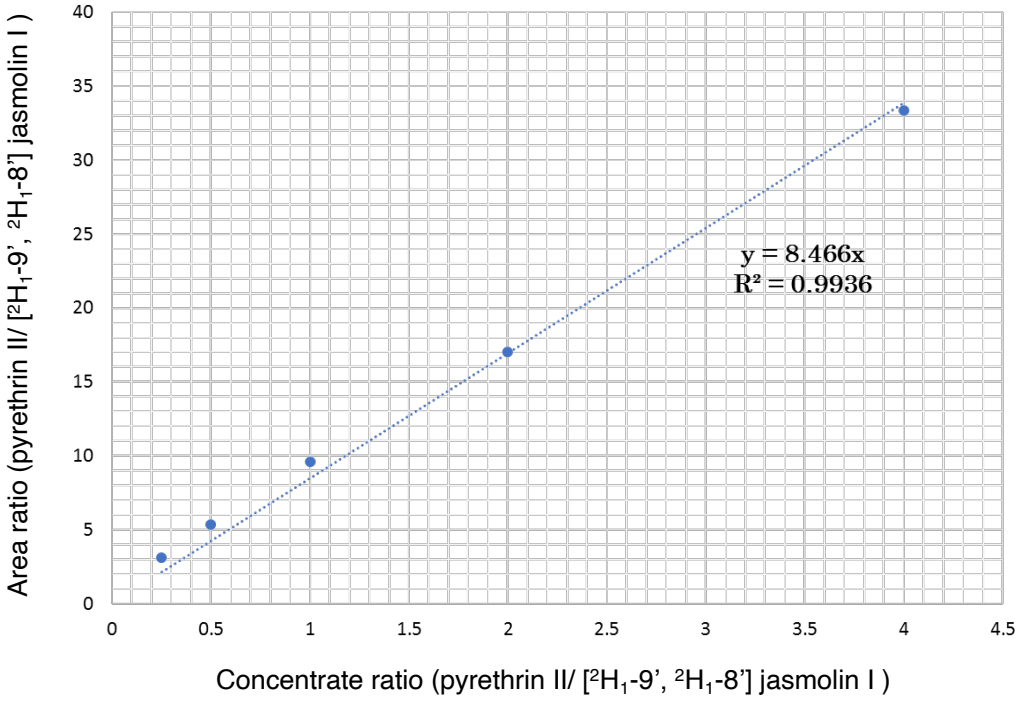

Figure 4.3. Calibration curve to evaluate the amount of pyrethrin II using [$^2H_1$-9', $^2H_1$-8']-jasmolin I as an internal standard.

4.2. Material and Method

General experimental procedures: Ultra-performance liquid chromatography (UPLC) was performed on a Waters ACQUITY UPLC system (Waters, USA), and the system was run by MassLynx 4.0. MS/MS was conducted on a Waters Micromass Quattro Premier tandem quadrupole mass spectrometer in multiple reaction monitoring (MRM) mode.

Plant material and growth condition: Seeds of pyrethrum (*T. cinerariifolium*) were planted into a Jiffy-7 (ϕ 42 mm) pot, which had absorbed 20 mL of water, and seedlings were grown in the growth chamber. The temperature and moisture of the chamber were set at 23 °C and 60%, respectively, and the conditions of day length were light for 14 h and dark for 10 h.

Air propagation of MeJA and MeSA: The experiment was performed according to the reported methods[37-39]. Pyrethrum plants (6 plants, 6 weeks old) grown with Jiffy-7 (ϕ 42 mm) and three filter papers with MeJA (1 mg) or MeSA (1 mg) were placed in a semi-closed container (9.5 L). After 24 h, aerial parts of plant materials were harvested. The target compounds were analyzed according to following section.

Irrigation treatments of ABA, PEG, NaCl and EtOH: Pyrethrum plants (6 plants, 6 weeks old) grown using Jiffy-7 (ϕ 42 mm) were fed aqueous solutions of ABA (200 μM, 20 mL/plant), PEG6000 (15%, 20 mL/plant), and NaCl (200 mM, 20 mL/plant) and EtOH (3%, 20 mL/plant). For control plants, solutions of H_2O were given to the plants with same manner. After 7 days, aerial pats of plant materials were harvested. The target compounds were analyzed according to following section.

Quantification of pyrethrin II, JA, SA and ABA: The plant material (300 ~ 1000 mg) was harvested, frozen using liquid nitrogen, crushed, and soaked in EtOH (20 mL). The extract was filtered, and 10 μg of [$^{2}H_{1}$-9', $^{2}H_{1}$-8']-jasmolin I , 100 ng of JA-d6, 25 ng of ABA-d6, 25 ng of SA-d4 were added as internal standards. The volatile components of the extract were removed under reduced pressure. The obtained residue was dissolved in 90% MeOH (2 mL). The solution was applied to a Bond Elute C18 cartridge column (Agilent Technologies, USA), and the column was successively eluted using a solution of 90% MeOH (4 mL). The volatile components of the combined eluents were removed in vacuo to afford a residue, which was resuspended in a solution of 80% MeOH (0.5 mL). A portion of the mixture (5 μL) was subjected to UPLC-MS/MS. Based on the calibration curve (Figure 4.3), the endogenous amount of pyrethrin II was calculated based on the following equation:

$$\text{Pyrethrin II endogenous amounts (μg/ g FW)} = \frac{\text{[Pyrethrin II area]} \times 10\ (\mu g)}{8.46 \times [[^{2}H_{1}\text{-9'}, {}^{2}H_{1}\text{-8'}]\text{-jasmolin I area}] \times \text{[Sample weight (g FW)]}}$$

Analytical conditions of UPLC-MS/MS: UPLC separation was performed on an ACQUITY ethylene-bridged (BEH) C18 column (1.7 mm, 2.1 × 100 mm) at 38 °C using 20% MeOH with 0.05% AcOH (solvent A) and MeOH with 0.05% AcOH (solvent B) as eluents. The detailed UPLC conditions are described in Tables 4.1-3. For MRM data collection, the capillary voltage was set at 3.5 kV, the source temperature was 120 °C, the desolation temperature was 350 °C, the desolation gas flow was 800 L/h, and the cone gas flow was 50 L/h. During each UPLC injection, the mass spectrometer was set to collect data in MRM mode using electrospray ionization in the positive and negative ion mode. Table 4.4-5 shows the precursor ion (*m*/*z*), product ion (*m*/*z*), cone voltage (V), and collision energy (eV) for the analysed compounds.

Table 4.1. LC condition for analysis of pyrethrin II

Time (min)	Flow (mL/min)	%A	%B	Curve
0.0	0.25	20	80	-
0.2	0.25	20	80	6
4.0	0.25	0	100	6
7.5	0.25	0	100	6
8.0	0.25	20	80	6
9.0	0.25	20	80	6

A: 20% aq. MeOH + 0.05% AcOH, B: 100% MeOH + 0.05% AcOH

Table 4.2. LC condition for analysis of JA and ABA

Time (min)	Flow (mL/min)	%A	%B	Curve
0.0	0.25	100	0	-
0.2	0.25	100	0	6
8.0	0.25	10	90	6
8.5	0.25	0	100	6
9.5	0.25	0	100	6
10.0	0.25	100	0	6
12.0	0.25	100	0	6

A: 20% aq. MeOH + 0.05% AcOH, B: 100% MeOH + 0.05% AcOH

Table 4.3. LC condition for analysis of SA

Time (min)	Flow (mL/min)	%A	%B	Curve
0.0	0.25	100	0	-
0.2	0.25	100	0	6
7.0	0.25	45	55	6
7.5	0.25	0	100	6
9.0	0.25	0	100	6
9.3	0.25	100	0	6
10.0	0.25	100	0	6

A: 20% aq. MeOH + 0.05% AcOH, B: 100% MeOH + 0.05% AcOH

Table 4.4. MRM condition in positive mode for analysis of pyrerthrin II and [$^{2}H_{1}$-9', $^{2}H_{1}$-8'] jasmolin I

Compound	$[M+H]^{+}$ (*m/z*)	Transition ion (*m/z*)	Dwell time (Secs)	Cone voltage (V)	Collision energy (eV)
Pyrethrin II	373.50	161.01	0.100	15.00	12.00
Jasmolin I–d2	333.76	165.54	0.100	15.00	12.00

Table 4.5. MRM condition in negative mode for analysis of JA, ABA and SA

Compound	$[M-H]^{-}$ (*m/z*)	Transition ion (*m/z*)	Dwell time (Secs)	Cone voltage (V)	Collision energy (eV)
JA	209.00	58.71	0.090	24.00	16.00
JA-d6	215.00	58.71	0.090	24.00	16.00
ABA	262.90	152.62	0.080	26.00	12.00
ABA-d6	268.90	158.62	0.080	26.00	12.00
SA	136.83	92.50	0.100	26.00	16.00
SA-d4	140.83	96.63	0.100	26.00	16.00

Statistical processing: Smirnov-Grubbs test was conducted to exclude outliers from the significant level of 5% in each data set. Determination of a significant difference between the two data sets was examined using Student's *t*-test.

4.3. Result

4.3.1. Air propagation of MeJA and MeSA

JA and SA treatments are conducted. In general, JA and SA are converted into their volatile forms, MeJA and MeSA, which can induce defence responses in neighboring plants through air propagation. To mimic this mechanism, MeJA and MeSA were applied to pyrethrum seedlings according to previously reported methods[38, 39]. In brief, six pyrethrum plants and three filter papers with MeJA (1 mg) or MeSA (1 mg) were placed in a semi-closed container (9.5 L). After 24 h, aerial parts of plant materials were harvested to analyze. It was found that MeJA and MeSA treatments resulted in significantly higher endogenous levels of JA and SA (Figure 4.4.a-b), respectively, compared with those of the control. However, neither treatment led to a significant increase in endogenous pyrethrin II content (Figure 4.4.c).

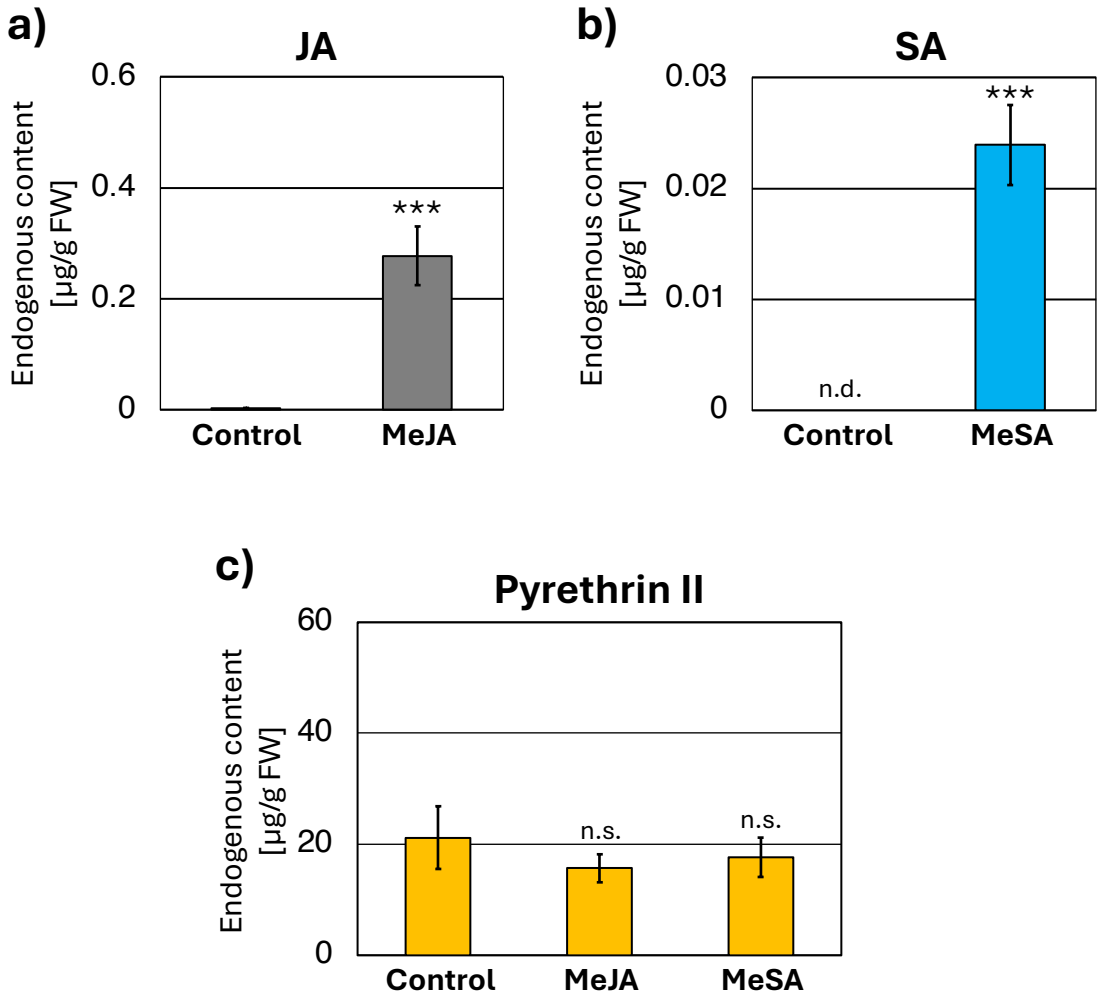

Figure 4.4. Air propagation of MeJA and MeSA to Pyrethrum plants.

(**a**) JA contents in MeJA-treated plants (n= 6 for the treated plants, 6 for non-treated plants).

(**b**) SA contents in MeSA-treated plants (n= 6 for the treated plants, 6 for non-treated plants).

(**c**) Pyrethrin II contents in MeJA- or MeSA-treated plants (n= 6 for the MeJA treated plants, n= 6 for the MeSA, treated plants 6 for non-treated plants).

Each value represents the mean ± SE.

Student's *t*-test (n.s., not significant; ***$p < 0.001$; n.d., not detected).

4.3.2. Irrigation treatment of ABA

Next, ABA treatment was examined. Unlike JA and SA, no researchers reported that ABA acted as a volatile signal mediating communication between plants. Therefore, instead of the airborne treatment, irrigation treatment with a solution of ABA was performed according to a previously reported method[50, 51]. Briefly, pyrethrum plants were irrigated with 200 μM ABA solution instead of water. After 7 days, aerial pats of plant materials were harvested to analyze. As a result of ABA treatment, the endogenous amount of ABA was increased by the treatment (Figure 4.5.a). Furthermore, the endogenous amount of pyrethrin II was also increased (Figure 4.5.b), which was 3.5-fold higher than that of the mock treatment.

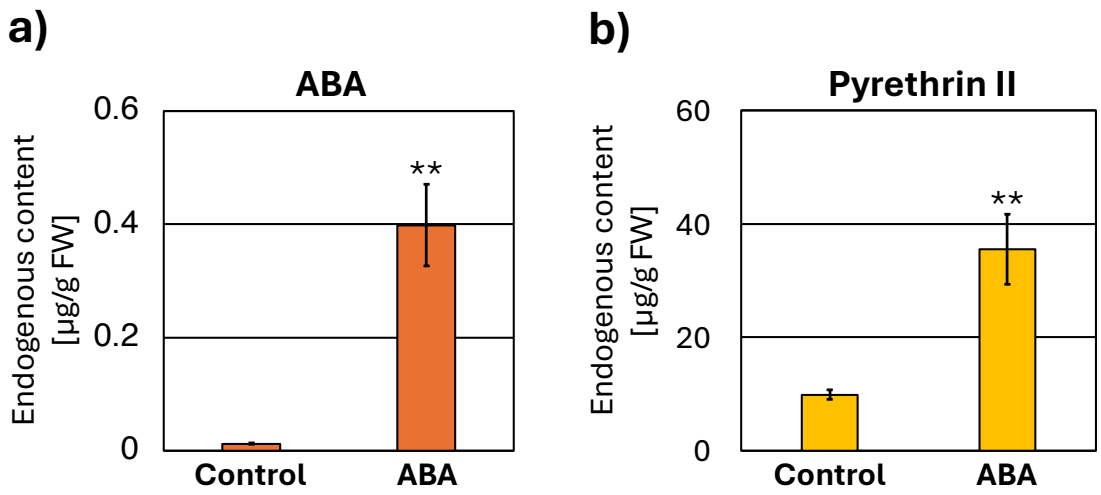

Figure 4.5. Irrigation treatment with ABA to pyrethrum seedlings

(**a**) ABA contents in ABA-treated plants (n= 7 for the treated plants, n=6 for non-treated plants).

(**b**) Pyrethrin II contents in ABA-treated plants (n= 8 for the treated plants, n=7 for non-treated plants).

Each value is represented as the mean ± SE.

4.3.3. PEG, NaCl and EtOH treatment

Because irrigation treatment with ABA upregulated the biosynthesis of pyrethrin II, it was hypothesized that external stimuli which induce ABA biosynthesis could upregulate the pyrethrin II biosynthesis, such as treatments with aqueous solutions of PEG, NaCl and EtOH. The solutions of PEG (15%), NaCl (200 mM), EtOH (2%) were treated in the same manner as for the irrigation ABA, and the endogenous amounts of ABA and pyrethrin II were evaluated. The treatments with PEG (15%) and NaCl (200 mM) increased the endogenous amount of ABA (Figure 4.6.a and c), however that with EtOH (2%) showed an increase without a significant difference (P = 0.06, Figure 4.6.e). Regarding the amount of pyrethrin II, all treatments increased the endogenous amount of pyrethrin II, whose accumulated amounts were 2.3-fold higher in the PEG treatment (Figure 4.6.b), 1.8-fold higher in the NaCl treatment (Figure 4.6.d), and 1.7-fold higher in the EtOH treatment (Figure 4.6.f)

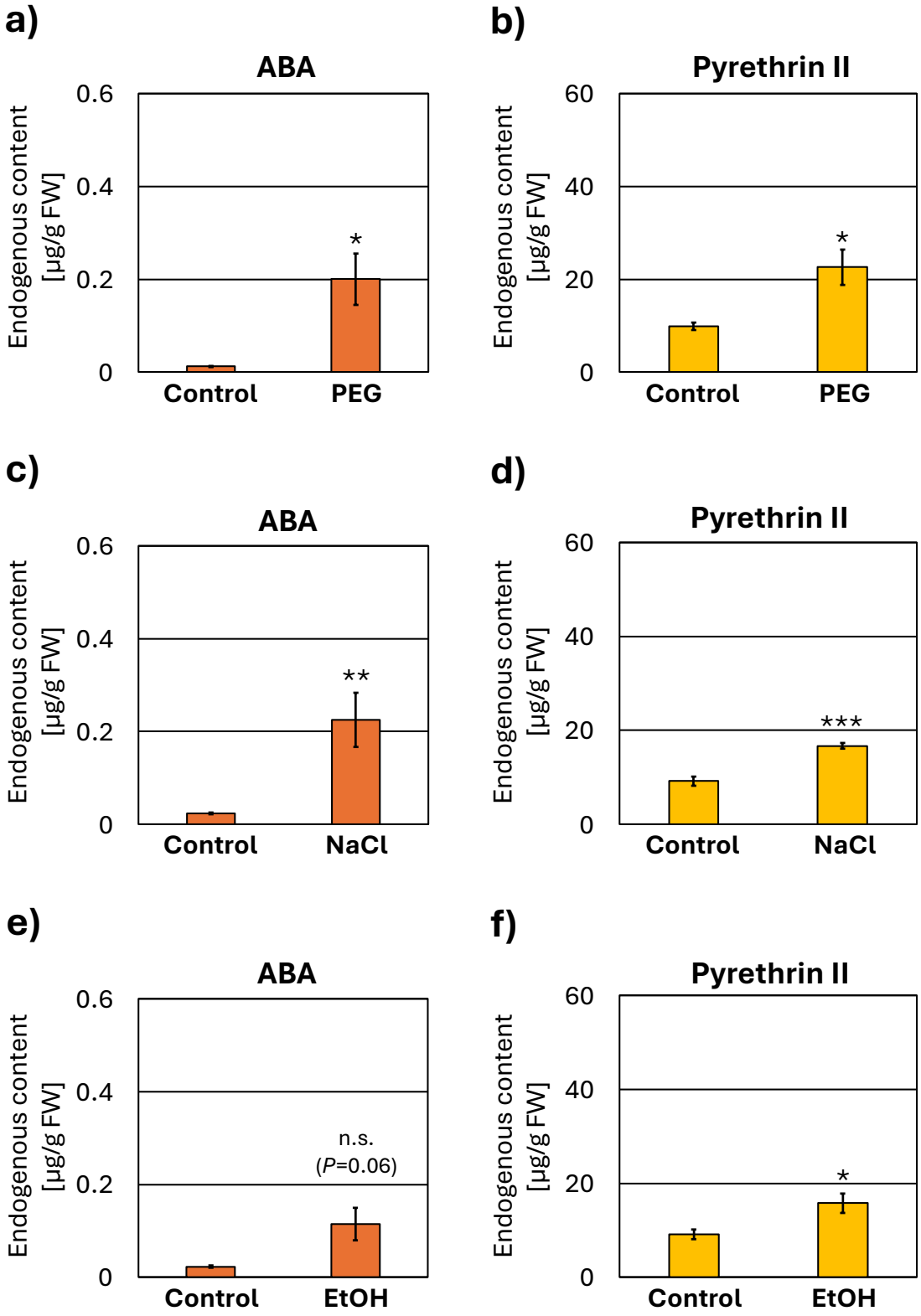
a)
ABA
Endogenous content [µg/g FW]
0.6
0.4
0.2
0
*
Control
PEG
b)
Pyrethrin II
Endogenous content [µg/g FW]
60
40
20
0
*
Control
PEG
c)
ABA
Endogenous content [µg/g FW]
0.6
0.4
0.2
0
**
Control
NaCl
d)
Pyrethrin II
Endogenous content [µg/g FW]
60
40
20
0
***
Control
NaCl
e)
ABA
Endogenous content [µg/g FW]
0.6
0.4
0.2
0
n.s.
(P=0.06)
Control
EtOH
f)
Pyrethrin II
Endogenous content [µg/g FW]
60
40
20
0
*
Control
EtOH

Figure 4.6. Irrigation treatment with PEG, NaCl, and EtOH to pyrethrum seedlings

(**a**) ABA contents in PEG-treated plants (n= 8 for the treated plants, n= 7 for non-treated plants).

(**b**) Pyrethrin II contents in PEG-treated plants (n= 8 for the treated plants, n= 7 for non-treated plants).

(**c**) ABA contents in NaCl-treated plants (n= 6 for the treated plants, n= 5 for non-treated plants).

(**d**) Pyrethrin II contents in NaCl-treated plants (n= 6 for the treated plants, n= 4 for non-treated plants).

(**e**) ABA contents in EtOH-treated plants (n= 6 for the treated plants, n= 6 for non-treated plants).

(**f**) Pyrethrin II contents in EtOH-treated plants (n= 6 for the treated plants, n= 5 for non-treated plants).

Each value is represented as the mean ± SE.

Student's *t*-test (n.s., not significant; * p <0.05; ** p <0.01; *** p <0.001).

4.4. Conclusion

Treatments with JA and SA, which are considered biotic stress signals such as herbivory and pathogen infection, did not result in an increase in endogenous pyrethrin levels (Figure 4.4). In contrast, ABA treatments, which are associated with responses to abiotic stresses such as drought and salinity, led to a marked increase in endogenous pyrethrin levels (Figure 4.5). Furthermore, treatments with NaCl, PEG, and EtOH, which are known to induce ABA biosynthesis in plants, resulted in increased endogenous ABA levels together with a significant increase in endogenous pyrethrin levels (Figure 4.6).

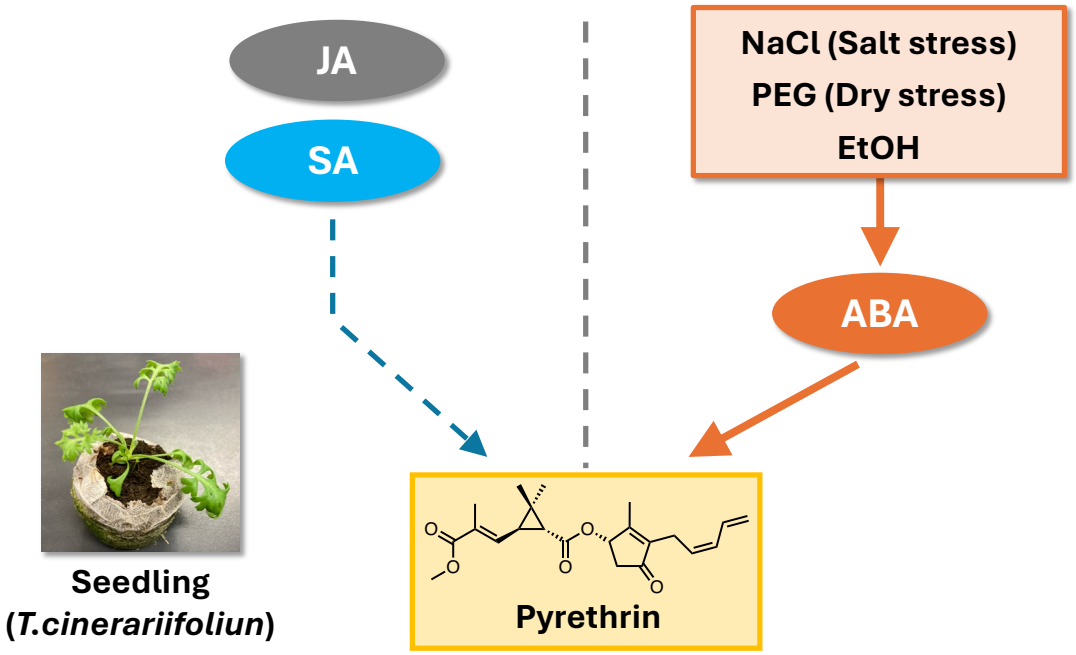

Figure 4.6. Graphical summary of this section

5. Discussion

5.1. Applicability of the *iso*-OPDA synthetic method developed in this study

The *iso*-OPDA synthetic method established in this study (Figure 2.1) was widely applied in other research, demonstrating its high versatility and utility. In the study by Hirota *et al*., (±)-*trans*-OPDA synthesized based on this method was employed to determine the stereochemistry of a novel compound, α-*cis*-OPDA glyceride, isolated from Arabidopsis thaliana[52]. By comparing the ^{1}H-NMR spectra of the isolated compound with those of the authentic standards, (±)-*trans*-OPDA and *cis*-OPDA, it was clearly demonstrated that the OPDA moiety of the isolated compound possessed a *cis* configuration rather than a *trans* configuration.

Furthermore, *iso*-OPDA, (±)-*trans*-OPDA-d6, and dn-*iso*-OPDA synthesized according to the present method was utilized in studies by Tsuzuki *et al.*[53] and Ersalena *et al.*[54] In the work by Tsuzuki *et al.*, the use of synthetic dn-*iso*-OPDA as an authentic standard enabled the accurate quantification of dn-*iso*-OPDA in *Marchantia polymorpha*[53]. Ersalena *et al.* successfully achieved precise quantification of *iso*-OPDA and dn-*iso*-OPDA in four kinds of moss species, such as *Calohypnum plumiforme* (formerly *Hypnum plumaeforme*), *Leucobryum bowringii*, *Pyrrhobryum dozyanum*, and *Bartramia pomiformis*, using *iso*-OPDA and dn-*iso*-OPDA as authentic compounds and (±)-*trans*-OPDA-d6 as an internal standard[54].

Collectively, these findings demonstrated that the *iso*-OPDA synthetic method developed in this study was highly effective and broadly applicable for the synthesis to give OPDA-related compounds.

5.2. Biosynthetic pathway from JA to CJ

Feeding experiments demonstrated that neither JA nor 4,5-ddh-JA was metabolized to CJ in *M. suaveolens* (Figure 3.7). This observation was consistent with previous reports by Matsui *et al*.[23] and Dabrowska *et al*.[16], which revealed that CJ was biosynthesized via the OPDA-isomerizing pathway rather than the OPDA-reducing pathway. However, these results appeared to contradict the findings of Koch *et al*.[22], which reported that (±)-JA was metabolized to CJ through 3,7-ddh-JA.

In the study by Koch *et al*., a 3 mM solution of (±)-MeJA-d5 were supplied to plants through the cut surface of stems by soaking. Using this method, the authors detected the corresponding CJ-d4 in Lima bean (*Phaseolus lunatus cv. Sieva*), white willow (*Salix alba*), and jasmine (*Jasminum ryncospermum*), thereby proposing a biosynthetic pathway from JA to CJ[22]. In contrast, no labeled CJ was detected in cotton (*Gossypium hirsutum*), tomato (*Lycopersicon lycopersicum*), tobacco (*Nicotiana tabacum*), or maize (*Zea mays*) following the administration of JA. Interestingly, when 3,7-ddh-MeJA-d2 was supplied, the formation of CJ-d2 was observed in all seven plant species mentioned above.

To evaluate whether the discrepancy among these studies were derivrd from differences in the method of applying the compounds, an additional experiment was performed according to the protocol of Koch *et al*. A 3 mM solution of JA-d6 was supplied to *M. suaveolens* via the cut end of the stem. After 24 h, EtOAc extracts from the leaves of the plants were subjected to GC–MS analysis. Although endogenous CJ was detected, no CJ-d6 was observed (data not shown). This result strongly supported the finding of the present study (Figure 3.6), suggesting that JA wa not metabolized to CJ in *M. suaveolens*.

5.3. Biosynthesis of JA from 3,7-ddh-JA

Feeding treatments performed in this study revealed that 3,7-ddh-JA was not metabolized to 4,5-ddh-JA and JA (Figure 3.7). The result supported the findings reported by Miyawaki *et al.*, which showed that feeding of 3,7-ddh-JA to potato single node stem did not induce potato tubers, although (±)-4,5-ddh-JA and (±)-JA induced potato tubers[55]. This result suggested that 3,7-ddh-JA is not metabolized into JA.

These findings showed that the OPDA-isomerizing and OPDA-reducing biosynthesis pathways should be independent and that the biosynthetic intermediates of the OPDA-isomerizing and OPDA-reducing pathways do not complement each other, although *cis*-OPDA was employed as a common biosynthetic intermediate.

5.4. Relationship of OPDA isomerases between early diverging land plants and vascular plants

Previous study suggested the presence of the OPDA-isomerizing pathway and the key enzyme, OPDA isomerase, in the biosynthesis of pyrethrins in pyrethrum[23]. In this study, the presence of the OPDA-isomerizing pathway and OPDA isomerase in the biosynthesis of CJ in Lamiaceae species was also suggested. Furthermore, in liverworts and various moss species, the presence of *iso*-OPDA and dn-*iso*-OPDA has been reported, suggesting that an OPDA-isomerizing pathway and OPDA isomerase are also present[33, 56]. In addition, dn-*iso*-OPDA was recently detected in many species of bryophytes and lycophytes (Figure 5.1)[57]. These results raised two competing hypotheses regarding whether OPDA isomerases share a common evolutionary origin or emerged independently in early diverging land plants (bryophytes and lycophytes) and some vascular plants (Figure 5.2).

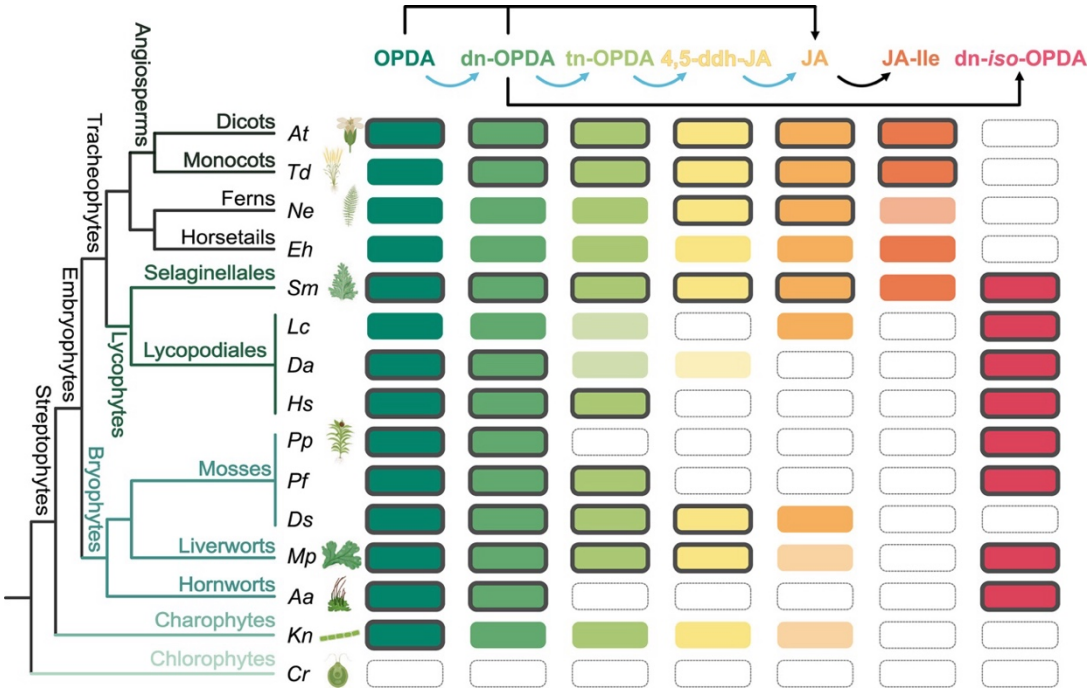

Figure 5.1. dn-*iso*-OPDA was widely detected in bryophytes and lycophytes[57].

The first hypothesis suggests that OPDA isomerase has been broadly conserved since early stages of land plant evolution. The OPDA isomerizing pathway functioned as a biosynthetic route for dn-*iso*-OPDA, the bioactive ligand of jasmonate signaling in ancestral land plants. However, with the co-evolution of the ligand–receptor system, the primary function of this pathway shifted toward the OPDA-reducing pathway. Instead, this pathway was repurposed for the biosynthesis of biologically active secondary metabolites, such as CJ and pyrethrins. In this model, OPDA isomerases from pyrethrum, Lamiaceae, bryophytes, and lycophytes are expected to form a monophyletic clade, indicating descent from a common ancestral OPDA isomerase.

In construct, the second hypothesis suggests that OPDA isomerase of vascular plants is evolutionarily distinct from that of early diverging land plants. Although the OPDA isomerizing pathway originally functioned in jasmonate signaling in ancestral land plants, its functional significance diminished during evolution, leading to the loss of the ancestral land plant–type OPDA isomerase in vascular plants. Subsequently, vascular plants acquired a new type of OPDA isomerase that is evolutionarily distinct from that of early-diverging land plants later contributing to the biosynthesis of CJ or pyrethrins. This model suggests that the OPDA isomerizing function of early diverging land plants and vascular plants emerged through convergent evolution rather than common origin. In this case, the OPDA isomerases from some vascular plants (pyrethrum and Lamiaceae) are expected to share extremely low sequence homology with those from early-diverging land plants (bryophytes and lycophytes), or they may even belong to entirely different enzyme families.

A similar case can be found in the biosynthesis of momilactones. Momilactones are phytoalexins produced by grasses such as rice (*Oryza sativa*) and barnyard grass

(*Echinochloa crus-galli*). Moreover, momilactone biosynthesis was identified in the bryophyte, *Hypnum plumaeforme*, and its biosynthetic mechanism was extensively studied. These studies revealed that gene cluster for momilactone biosynthesis in *H. plumaeforme* is functionally similar to that in rice and barnyard grass. However, no such candidate gene clusters were identified in bryophytes and lycophytes other than *H. plumaeforme*. Similarly, among vascular plants, these clusters were only detected in a few species, such as rice and barnyard grass. These findings indicated that momilactone biosynthetic pathways emerged through convergent evolution in such evolutionarily distant lineages as *H. plumaeforme* and these specific grasses.

This case differs from momilactone biosynthesis in that the OPDA isomerizing pathway is observed across a much wider range of species. Therefore, the former hypothesis is more plausible. In fact, the findings show that dn-*iso*-OPDA was widely detected in various bryophytes and lycophytes (Figure 5.1). Ultimately, the identification of OPDA isomerases across diverse species, combined with comprehensive phylogenetic analyses, will be essential to determine which hypothesis is correct.

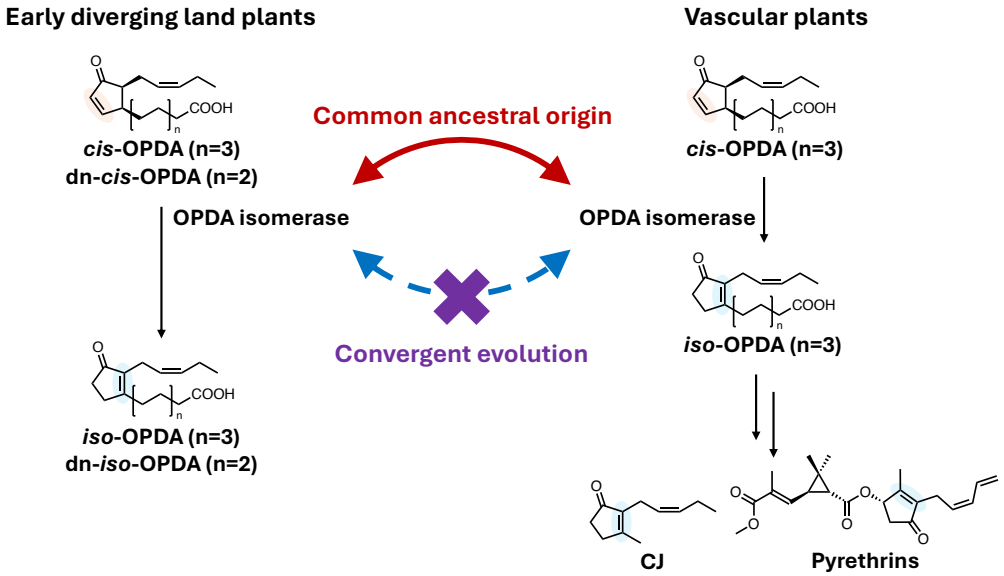

Figure 5.2. Proposed the relationship of OPDA isomerases between early diverging land plants and vascular plants.

5.5. Air propagation of MeJA and MeSA do not induce pyrethrin biosynthesis.

Ueda *et al*. reported that wounding treatment generated systemic signals that upregulated pyrethrin biosynthesis in systemic leaves, resulting in increases of endogenous pyrethrin I and II contents to 1.6- and 1.7-fold, respectively, compared with mock-treated plants[58]. Similarly, Kikuta *et al.* showed that the endogenous levels of pyrethrin I and II in the leaves of plants neighboring wounded plants increased by 1.3-fold relative to those of mock plants[59]. Based on these results, it was anticipated that JA signaling, which is involved in wound responses, would induce the biosynthesis of pyrethrins. In addition, Zeng *et al*. reported that the expression levels of LOX1, AOS, AOC, JMH, CDS, ADH2, ALDH1, and GLIP were significantly upregulated 6 or 12 hours after foliar application of MeJA treatment[29]. Considering the insecticidal function of pyrethrins, it is biologically reasonable that their biosynthesis is induced as part of a JA-mediated defense response.

Based on the antagonistic relationship between JA and SA signaling, it was hypothesized that an increase in endogenous pyrethrin content were expected by air propagation of MeJA, whereas a decrease was anticipated by air propagation of MeSA. However, no significant changes in endogenous pyrethrin levels were observed under either treatment (Figure 4.4). These results suggested that the MeJA-induced upregulation of pyrethrin biosynthetic gene expression might be transient or insufficient to cause a measurable increase in pyrethrin accumulation.

5.6. ABA treatment induces pyrethrin biosynthesis

In this study, treatment with 200 μM ABA significantly increased the endogenous level of pyrethrin II by 3.5-fold (Figure 4.5.b). Since ABA is primarily a plant hormone involved in responses to osmotic stress, such as drought, it remains unclear why ABA treatment leads to a pronounced increase in endogenous levels of pyrethrin, the insecticidal compound.

First, I hypothesized that ABA treatment would enhance pyrethrin accumulation through transcriptional upregulation of pyrethrin biosynthetic genes. However, when gene expression levels were compared between the ABA treatment and the control using RNA-seq analysis, no significant upregulation of the known pyrethrin biosynthetic genes (AOS, AOC, JMH, CDS, CCMT, PYS, ADH2, ALDH1, and GLIP) was observed (no data shown).

Next, based on the known physiological functions of ABA, I considered the possibility that ABA enhances pyrethrin accumulation through modulation of enzyme activity rather than transcriptional regulation. It is known that an increase in endogenous ABA under osmotiic stress conditions, such as drought, can lead to alkalization of the apoplast[60]. Indeed, it was reported that a stress of soil drying for 11 days gave impact to faba bean changing pH from 4.4 to 5.7 in the leaves[61]. In pyrethrin biosynthesis, the carboxylic acid and alcohol moieties, which are synthesized in the cytoplasm, are transported extracellularly and subsequently esterified in the apoplast by TcGLIP to form pyrethrin[25]. TcGLIP exhibits maximal activity at approximately pH 7.5, whereas its activity drops to less than one-tenth of the optimum at pH values below 6. However, the enzyme activity increases sharply between pH 6 and 7.5[25]. Taken together, these findings suggested that ABA-induced alkalization of the apoplast might enhance TcGLIP activity, thereby resulting in an increased endogenous pyrethrin level.

There are several reports on how much amounts of ABA plants accumulate during dry

stress. Cai *et al.*, Chen *et al.*, Tureckova *et al.* and Perreca *et al.* reported that rice, cotton, wheat, and conifer Picea glauca accumulated ABA at almost 400 ng/g FW, 2000 ng/g FW, 19 ng/g FW, and 400 ng/g FW, respectively[62-65]. Although it is difficult to make a general statement because the formulation of desiccation stress differs in each report, it may be safe to say that the endogenous amount of ABA (400 ng/g FW in Figure 4.5.a) that increased by ABA irrigation treatment in this study was close to the physiologically relevant concentration

5.7 PEG, NaCl and EtOH treatments induce ABA and Pyrethrin accumulation.

Treatments with NaCl, PEG, and EtOH, which are known to induce ABA biosynthesis in plants, resulted in increased endogenous ABA levels together with a significant increase in endogenous pyrethrin levels (Figure 4.6.b, d and f).

These results strongly supported the evidence that ABA enhances pyrethrin accumulation. Upon ABA treatment, endogenous ABA levels increased to 400 ng/g FW, resulting in a 3.5-fold increase in Pyrethrin II content. In comparison, PEG, NaCl, and EtOH treatments led to ABA levels of 200, 230, and 120 ng/g FW (Figure 4.6.a, c and e), respectively, and corresponding increases in Pyrethrin II content of 2.2-, 1.9-, and 1.7-fold. These findings indicated a clear correlation between endogenous ABA accumulation and Pyrethrin II production. Further optimization of PEG, NaCl, and EtOH concentrations and the application of more intense stress treatments may lead to even higher pyrethrin accumulation.

Moreover, it was thought that EtOH treatment should have potential for practical application among the stress treatments tested, due to its high biodegradability, low environmental impact, and cost-effectiveness. Although further validation, such as field trials involving foliar ethanol spraying on pyrethrum flowers, is required, this approach holds potential for enhancing pyrethrin production at an industrial scale.

6. Reference

(1) Ryan, C. A. The search for the proteinase inhibitor-inducing factor, PIIF. *Plant Molecular Biology* **1992**, *19* (1), 123-133. DOI: 10.1007/bf00015610.

(2) McDowell, J. M. Signal transduction in the plant immune response. *Trends in biochemical sciences (Amsterdam. Regular ed.)* **2000**, *25* (2), 79-82. DOI: 10.1016/s0968-0004(99)01532-7.

(3) Ishiguro, S.; Kawai-Oda, A.; Ueda, J.; Nishida, I.; Okada, K. The DEFECTIVE IN ANTHER DEHISCENCE1 Gene Encodes a Novel Phospholipase A1 Catalyzing the Initial Step of Jasmonic Acid Biosynthesis, Which Synchronizes Pollen Maturation, Anther Dehiscence, and Flower Opening in Arabidopsis. *The Plant Cell* **2001**, *13* (10), 2191-2209. DOI: 10.1105/tpc.010192

(4) Bannenberg, G.; Martínez, M.; Hamberg, M.; Castresana, C. Diversity of the Enzymatic Activity in the Lipoxygenase Gene Family of *Arabidopsis thaliana*. *Lipids* **2009**, *44* (2), 85-95. DOI: 10.1007/s11745-008-3245-7.

(5) Laudert, D.; Pfannschmidt, U.; Lottspeich, F.; Holländer-Czytko, H.; Weiler, E. W. Cloning, molecular and functional characterization of *Arabidopsis thaliana* allene oxide synthase (CYP 74), the first enzyme of the octadecanoid pathway to jasmonates. *Plant Molecular Biology* **1996**, *31* (2), 323-335. DOI: 10.1007/BF00021793.

(6) Stenzel, I.; Hause, B.; Miersch, O.; Kurz, T.; Maucher, H.; Weichert, H.; Ziegler, J.; Feussner, I.; Wasternack, C. Jasmonate biosynthesis and the allene oxide cyclase family of *Arabidopsis thaliana*. *Plant Molecular Biology* **2003**, *51* (6), 895-911. DOI: 10.1023/A:1023049319723.

(7) Stintzi, A.; Browse, J. The *Arabidopsis* male-sterile mutant, *opr3*, lacks the 12-oxophytodienoic acid reductase required for jasmonate synthesis. *Proceedings of the*

National Academy of Sciences **2000**, *97* (19), 10625-10630. DOI: 10.1073/pnas.190264497.

(8) Staswick, P. E.; Tiryaki, I. The Oxylipin Signal Jasmonic Acid Is Activated by an Enzyme That Conjugates It to Isoleucine in *Arabidopsis*. *The Plant Cell* **2004**, *16* (8), 2117-2127. DOI: 10.1105/tpc.104.023549.

(9) Seo, H. S.; Song, J. T.; Cheong, J.-J.; Lee, Y.-H.; Lee, Y.-W.; Hwang, I.; Lee, J. S.; Choi, Y. D. Jasmonic acid carboxyl methyltransferase: A key enzyme for jasmonate-regulated plant responses. *Proceedings of the National Academy of Sciences* **2001**, *98* (8), 4788-4793. DOI: 10.1073/pnas.081557298.

(10) Stuhlfelder, C.; Lottspeich, F.; Mueller, M. J. Purification and partial amino acid sequences of an esterase from tomato. *Phytochemistry* **2002**, *60* (3), 233-240. DOI: 10.1016/s0031-9422(02)00126-7

(11) Chini, A.; Monte, I.; Zamarreño, A. M.; Hamberg, M.; Lassueur, S.; Reymond, P.; Weiss, S.; Stintzi, A.; Schaller, A.; Porzel, A.; García-Mina, J. M.; Solano, R. An OPR3-independent pathway uses 4,5-didehydrojasmonate for jasmonate synthesis. *Nature Chemical Biology* **2018**, *14* (2), 171-178. DOI: 10.1038/nchembio.2540.

(12) Thines, B.; Katsir, L.; Melotto, M.; Niu, Y.; Mandaokar, A.; Liu, G.; Nomura, K.; He, S. Y.; Howe, G. A.; Browse, J. JAZ repressor proteins are targets of the SCFCOI1 complex during jasmonate signalling. *Nature* **2007**, *448* (7154), 661-665. DOI: 10.1038/nature05960.

(13) Zheng, N.; Schulman, B. A.; Song, L.; Miller, J. J.; Jeffrey, P. D.; Wang, P.; Chu, C.; Koepp, D. M.; Elledge, S. J.; Pagano, M.; et al. Structure of the Cul1–Rbx1–Skp1–F boxSkp2 SCF ubiquitin ligase complex. *Nature* **2002**, *416* (6882), 703-709. DOI: 10.1038/416703a.

(14) Ruzicka, L.; Pfeiffer, M. Über Jasminriechstoffe I. Die Konstitution des Jasmons.

Helvetica Chimica Acta **1933**, *16* (1), 1208-1214. DOI: https://doi.org/10.1002/hlca.193301601153.

(15) Demole, E.; Lederer, E.; Mercier, D. Isolement et détermination de la structure du jasmonate de méthyle, constituant odorant caractéristique de l'essence de jasmin. *Helvetica Chimica Acta* **1962**, *45* (2), 675-685. DOI: 10.1002/hlca.19620450233.

(16) Dąbrowska, P.; Boland, W. *iso*-OPDA: An Early Precursor of *cis*-Jasmone in Plants? *ChemBioChem* **2007**, *8* (18), 2281-2285. DOI: https://doi.org/10.1002/cbic.200700464.

(17) Birkett, M. A.; Campbell, C. A. M.; Chamberlain, K.; Guerrieri, E.; Hick, A. J.; Martin, J. L.; Matthes, M.; Napier, J. A.; Pettersson, J.; Pickett, J. A.; Poppy, G. M.; Pow, E. M.; Pye, B. J.; Smart, L. E.; Wadhams, G. H.; Wadhams, L. J.; Woodcock, C. M. New roles for *cis*-jasmone as an insect semiochemical and in plant defense. *Proceedings of the National Academy of Sciences* **2000**, *97* (16), 9329-9334. DOI: 10.1073/pnas.160241697.

(18) Ali, J.; Covaci, A. D.; Roberts, J. M.; Sobhy, I. S.; Kirk, W. D. J.; Bruce, T. J. A. Effects of *cis*-Jasmone Treatment of Brassicas on Interactions With *Myzus persicae* Aphids and Their Parasitoid *Diaeretiella rapae*. *Frontiers in Plant Science* **2021**, *12*. DOI: 10.3389/fpls.2021.711896.

(19) Agbessenou, A.; Akutse, K. S.; Yusuf, A. A.; Khamis, F. M. The Endophyte *Trichoderma asperellum* M2RT4 Induces the Systemic Release of Methyl Salicylate and (Z)-jasmone in Tomato Plant Affecting Host Location and Herbivory of *Tuta absoluta*. *Frontiers in Plant Science* **2022**, *13*. DOI: 10.3389/fpls.2022.860309.

(20) Moraes, M. C. B.; Birkett, M. A.; Gordon-Weeks, R.; Smart, L. E.; Martin, J. L.; Pye, B. J.; Bromilow, R.; Pickett, J. A. *cis*-Jasmone induces accumulation of defence compounds in wheat, *Triticum aestivum*. *Phytochemistry* **2008**, *69* (1), 9-17. DOI: 10.1016/j.phytochem.2007.06.020.

(21) Matthes, M. C.; Bruce, T. J. A.; Ton, J.; Verrier, P. J.; Pickett, J. A.; Napier, J. A. The transcriptome of *cis*-jasmone-induced resistance in *Arabidopsis thaliana* and its role in indirect defence. *Planta* **2010**, *232* (5), 1163-1180. DOI: 10.1007/s00425-010-1244-4.

(22) Koch, T.; Bandemer, K.; Boland, W. Biosynthesis of *cis*-Jasmone: a pathway for the inactivation and the disposal of the plant stress hormone jasmonic acid to the gas phase? *Helvetica Chimica Acta* **1997**, *80* (3), 838-850. DOI: 10.1002/hlca.19970800318.

(23) Matsui, R.; Takiguchi, K.; Kuwata, N.; Oki, K.; Takahashi, K.; Matsuda, K.; Matsuura, H. Jasmonic acid is not a biosynthetic intermediate to produce the pyrethrolone moiety in pyrethrin II. *Scientific Reports* **2020**, *10* (1). DOI: 10.1038/s41598-020-63026-3.

(24) Lybrand, D. B.; Xu, H.; Last, R. L.; Pichersky, E. How Plants Synthesize Pyrethrins: Safe and Biodegradable Insecticides. *Trends in Plant Science* **2020**, *25* (12), 1240-1251. DOI: 10.1016/j.tplants.2020.06.012.

(25) Kikuta, Y.; Ueda, H.; Takahashi, M.; Mitsumori, T.; Yamada, G.; Sakamori, K.; Takeda, K.; Furutani, S.; Nakayama, K.; Katsuda, Y.; et al. Identification and characterization of a GDSL lipase-like protein that catalyzes the ester-forming reaction for pyrethrin biosynthesis in Tanacetum cinerariifolium– a new target for plant protection. *The Plant Journal* **2012**, *71* (2), 183-193. DOI: 10.1111/j.1365-313X.2012.04980.x.

(26) Rivera, S. B.; Swedlund, B. D.; King, G. J.; Bell, R. N.; Hussey, C. E.; Shattuck-Eidens, D. M.; Wrobel, W. M.; Peiser, G. D.; Poulter, C. D. Chrysanthemyl diphosphate synthase: Isolation of the gene and characterization of the recombinant non-head-to-tail monoterpene synthase from *Chrysanthemum cinerariaefolium*. *Proceedings of the National Academy of Sciences* **2001**, *98* (8), 4373-4378. DOI: 10.1073/pnas.071543598.

(27) Xu, H.; Li, W.; Schilmiller, A. L.; Van Eekelen, H.; De Vos, R. C. H.; Jongsma, M. A.; Pichersky, E. Pyrethric acid of natural pyrethrin insecticide: complete pathway elucidation

and reconstitution in *Nicotiana benthamiana*. *New Phytologist* **2019**, *223* (2), 751-765. DOI: 10.1111/nph.15821.

(28) Xu, H.; Moghe, G. D.; Wiegert-Rininger, K.; Schilmiller, A. L.; Barry, C. S.; Last, R. L.; Pichersky, E. Coexpression Analysis Identifies Two Oxidoreductases Involved in the Biosynthesis of the Monoterpene Acid Moiety of Natural Pyrethrin Insecticides in *Tanacetum cinerariifolium*. *Plant Physiology* **2017**, *176* (1), 524-537. DOI: 10.1104/pp.17.01330

(29) Li, W.; Zhou, F.; Pichersky, E. Jasmone Hydroxylase, a Key Enzyme in the Synthesis of the Alcohol Moiety of Pyrethrin Insecticides. *Plant Physiol* **2018**, *177* (4), 1498-1509. DOI: 10.1104/pp.18.00748

(30) Li, W.; Lybrand, D. B.; Zhou, F.; Last, R. L.; Pichersky, E. Pyrethrin Biosynthesis: The Cytochrome P450 Oxidoreductase CYP82Q3 Converts Jasmolone To Pyrethrolone. *Plant Physiol* **2019**, *181* (3), 934-944. DOI: 10.1104/pp.19.00499

(31) Bowman, J. L.; Kohchi, T.; Yamato, K. T.; Jenkins, J.; Shu, S.; Ishizaki, K.; Yamaoka, S.; Nishihama, R.; Nakamura, Y.; Berger, F.; Adam, C.; Sugamata Aki, S.; Althoff, F.; Araki, T.; Arteaga-Vazquez, M. A.; Balasubrmanian, S.; Barry, K.; Bauer, D.; Boehm, C. R.; Briginshaw, L.; Schmutz, J. Insights into Land Plant Evolution Garnered from the *Marchantia polymorpha* Genome. *Cell* **2017**, *171* (2), 287-304.e215. DOI: 10.1016/j.cell.2017.09.030.

(32) Yamamoto, Y.; Ohshika, J.; Takahashi, T.; Ishizaki, K.; Kohchi, T.; Matusuura, H.; Takahashi, K. Functional analysis of allene oxide cyclase, MpAOC, in the liverwort *Marchantia polymorpha*. *Phytochemistry* **2015**, *116*, 48-56. DOI: 10.1016/j.phytochem.2015.03.008.

(33) Monte, I.; Ishida, S.; Zamarreño, A. M.; Hamberg, M.; Franco-Zorrilla, J. M.; García-

Casado, G.; Gouhier-Darimont, C.; Reymond, P.; Takahashi, K.; García-Mina, J. M.; Nishihama, R.; Kohchi, T.; Solano, R. Ligand-receptor co-evolution shaped the jasmonate pathway in land plants. *Nature Chemical Biology* **2018**, *14* (5), 480-488. DOI: 10.1038/s41589-018-0033-4.

(34) Monte, I.; Caballero, J.; Zamarreño, A. M.; Fernández-Barbero, G.; García-Mina, J. M.; Solano, R. JAZ is essential for ligand specificity of the COI1/JAZ co-receptor. *Proceedings of the National Academy of Sciences* **2022**, *119* (49), e2212155119. DOI:10.1073/pnas.2212155119.

(35) Soriano, G.; Kneeshaw, S.; Jimenez-Aleman, G.; Zamarreño, Á. M.; Franco-Zorrilla, J. M.; Rey-Stolle, M. F.; Barbas, C.; García-Mina, J. M.; Solano, R. An evolutionarily ancient fatty acid desaturase is required for the synthesis of hexadecatrienoic acid, which is the main source of the bioactive jasmonate in *Marchantia polymorpha*. *New Phytologist* **2022**, *233* (3), 1401-1413. DOI: 10.1111/nph.17850.

(36) Lauchli, R.; Boland, W. Efficient synthesis of [$^2H_2$]-tetrahydrodicranenone B and a 3-oxa-analogue resistant against β-oxidation. *Tetrahedron* **2003**, *59* (2), 149-153. DOI: 10.1016/S0040-4020(02)01484-9.

(37) Tamogami, S.; Rakwal, R.; Agrawal, G. K. Interplant communication: Airborne methyl jasmonate is essentially converted into JA and JA-Ile activating jasmonate signaling pathway and VOCs emission. *Biochemical and Biophysical Research Communications* **2008**, *376* (4), 723-727. DOI: 10.1016/j.bbrc.2008.09.069.

(38) Oki, K.; Masimbula, R.; Miyawaki, K.; Takata, Y.; Takahashi, K.; Matsuura, H. 12OHJA, 12OGlcJA, and JA-L-Val as airborne MeJA metabolites. *Bioscience, Biotechnology, and Biochemistry* **2019**, *83* (9), 1709-1712. DOI: 10.1080/09168451.2019.1611408.

(39) Masimbula, R.; Oki, K.; Shibata, H.; Osawa, H.; Kondo, N.; Takahashi, K.; Matsuura,

H. Ability of plant pathogenic fungi *Gibberella fujikuroi* and *Fusarium commune* to react with airborne methyl jasmonate. *Bioscience, Biotechnology, and Biochemistry* **2019**, *83* (9), 1650-1654. DOI: 10.1080/09168451.2019.1617108.

(40) El-Sayed, A. M.; Mitchell, V. J.; McLaren, G. F.; Manning, L. M.; Bunn, B.; Suckling, D. M. Attraction of New Zealand Flower Thrips, Thrips obscuratus, to *cis*-Jasmone, a Volatile Identified from Japanese Honeysuckle Flowers. *Journal of Chemical Ecology* **2009**, *35* (6), 656-663. DOI: 10.1007/s10886-009-9619-3.

(41) Wu, L.-C.; Lin, C.-L.; Peng, C.-C.; Huang, T.-L.; Tsai, T.-H.; Kuan, Y.-E.; Chung, Y.-C. Development from *Jasminum sambac* Flower Extracts of Products with Floral Fragrance and Multiple Physiological Activities. *Evidence-Based Complementary and Alternative Medicine* **2021**, *2021*, 1-12. DOI: 10.1155/2021/7657628.

(42) Matsui, R.; Amano, N.; Takahashi, K.; Taguchi, Y.; Saburi, W.; Mori, H.; Kondo, N.; Matsuda, K.; Matsuura, H. Elucidation of the biosynthetic pathway of *cis*-jasmone in *Lasiodiplodia theobromae*. *Scientific Reports* **2017**, *7* (1). DOI: 10.1038/s41598-017-05851-7.

(43) Acheampong, A. K.; Zheng, C.; Halaly, T.; Giacomelli, L.; Takebayashi, Y.; Jikumaru, Y.; Kamiya, Y.; Lichter, A.; Or, E. Abnormal Endogenous Repression of GA Signaling in a Seedless Table Grape Cultivar with High Berry Growth Response to GA Application. *Frontiers in Plant Science* **2017**, *8*. DOI: 10.3389/fpls.2017.00850.

(44) Liu, W.; Li, T.; Yuan, H.; Tan, D.; Wang, A. Enhancement of apple coloration using jasmonate treatment without sacrificing storage potential. *Plant Signaling & Behavior* **2018**, *13* (1), e1422467. DOI: 10.1080/15592324.2017.1422467.

(45) Gundlach, H.; Müller, M. J.; Kutchan, T. M.; Zenk, M. H. Jasmonic acid is a signal transducer in elicitor-induced plant cell cultures. *Proceedings of the National Academy of*

Sciences **1992**, *89* (6), 2389-2393. DOI: doi:10.1073/pnas.89.6.2389.

(46) van Butselaar, T.; Van den Ackerveken, G. Salicylic Acid Steers the Growth&Immunity Tradeoff. *Trends in Plant Science* **2020**, *25* (6), 566-576. DOI: 10.1016/j.tplants.2020.02.002

(47) Fu, Z. Q.; Dong, X. Systemic Acquired Resistance: Turning Local Infection into Global Defense. *Annual Review of Plant Biology* **2013**, *64*, 839-863. DOI: 10.1146/annurev-arplant-042811-105606.

(48) Cutler, S. R.; Rodriguez, P. L.; Finkelstein, R. R.; Abrams, S. R. Abscisic Acid: Emergence of a Core Signaling Network. *Annual Review of Plant Biology* **2010**, *61*, 651-679. DOI: 10.1146/annurev-arplant-042809-112122.

(49) Grdiša, M.; Babić, S.; Periša, M.; Carović-Stanko, K.; Kolak, I.; Liber, Z.; Jug-Dujaković, M.; Satovic, Z. Chemical Diversity of the Natural Populations of Dalmatian Pyrethrum (*Tanacetum cinerariifolium* (Trevir.) Sch.Bip.) in Croatia. *Chemistry & Biodiversity* **2013**, *10* (3), 460-472. DOI: 10.1002/cbdv.201200015.

(50) Yu, D.; Wildhagen, H.; Tylewicz, S.; Miskolczi, P. C.; Bhalerao, R. P.; Polle, A. Abscisic acid signalling mediates biomass trade-off and allocation in poplar. *New Phytologist* **2019**, *223* (3), 1192-1203. DOI: 10.1111/nph.15878.

(51) Yamashita, Y.; Ota, M.; Inoue, Y.; Hasebe, Y.; Okamoto, M.; Inukai, T.; Masuta, C.; Sakihama, Y.; Hashidoko, Y.; Kojima, M.; Sakakibara, H.; Inage, Y.; Takahashi, K.; Yoshihara, T.; Matsuura, H. Chemical Promotion of Endogenous Amounts of ABA in *Arabidopsis thaliana* by a Natural Product, Theobroxide. *Plant and Cell Physiology* **2016**, *57* (5), 986-999. DOI: 10.1093/pcp/pcw037.

(52) Hirota, S.; Ito, Y.; Inoue, S.; Kitaoka, N.; Taniguchi, T.; Monde, K.; Takahashi, K.; Matsuura, H. Isolation and Structure Determination of *cis*-OPDA-α-Monoglyceride from

Arabidopsis thaliana. *Journal of Natural Products* **2024**, *87* (5), 1358-1367. DOI: 10.1021/acs.jnatprod.3c01237.

(53) Tsuzuki, H.; Kitaoka, N.; Inoue, S.; Takahashi, K.; Matsuura, H. Airborne Methyl Jasmonate is Metabolized to Jasmonic Acid and 12-Hydroxyjasmonic Acid, and Induces Jasmonate Biosynthesis in *Marchantia polymorpha*. *ChemistrySelect* **2023**, *8* (21), e202300117. DOI: 10.1002/slct.202300117.

(54) Ersalena, V. F.; Kitaoka, N.; Matsuura, H. Unveiling the presence of jasmonoyl-L-isoleucine in 3 species of moss belonging to Bryophytes. *Bioscience, Biotechnology, and Biochemistry* **2025**, *89* (8), 1177-1181. DOI: 10.1093/bbb/zbaf072

(55) Miyawaki, K.; Inoue, S.; Kitaoka, N.; Matsuura, H. Potato tuber-inducing activities of jasmonic acid and related-compounds (II). *Bioscience, Biotechnology, and Biochemistry* **2021**, *85* (12), 2378-2382. DOI: 10.1093/bbb/zbab161 (acccessed 12/8/2025).

(56) Mukhtarova, L. S.; Lantsova, N. V.; Khairutdinov, B. I.; Grechkin, A. N. Lipoxygenase pathway in model bryophytes: 12-oxo-9(13),15-phytodienoic acid is a predominant oxylipin in *Physcomitrella patens*. *Phytochemistry* **2020**, *180*, 112533. DOI:10.1016/j.phytochem.2020.112533.

(57) Chini, A.; Monte, I.; Zamarreño, A. M.; García-Mina, J. M.; Solano, R. Evolution of the jasmonate ligands and their biosynthetic pathways. *New Phytologist* **2023**, *238* (5), 2236-2246. DOI: 10.1111/nph.18891.

(58) Ueda, H.; Matsuda, K. VOC-mediated within-plant communications and nonvolatile systemic signals upregulate pyrethrin biosynthesis in wounded seedlings of *Chrysanthemum cinerariaefolium*. *Journal of Plant Interactions* **2011**, *6* (2-3), 89-91. DOI: 10.1080/17429145.2011.555566.

(59) Kikuta, Y.; Ueda, H.; Nakayama, K.; Katsuda, Y.; Ozawa, R.; Takabayashi, J.;

Hatanaka, A.; Matsuda, K. Specific Regulation of Pyrethrin Biosynthesis in *Chrysanthemum cinerariaefolium* by a Blend of Volatiles Emitted from Artificially Damaged Conspecific Plants. *Plant and Cell Physiology* **2011**, *52* (3), 588-596. DOI: 10.1093/pcp/pcr017.

(60) Geilfus, C.-M. The pH of the Apoplast: Dynamic Factor with Functional Impact Under Stress. *Molecular Plant* **2017**, *10* (11), 1371-1386. DOI: 10.1016/j.molp.2017.09.018.

(61) Karuppanapandian, T.; Geilfus, C. M.; Mühling, K. H.; Novák, O.; Gloser, V. Early changes of the pH of the apoplast are different in leaves, stem and roots of *Vicia faba L*. under declining water availability. *Plant Science* **2017**, *255*, 51-58. DOI:10.1016/j.plantsci.2016.11.010.

(62) Cai, S.; Jiang, G.; Ye, N.; Chu, Z.; Xu, X.; Zhang, J.; Zhu, G. A Key ABA Catabolic Gene, *OsABA8ox3*, Is Involved in Drought Stress Resistance in Rice. *PLOS ONE* **2015**, *10* (2), e0116646. DOI: 10.1371/journal.pone.0116646.

(63) Chen, L.; Zhang, B.; Xia, L.; Yue, D.; Han, B.; Sun, W.; Wang, F.; Lindsey, K.; Zhang, X.; Yang, X. The GhMAP3K62-GhMKK16-GhMPK32 kinase cascade regulates drought tolerance by activating GhEDT1-mediated ABA accumulation in cotton. *Journal of Advanced Research* **2023**, *51*, 13-25. DOI: https://doi.org/10.1016/j.jare.2022.11.002.

(64) Turečková, V.; Novák, O.; Strnad, M. Profiling ABA metabolites in *Nicotiana tabacum L.* leaves by ultra-performance liquid chromatography–electrospray tandem mass spectrometry. *Talanta* **2009**, *80* (1), 390-399. DOI: 10.1016/j.talanta.2009.06.027.

(65) Perreca, E.; Rohwer, J.; González-Cabanelas, D.; Loreto, F.; Schmidt, A.; Gershenzon, J.; Wright, L. P. Effect of Drought on the Methylerythritol 4-Phosphate (MEP) Pathway in the Isoprene Emitting Conifer *Picea glauca*. *Frontiers in Plant Science* **2020**, *Volume 11 - 2020*, Original Research. DOI: 10.3389/fpls.2020.546295.

7. Acknowledgement

I would like to express my sincere gratitude to my supervisor, Professor Dr. Hideyuki Matsuura for his continuous guidance, encouragement, and insightful discussions during my study.

I am also deeply grateful to Associate Professor. Dr. Naoki Kitaoka for his valuable comments and constructive suggestions.

I am sincerely grateful to Dr. John Charles Dauria, Team Leader of the Metabolic Diversity Team at IPK, for his generous support and insightful discussions throughout my ten-month research stay.

I would like to thank Associate Professor, Dr. Wataru Sabori for his technical support in enzyme-related experiments, and Assistant Professor, Dr. Hayato Maruyama for his expertise and support in RNA-seq data analysis.

I really appreciate it Professor. Dr. Makoto Hashimoto, Professor. Dr. Yasuko Sakihama and Lecturer. Dr. Kengo Shigetomi for reviewing my thesis and thoughtful comments.

I also thank Dr. Eri Fukushi and Mr. Yusuke Takata for NMR and FD-MS measurements.

I would like to express my sincere gratitude to all the past and present members of the Laboratory of Natural product Chemistry for their support and togetherness.

This work was supported by the Hokkaido University–Hitachi Collaborative Research Support Program and the JSPS Research Fellowship for Young Scientists (DC2).

Finally, I would like to express my deepest gratitude to my family for their constant support and understanding throughout my doctoral studies.

8. Appendix

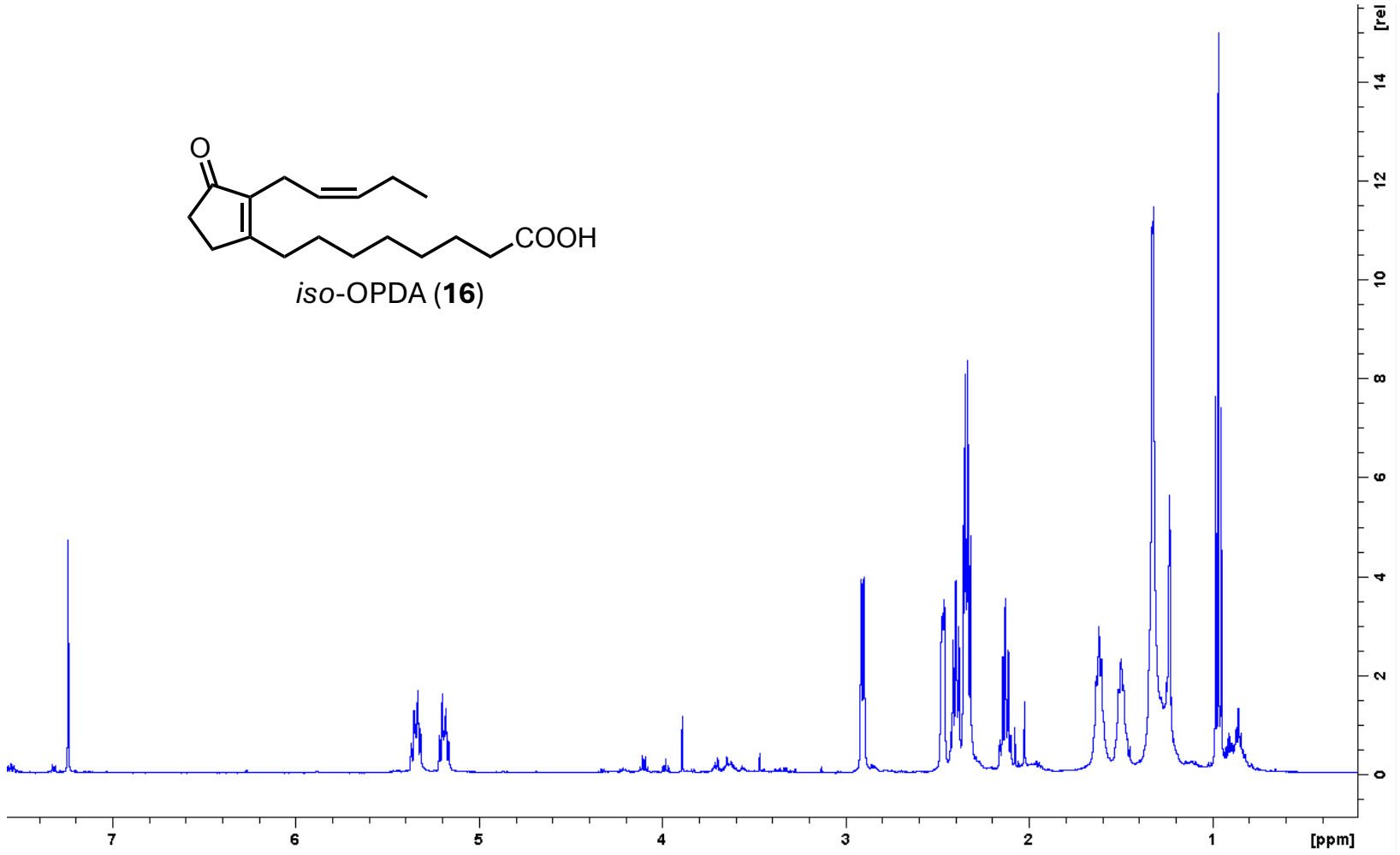

Chart 1: ^{1}H-NMR spectrum of *iso*-OPDA (16) in chapter 2

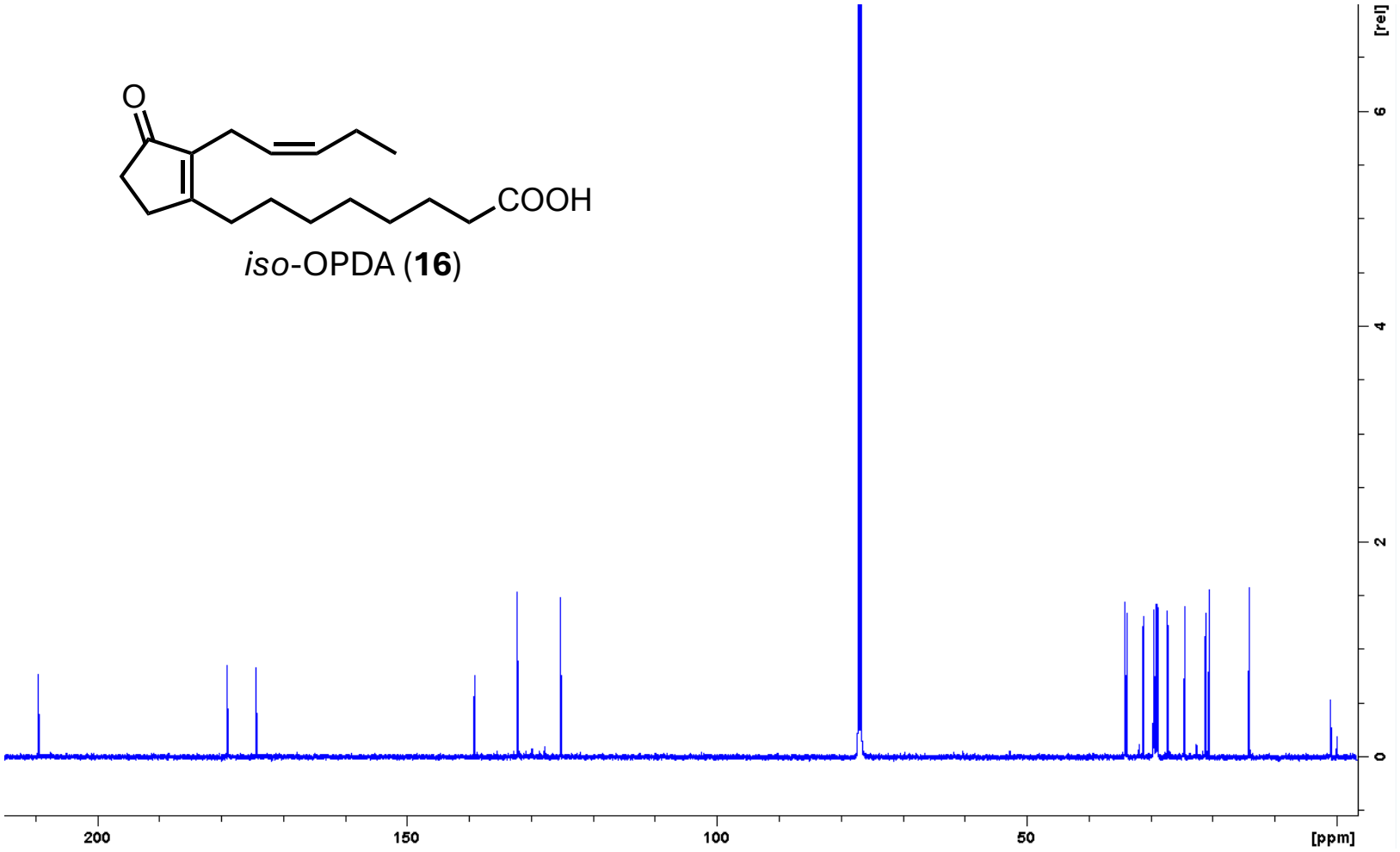

Chart 2: ^{13}C-NMR spectrum of *iso*-OPDA (16) in chapter 2

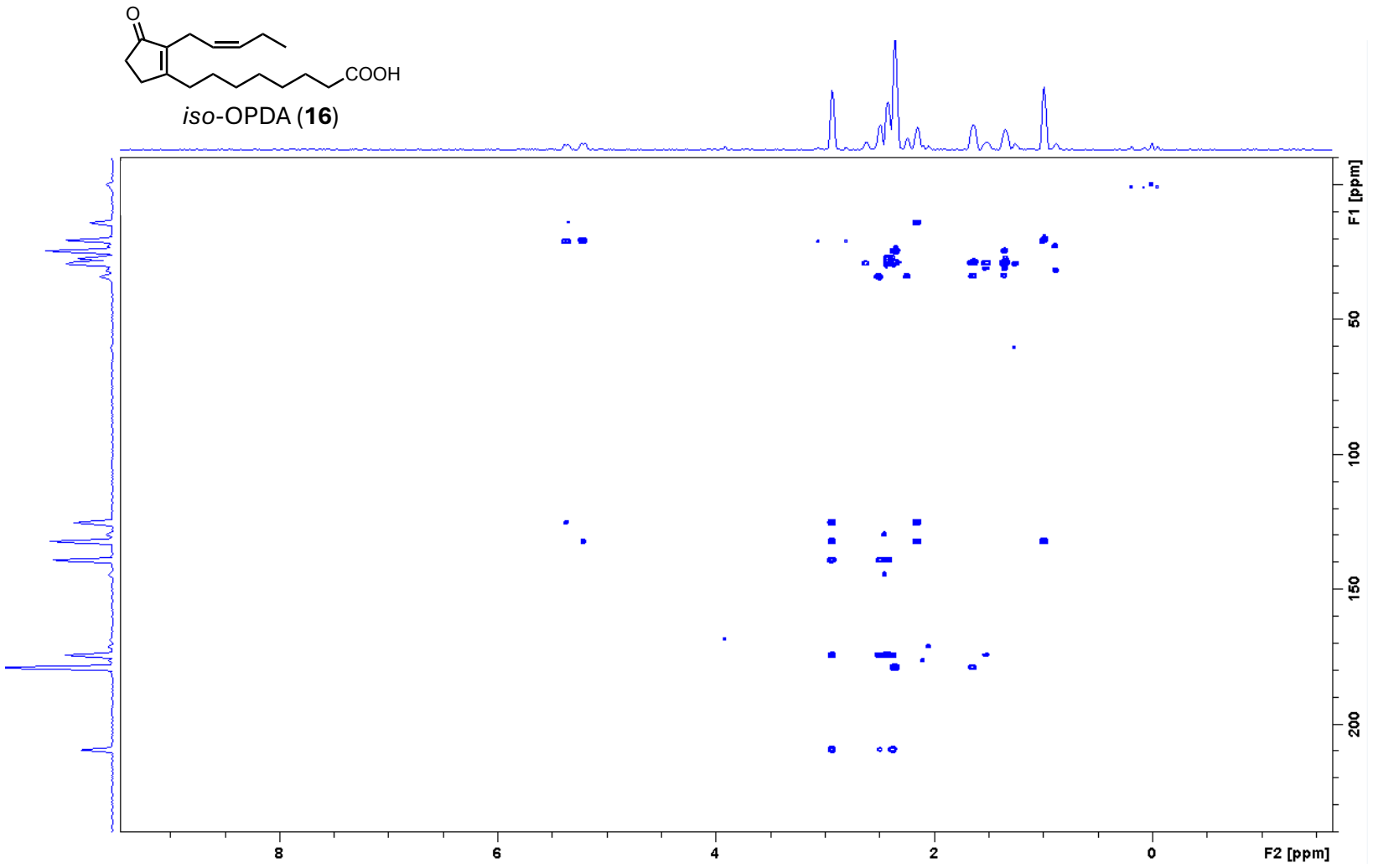

Chart 3: HMBC spectrum of *iso*-OPDA (16) in chapter 2

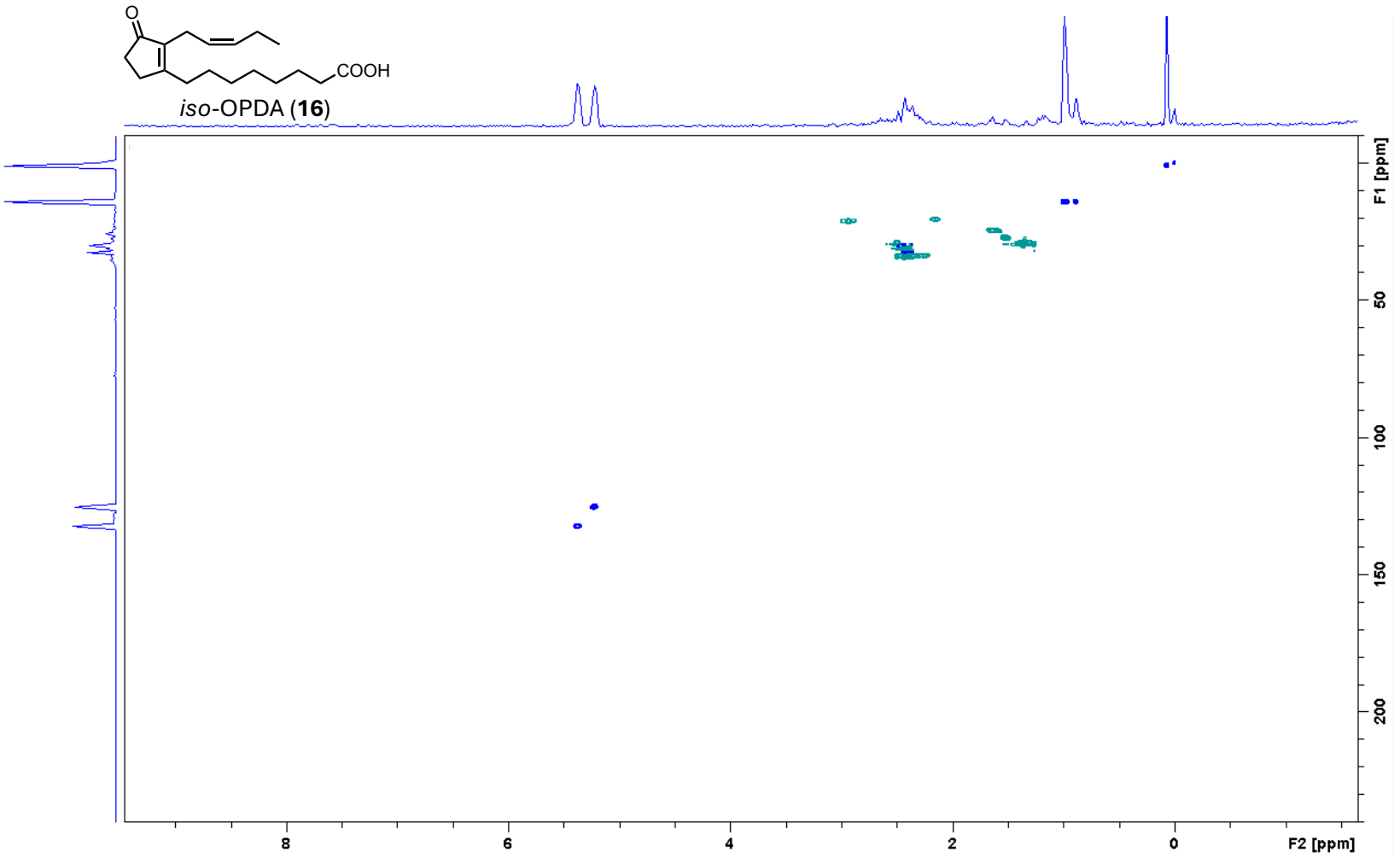

Chart 4: HSQC spectrum of *iso*-OPDA (16) in chapter 2

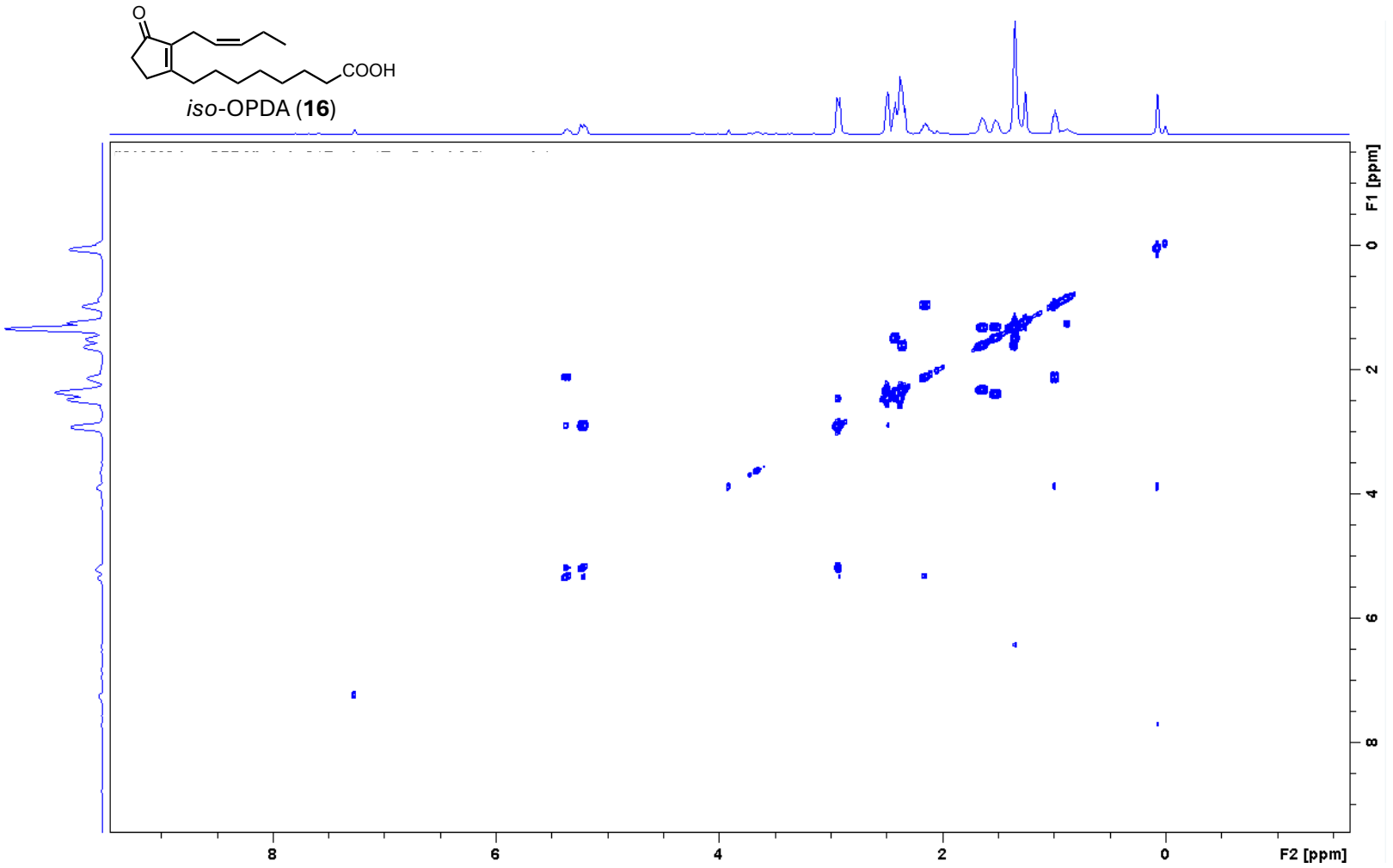

Chart 5: ^{1}H-^{1}H COSY spectrum of *iso*-OPDA (16) in chapter 2

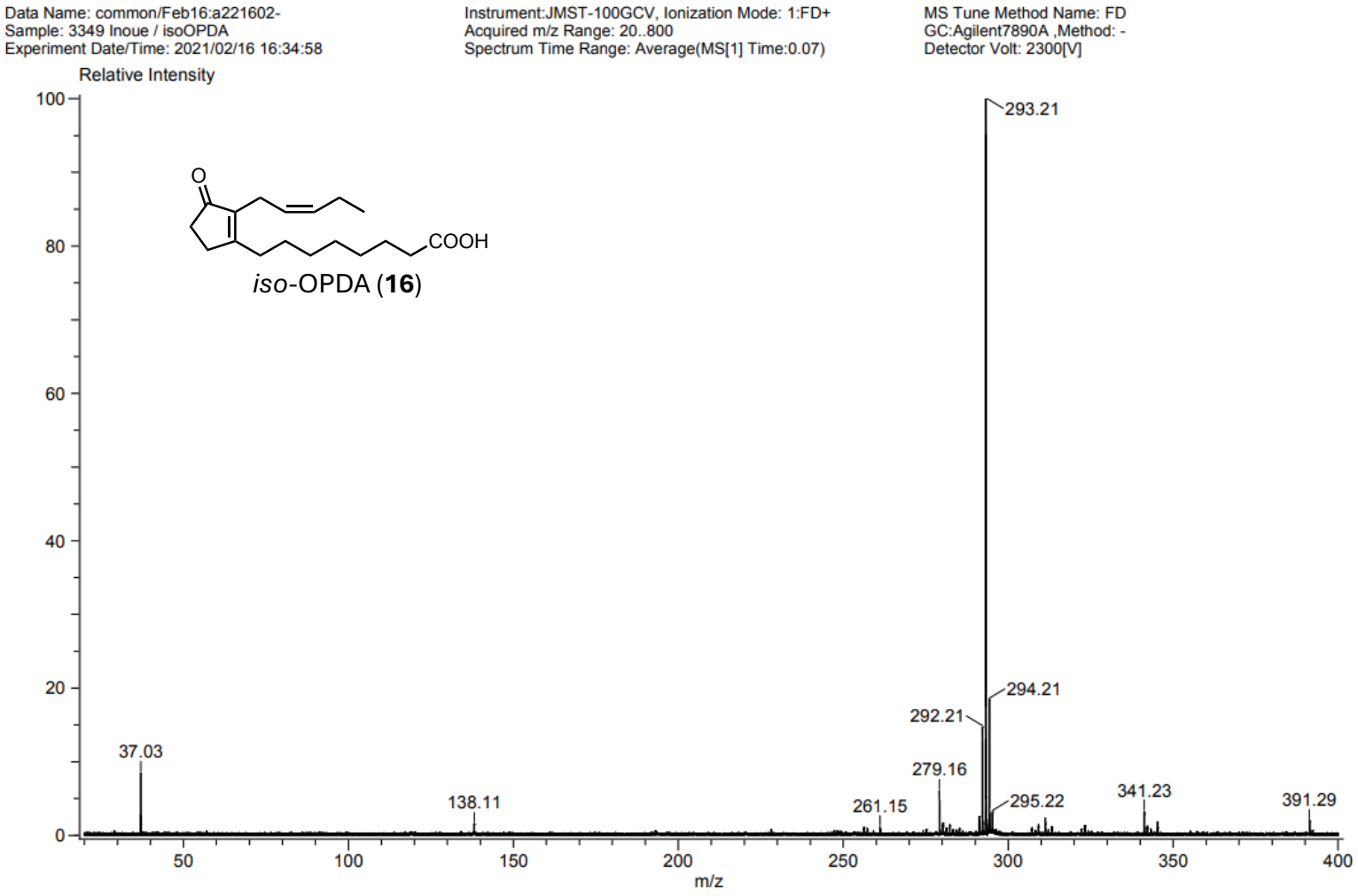

Chart 6: FD-MS spectrum of *iso*-OPDA (16) in chapter 2

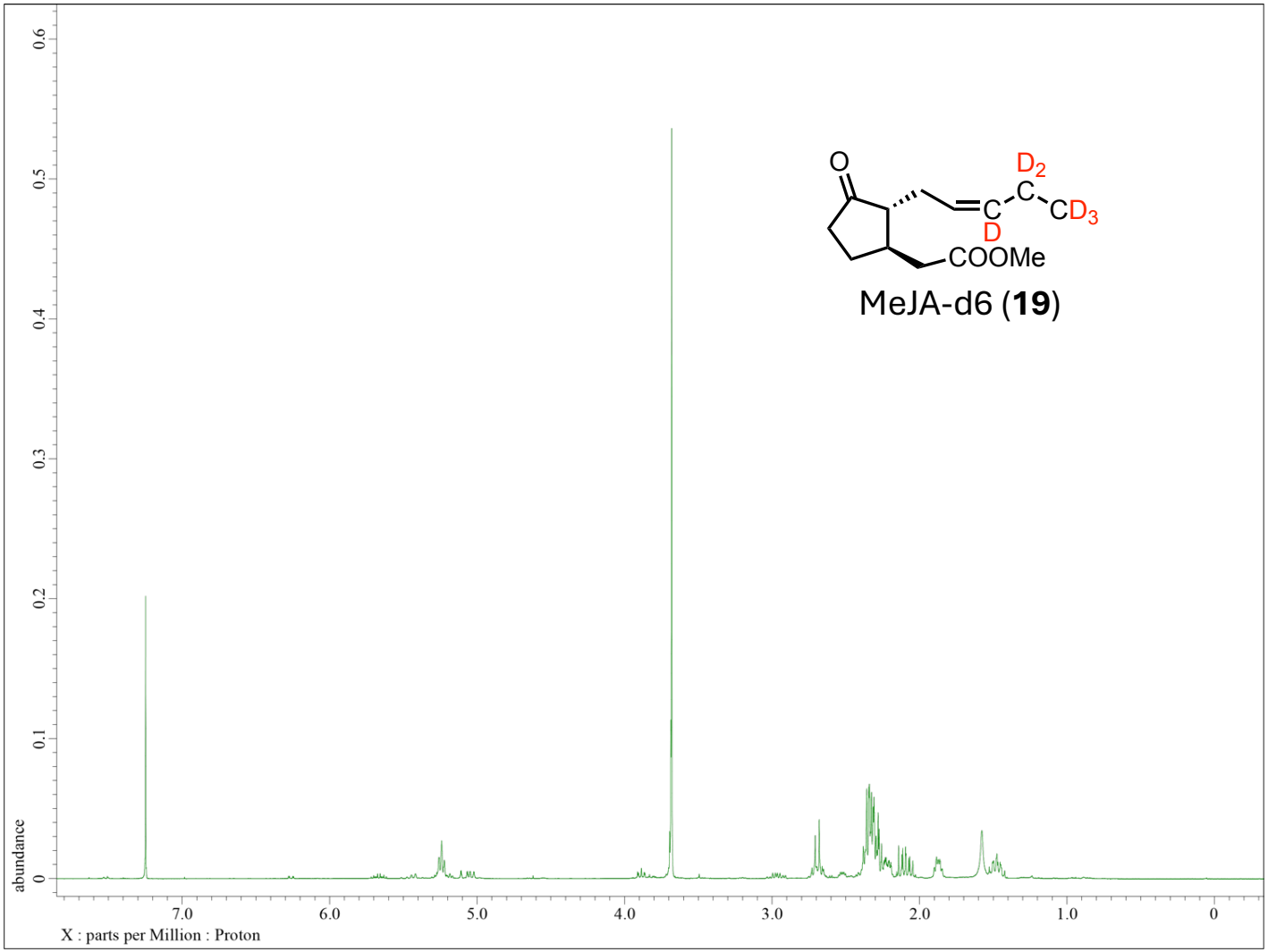

Chart 7: ^{1}H-NMR spectrum of MeJA-d6 (19) in chapter 3

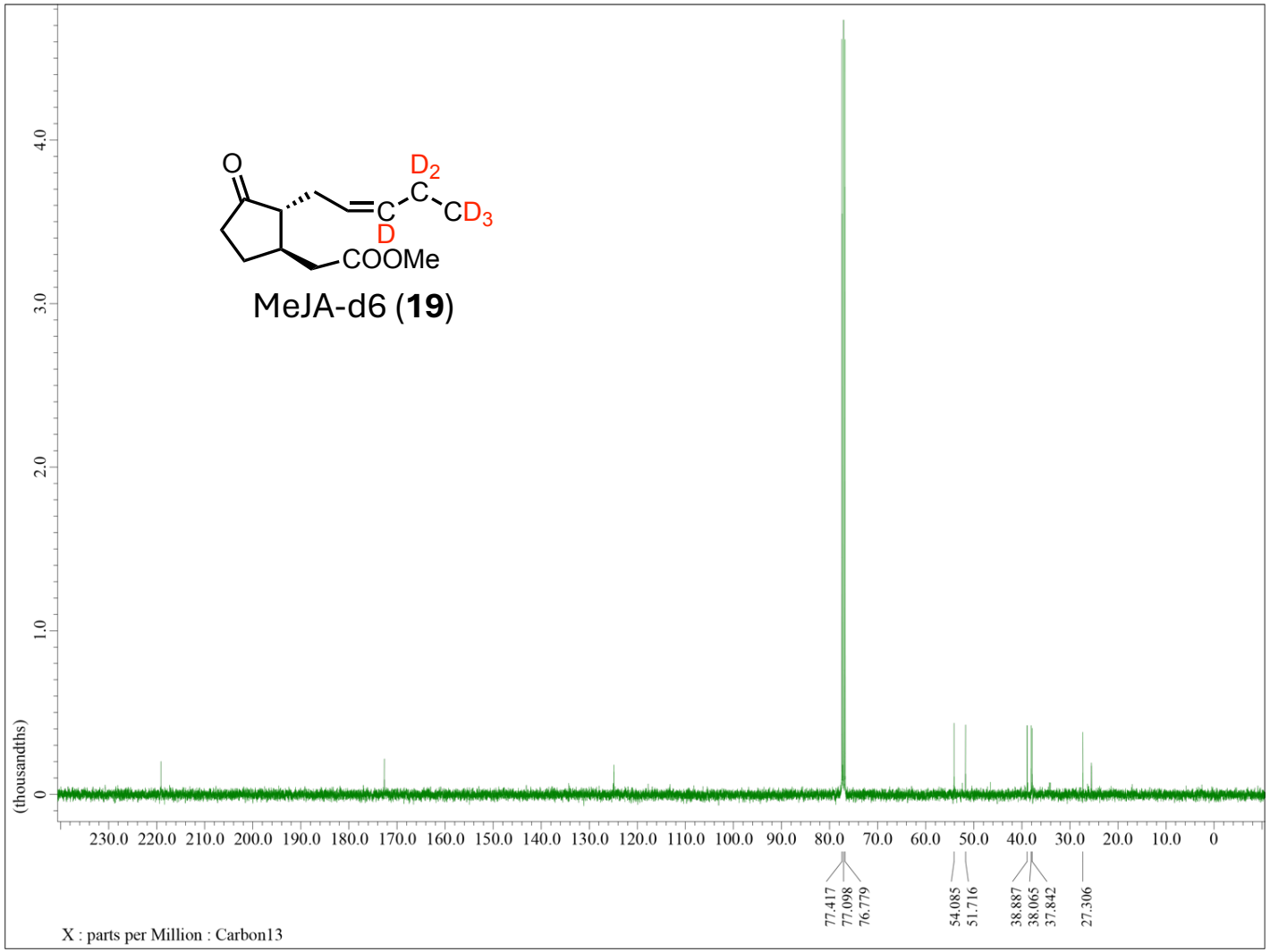

Chart 8: ^{13}C-NMR spectrum of MeJA-d6 (19) in chapter 3

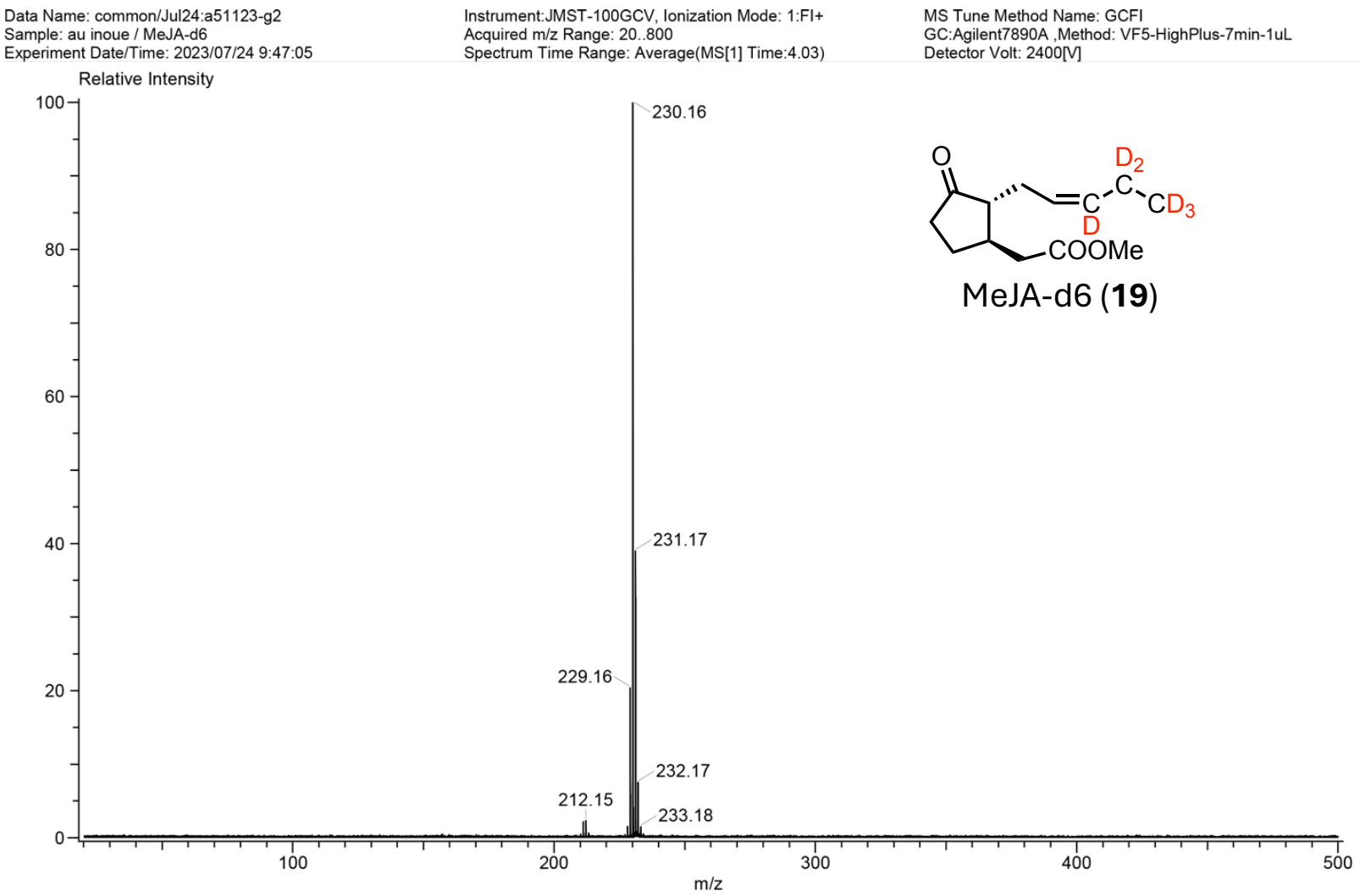

Chart 9: FD-MS spectrum of MeJA-d6 (19) in chapter 3

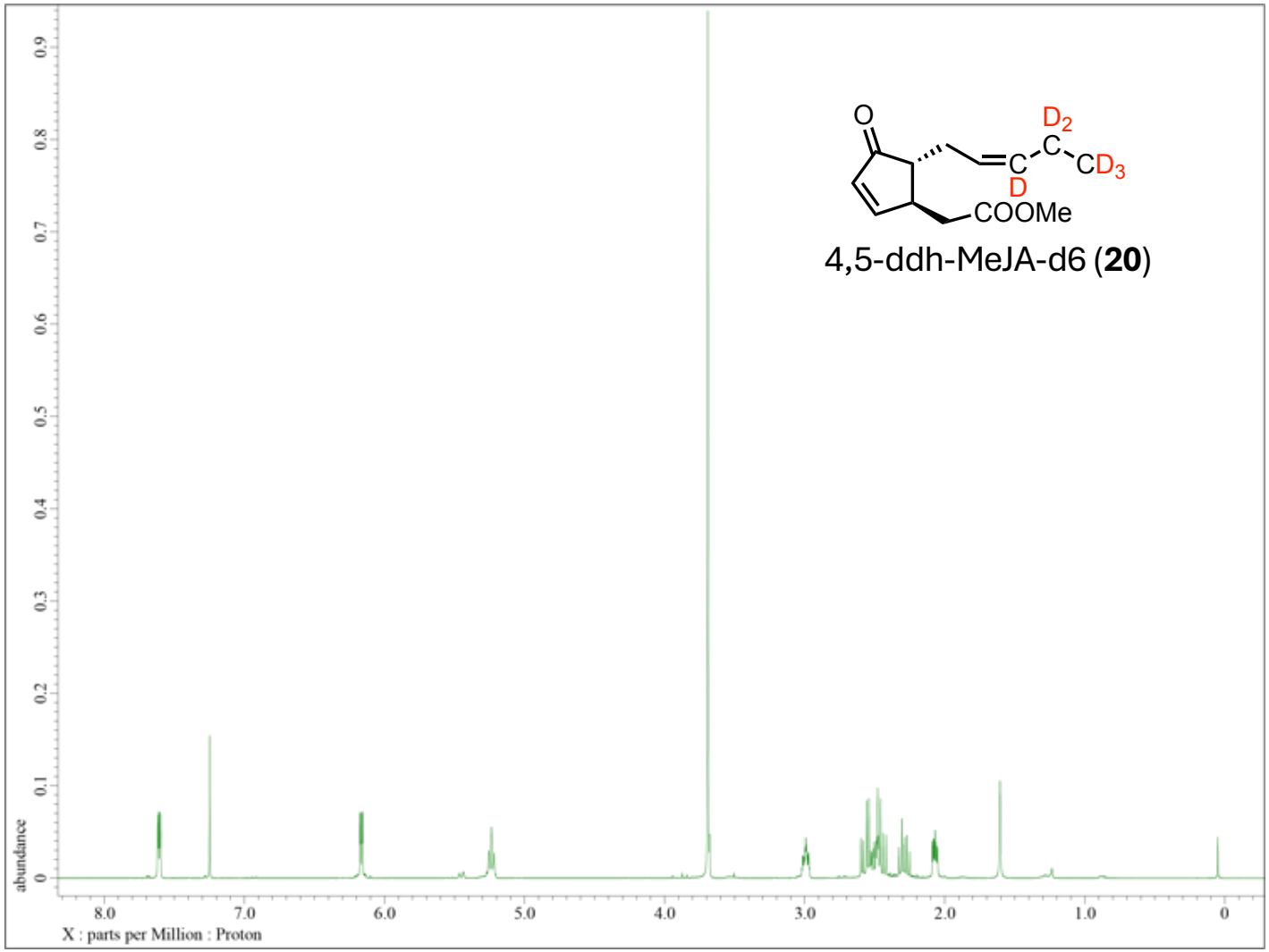

Chart 11: ^{13}C-NMR spectrum of 4,5-ddhMeJA-d6 (20) in chapter 3

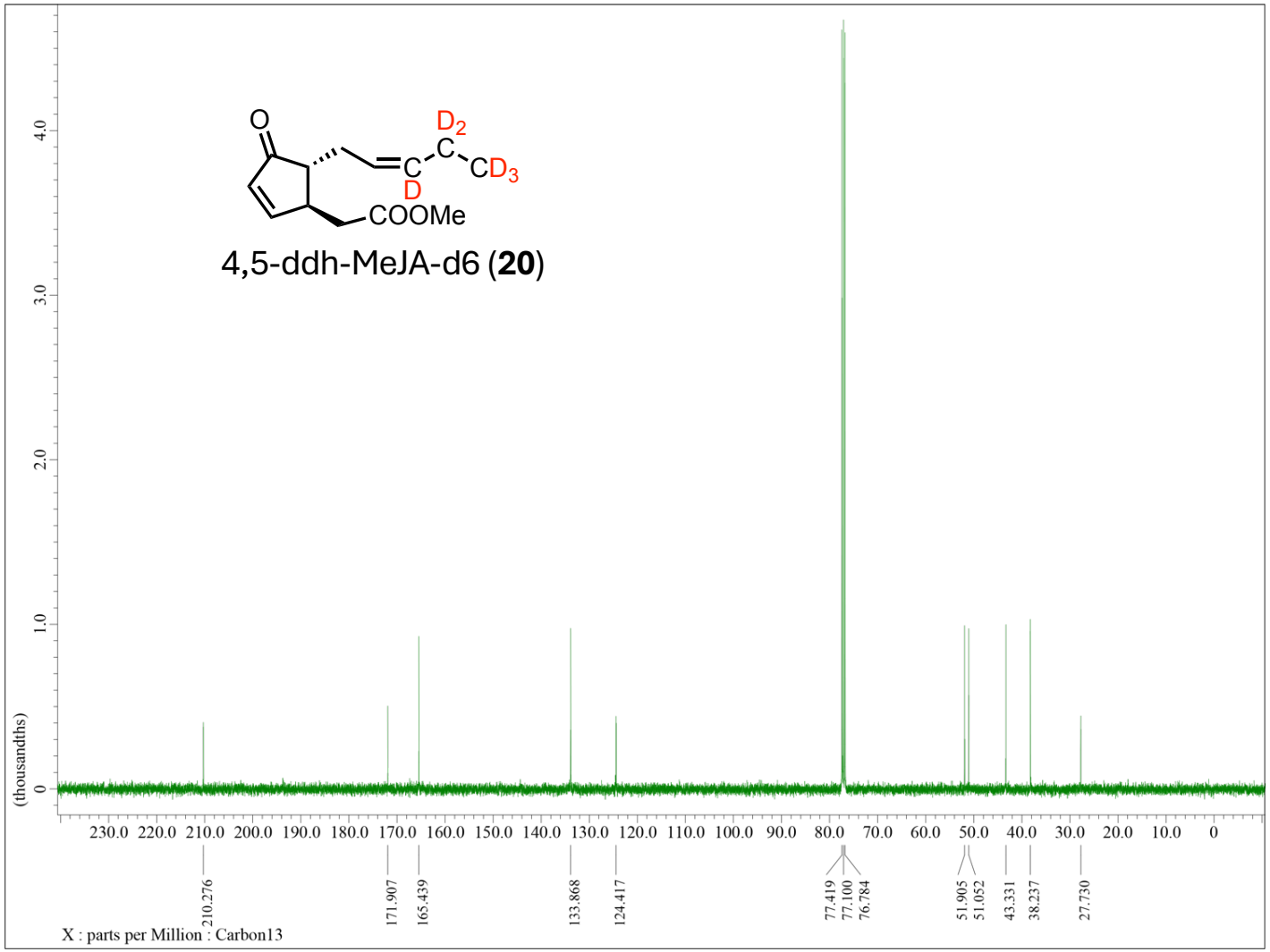

Chart 12: ^{13}C-NMR spectrum of 4,5-ddhMeJA-d6 (20) in chapter 3

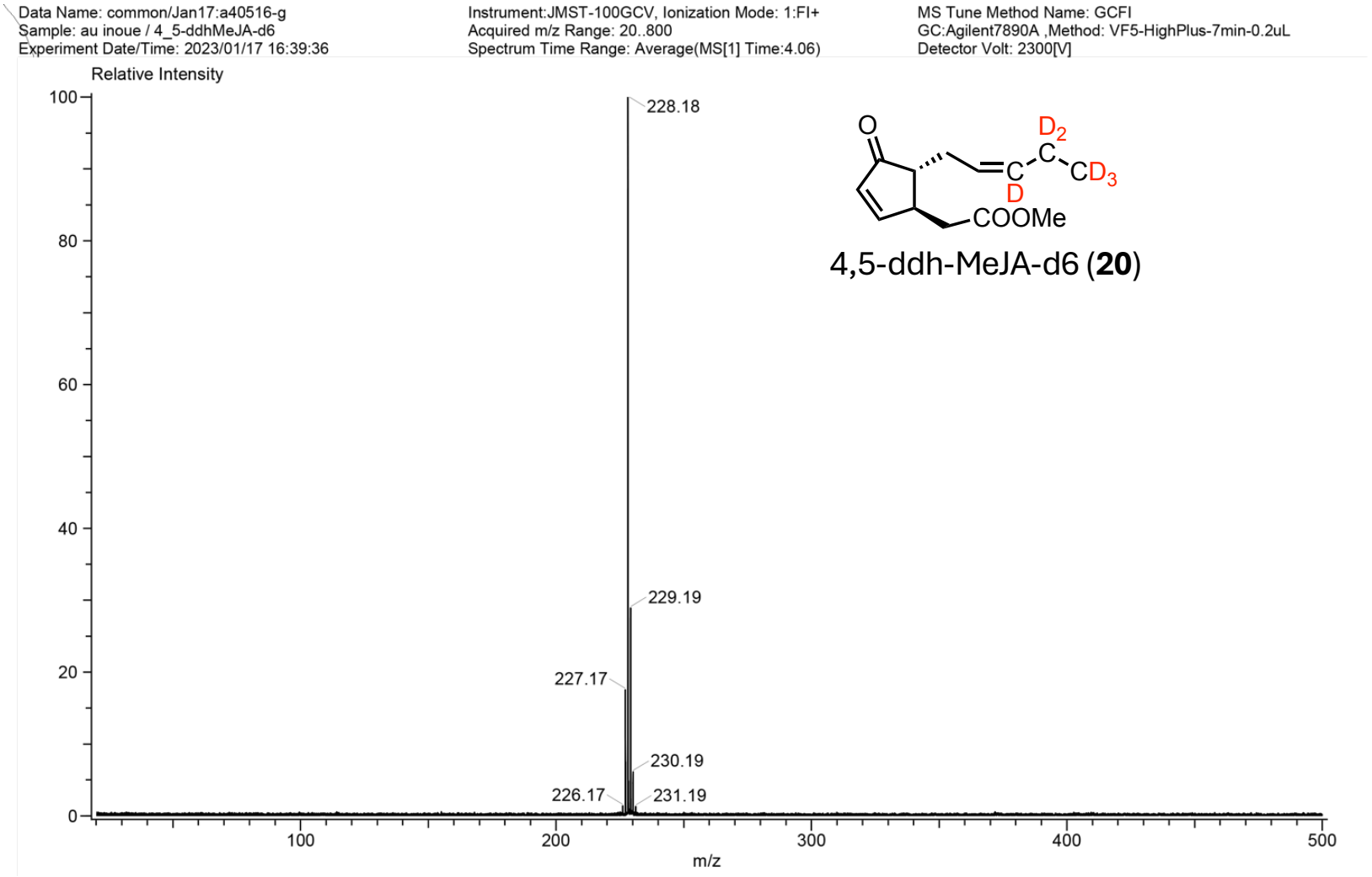

Chart 12: FD-MS spectrum of 4,5-ddh-MeJA-d6 (20) in chapter 3

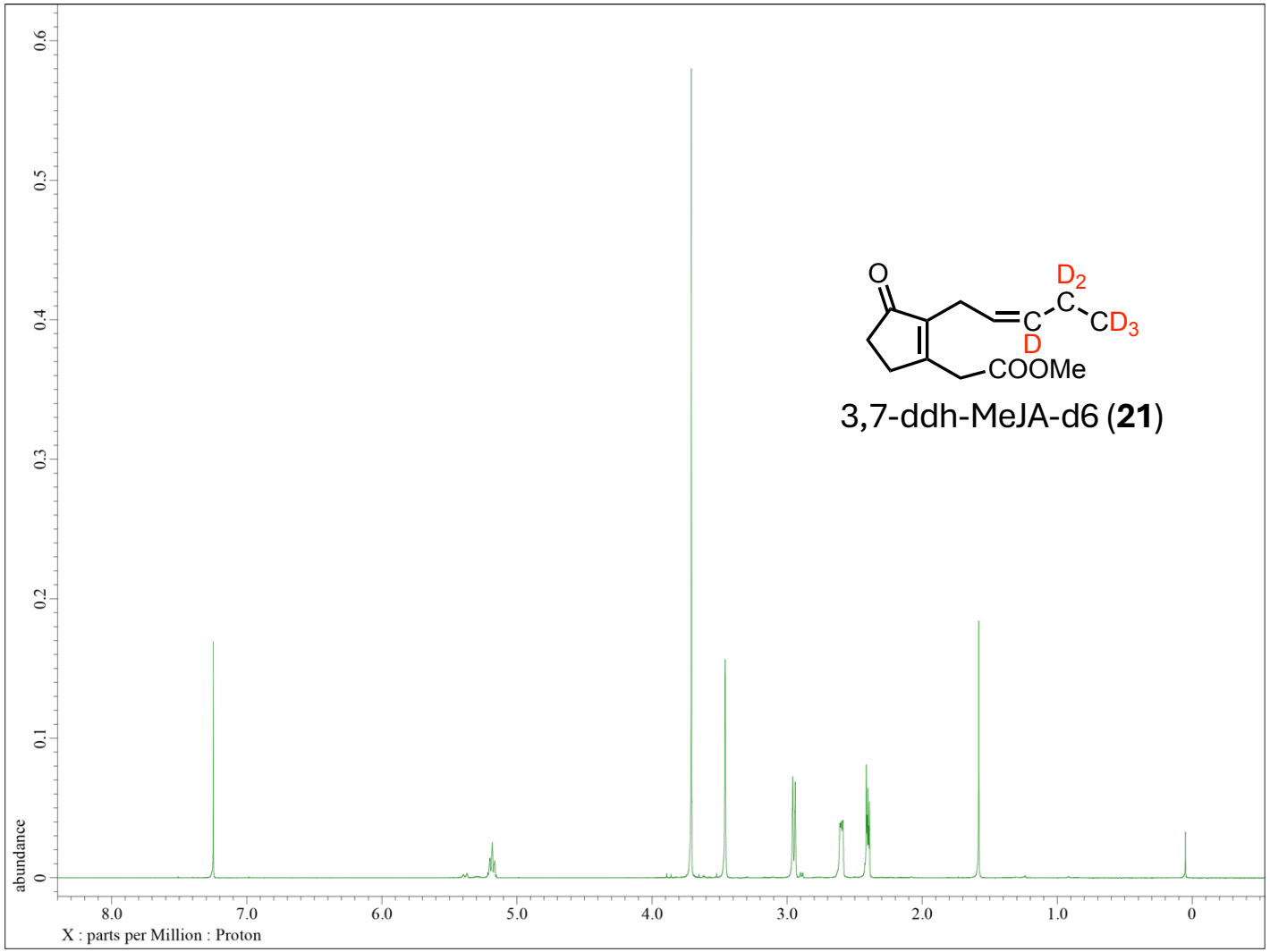

Chart 13: ^{1}H-NMR spectrum of 3,7-ddh-MeJA-d6 (21) in chapter 3

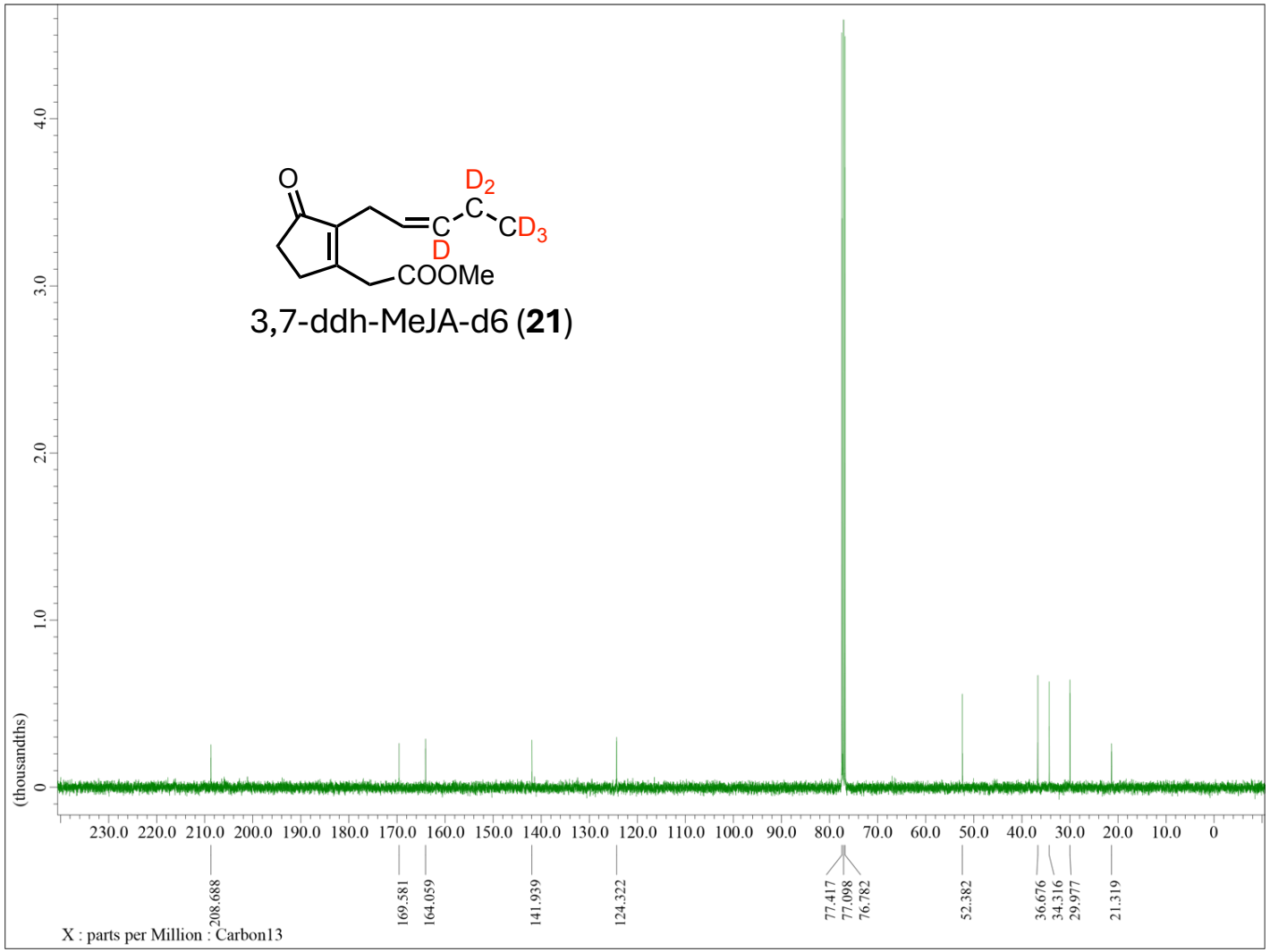

Chart 14: ^{13}C-NMR spectrum of 3,7-ddhMeJA-d6 (21) in chapter 3

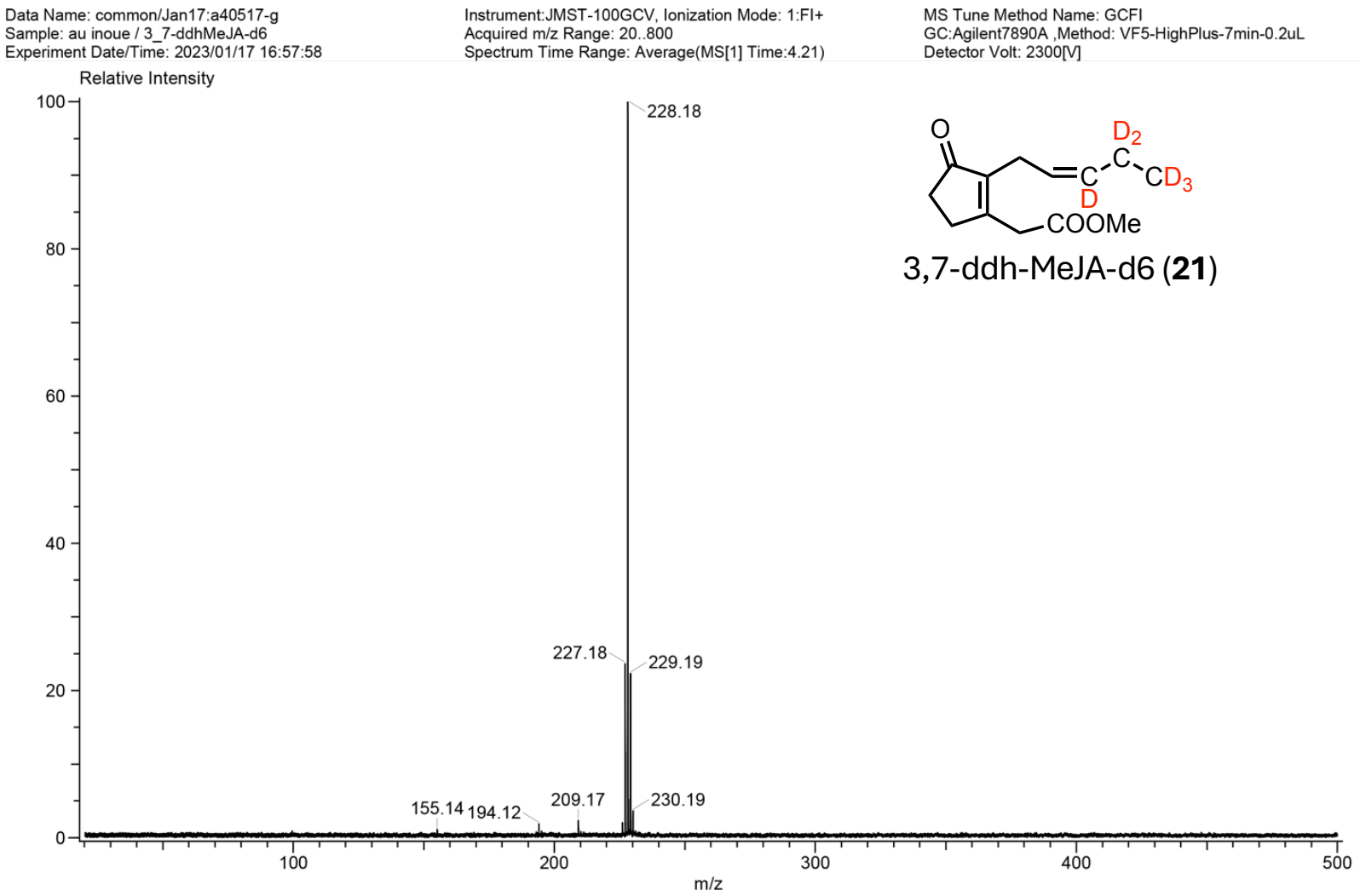

Chart 15: FD-MS spectrum of 3,7-ddhMeJA-d6 (21) in chapter 3